LA-13924-PR
Progress Report

Technology Development, Evaluation, and Application (TDEA) FY 2001 Progress Report

Environment, Safety, and Health (ESH) Division

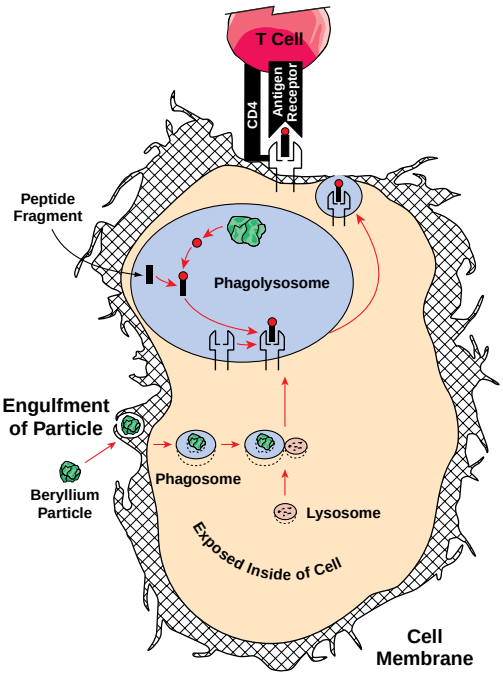

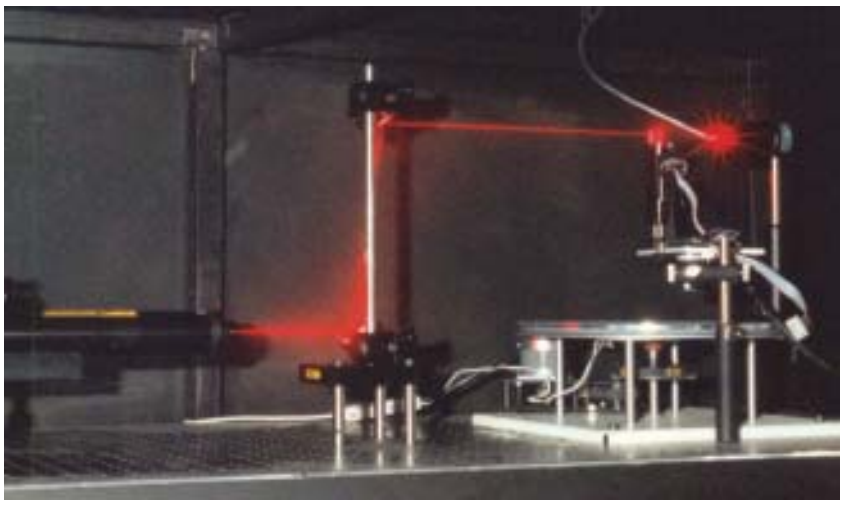

Los Alamos
NATIONAL LABORATORY

Los Alamos National Laboratory is operated by the University of California for the United States Department of Energy under contract W-7405-ENG-36.

Prepared by Larry G. Hoffman, Group ESH-10
Edited by Earlene Hammock, Comforce, Inc., for Group IM-1
Illustrations by Stacey Perez, Weirich Technical Associates, for Group IM-1, and Randy Summers, Comforce, Inc., for Group IM-1
Design and composition by Stacey Perez, Weirich Technical Associates, for Group IM-1
Printing coordinator Guadalupe Archuleta, Group IM-4

Abstract

This progress report presents the results of 11 projects funded ($500K) in FY01 by the Technology Development, Evaluation, and Application (TDEA) Committee of the Environment, Safety, and Health Division (ESH). Five projects fit into the Health Physics discipline, 5 projects are environmental science and one is industrial hygiene/ safety. As a result of their TDEA-funded projects, investigators have published sixteen papers in professional journals, proceedings, or Los Alamos reports and presented their work at professional meetings. Supplement funds and in-kind contributions, such as staff time, instrument use, and workspace, were also provided to TDEA-funded projects by organizations external to ESH Divisions.

The four most recent reports in the unclassified series are LA-13438-PR, LA-13579-PR, LA-13766-PR, and LA-13901-PR.

Photographs without negative numbers are the property of the author.

An Affirmative Action/Equal Opportunity Employer

On cover at left, the diagram shows chronic beryllium disease cellular processing of particles from phagocytosis to antigen presentation. T-cell receptors are triggered when they bind with molecular antigen presented by an antigen-presenting cell, such as pulmonary alveolar machrophages.

At top, an up-close picture shows a young black bear investigating the camera unit at the sampling station. A barbed-wire fur-snare appears in the background. The pictures help verify animal hair, tracks, and scat samples at the sampling station.

The third photo shows the DA-LITES instrument developed in conjunction with Georgia Institute of Technology, which measures scattered laser light. Here, the instrument had the measurement photodiode mounted on a turntable that can be positioned at the desired angle. (Photo courtesy of Heather J. Gepford).

Contents

Introduction

The public expects that the Los Alamos National Laboratory (LANL, Laboratory) will operate in a manner that prevents negative impacts to the environment and protects the safety and health of its employees and the public. To achieve this goal within budget, the Department of Energy (DOE) and the Laboratory must develop new and improved environment, safety, and health (ES&H) technologies and implement innovative, more cost effective ES&H approaches to operations.

The Environment, Health, and Safety Division (ESH) is a multifaceted division with activities and responsibilities that require technology development and application in addition to the technical and operational support of Laboratory activities. Protecting the health of LANL workers and the public is a major effort with expenditures of over $60 million dollars a year. In fiscal year (FY) 95, the division established the Technology Development, Evaluation, and Application (TDEA) Program. The program is managed by a steering committee with members from both within ESH Division as well as outside the division.

The program emphasizes cost effectively improving worker health and safety by becoming more efficient, making better use of resources, and addressing special needs and problems. Now in its seventh year, the program's success can more clearly be evaluated by comparing its accomplishments with the initial TDEA Committee priorities. In the body of this report, the reader will find a mini-progress report for each ES&H discipline represented in the TDEA. The program concentrates on four topical areas: 1) dosimetry, 2) hazards protection, 3) instrumentation, and 4) monitoring. However, the committee considers funding other topics that have compelling justification or significant immediate impact.

In its first year, the TDEA Committee allocated $300K to support five projects for six months. Over the past seven years, this allocation has remained steady at approximately $500K per year, and the allocation supports approximately ten projects each year. From the beginning, the committee decided to limit the duration of any one project's funding to three years. Much of the technology that has been developed from TDEA-funded projects is applied not only within the Laboratory and throughout the DOE complex, but nationally and internationally through government organizations and industry. The TDEA Committee maintains the following five program priorities.

Improve ES&H protection to Laboratory workers and the public. Although all funded projects contribute to protecting workers and the public, one ongoing project in particular has the potential to contribute to an understanding of the workplace hazards associated with beryllium. The information gained in this study may result in improved worker protection, not just at the Laboratory, but also in the DOE complex as well as the international industrial community, and may result in establishing new standards.

Support Laboratory mission objectives. One of the Laboratory's three mission objectives is to solve national problems in energy, environment, infrastructure, and health and safety. The Laboratory's primary operational goal is safety. It is evident from the information provided in this report, that the TDEA Program helps to directly achieve the mission objective and meet the goal in an efficient and cost effective manner.

Respond and build on the unique expertise of the Laboratory and Laboratory requirements. Investigators for TDEA-funded projects through the years have

- developed lightweight, more sensitive instrumentation to measure worker exposure to neutrons;
- applied sophisticated analytical chemistry techniques to bioassay sample measurement methods;
- determined the impacts to the environment with regard to wildlife interaction within the Laboratory;
- determined pressure-deformation correlation criteria to allow emergency responders to evaluate the hazards from pressurized drums;
- identified methods to reduce worker exposure to internally deposited hazardous and radioactive material, developing methods to determine the properties of respirable beryllium associated with chronic beryllium disease; and
- evaluated the reusability of organic vapor air-purifying respirator cartridges.

Achieve success within three years. This annual report summarizes the progress for the seventh year of this program. The success of the program is demonstrated by the implementation of funded project products in the workplace. We discuss successful implementation of these products in more detail in the body of this report.

Find potential to transfer technologies to other DOE sites. Information and methods generated by TDEA-funded projects are transferable to other DOE organizations with the same ES&H concerns. Other government organizations, universities, and private industry have also sought the developed technology.

The FY01 projects listed by discipline include the following three categories:

Environment

A Wildfire Behavior Model for the Los Alamos Region and an Evaluation of Options for Mitigating Fire Hazards;

Developing Genetic Analysis Capabilities as a Tool to Manage Large Carnivore Species at LANL in Response to the Cerro Grande Fire and Associated Impacts;

The Effects of Depleted Uranium on Amphibian Health;

Modification of the Los Alamos/ Canberra Environmental Continuous Air Monitor (ECAM) Inlet for Enhanced Performance by Removal of Fine Particles; and

Wildfire Effects on Contaminant Transport through Wind Erosion.

Health Physics

Neutron Extremity Dosimetry Based on Monte Carlo Computations of Magnetic Resonance Images;

Laser Illuminated Track Etch Scattering (LITES) Dosimetry System;

Personal Continuous Air Monitor (PCAM);

PRESCILA: Proton Recoil Scintillator Los Alamos Rem Meter; and

Rapid Discrimination of Personnel Contamination Due to Radon versus Other Alpha-Emitting Radionuclides.

Industrial Hygiene/ Safety

Development of Methods for Determining Physiochemical Properties of Respirable Beryllium Aerosol Materials Associated with Chronic Beryllium Disease.

The TDEA Committee evaluates TDEA Program success according to the following measures: publications and presentations, cost savings, new technologies, and external support. Peer review is an important part of confirming the validity of the work. The interest from organizations external to ESH Division, especially financial support, also is a measure. However, the primary factor illustrating success is the actual application of the results of a project toward better protection of workers and the environment. Measures of success, including applications of TDEA-funded project results, are discussed in the front of each topical section of this report.

Projects listed under FY96 are documented in LA-13264-PR, for FY97 in LA-13438-PR, FY98 in LA13579-PR, FY99 in LA-13766-PR, and FY00 in LA-13901-PR.

Environment

A Wildfire Behavior Model for the Los Alamos Region and an Evaluation of Options for Mitigating Fire Hazards

Developing Genetic Analysis Capabilities as a Tool to Manage Large Carnivore Species at LANL in Response to the Cerro Grande Fire and Associated Impacts

The Effects of Depleted Uranium on Amphibian Health

Modification of the Los Alamos/Canberra Environmental Continuous Air Monitor (ECAM) Inlet for Enhanced Performance by Removal of Fine Particles

Wildfire Effects on Contaminant Transport through Wind Erosion

Studies to Date

FY96

Seasonal Movements, Activity Patterns, and Radionuclide Concentrations of Rocky Mountain Elk (*Cervus elaphus nelsoni*) and Mule Deer (*Odocoileus heminous*) Inhabiting the Pajarito Plateau

FY97

Development and Evaluation of a Radio-Frequency Identification System to Measure Time Spent by Medium-Sized Mammals at Contaminated Sites at Los Alamos National Laboratory (LANL)

Seasonal Movements, Activity Patterns, and Radionuclide Concentrations of Rocky Mountain Elk (*Cervus elaphus nelsoni*) and Mule Deer (*Odocoileus heminous*) Inhabiting the Pajarito Plateau

FY98

Comparison of Two Permanent Plots within the 1977 La Mesa Fire and Observations from the OSO Fire

Development and Evaluation of a Radio-Frequency Identification System to Measure Time Spent by Medium-Sized Mammals at Contaminated Sites at Los Alamos National Laboratory (LANL)

Seasonal Movements, Activity Patterns, and Radionuclide Concentrations of Rocky Mountain Elk (*Cervus elaphus nelsoni*) Inhabiting the Pajarito Plateau

FY99

A Wildfire Behavior Model for the Los Alamos Region and an Evaluation of Options for Mitigating Fire Hazards

FY00

A Wildfire Behavior Model for the Los Alamos Region and an Evaluation of Options for Mitigating Fire Hazards

Performance Evaluation of LANL Environmental Radiological Air Monitoring Inlets at High-wind Velocities Associated with Resuspension

The Effects of Depleted Uranium on Amphibian Health

Summary of Progress

The ESH Division TDEA program funded five environmental studies in FY01. The diverse projects resulted in 24 publications and presentations with six of the papers being published in peer reviewed journals. Since 1996, a total of 65 publications and presentations have resulted from environmental studies funded by TDEA. Three of the studies funded this fiscal year were a direct result of a need for information to manage the environmental effects of the Cerro Grande fire. The LANL Principle Investigators collaborated with state and federal agencies and/or universities on each of the funded studies. The outside organizations contributed funding, personnel, and physical resources to the projects.

A Wildfire Behavior Model for the Los Alamos Region and an Evaluation of Options for Mitigating Fire Hazards

Principle Investigators: Randy G. Balice, Steven W. Koch, Ecology Group (ESH-20)

Coinvestigators: Jack Nyhan, Sam Loftin, Patrick Valerio, Ecology Group (ESH-20); George H. Fenton, Air Quality Group (ESH-17)

Funding: FY99, $93.5 K; FY00, $95.5 K; FY01, $95.9 K

Matching funds: FY 1999, $15 K (U.S. Forest Service); FY 2000, $45 K (U.S. Forest Service); FY 2001, $50 K (U.S. Forest Service), $325.4 K (Facilities and Waste Operations Division, LANL)

Introduction

Since the occurrence of the Dome Fire in 1996, Los Alamos National Laboratory (LANL) and its neighboring land managers have become increasingly interested in protecting their resources from potential damages caused by wildfires. This awareness was significantly heightened by the Cerro Grande fire in early May 2000.

To support LANL's efforts to protect facilities and property from damages caused by wildfire, we conducted a three-year project to develop a system for modeling the behavior of wildfires and the potential for soil erosion in the Los Alamos region. During the first year of this project, we assembled the databases for performing these modeling tasks (Balice et al. 2000a). During the second year, we conducted sensitivity analyses and validation exercises (Balice et al. 2001). The third year was devoted to updating the databases in the wake of the Cerro Grande fire and performing Monte Carlo simulations of fires and their economic impacts on LANL. This report is a summary of the fire behavior modeling activities conducted during the third year of this project. We conclude this report with evidence from the modeling results that previous thinning of overstocked forests at LANL reduced the expected loss to wildfire, such as the Cerro Grande fire, by approximately $44 M.

LANL is well-suited for this type of modeling activity because of the environmental diversity throughout LANL and the surrounding region (Balice et al. 1997, Balice 1998), the presence of mature programs for monitoring weather (Baars et al. 1998), soil (Nyhan et al. 1978) and vegetation (Balice et al. 1999, 2000b), and the availability of a strong computing and geographic information system (GIS) capability (Bennett et al. 2001). We were able to combine these attributes in an optimal fashion by adopting FARSITE and the Enhanced Universal Soil Loss Equation (USLE) for modeling wildfire behavior and soil erosion, respectively. FARSITE was integrated with selected GIS data layers to interactively produce outputs of wildfire effects, such as total area burned, heat per unit area, rate of spread, and occurrence of crown fires (Finney 1998). GIS data layers were also used to perform USLE estimations of annual soil erosion in tons per acre (Wischmeier and Smith 1978, Nyhan and Lane 1986). The USLE results are summarized and reviewed in Nyhan et al. (2001).

Methods

Database development before the Cerro Grande Fire. The specific inputs required by FARSITE and the USLE were derived from existing, locally collected, environmental data that had been converted to spatially explicit formats (Koch and Balice 1999). FARSITE required three general types of inputs: weather, topography, and fuels. Weather data for specific time periods and locations within the Los Alamos region, including temperature, relative humidity, wind speed, and wind direction, were downloaded from the LANL Weather Machine (Air Quality Group 2001). Topography, including slope, aspect, and elevation, was produced at 30-meter resolution from USGS digital elevation model (DEM) data. Characteristics of fuels in vegetated areas, including the fuel model (Anderson 1982), total height of the vegetation, percent cover of the forest canopy, and height from the ground to the live forest crown were summarized from existing vegetation data that had been collected for the Los Alamos region (Balice et al. 1999, 2000b). Additionally, crown bulk density information was adopted from Keane et al. (1998). Values for each of these parameters were assigned to a previously developed land cover classification (Koch et al. 1997, Balice et al. 1997, Balice 1998). In areas that did not support vegetation, such as areas with bare rock, or with buildings, facilities and paved areas of more than one acre in size, the fuel model was set to unburnable.

To develop a realistic database of fire starting points within the Los Alamos region, we adopted a dataset of lightning strikes that had been organized by geographic coordinates and by signal strength (Jacobson et al. 2000, Smith et al. 2001). The time period for these data extended from April 1, 1998, to October 1, 1998. To limit the data set to lightning strikes that would occur during the wildfire season and would have sufficient energy to start a fire, we eliminated all lightning strikes after July 11, as well as those with strengths less than 100 kiloamps. The resulting final dataset included 122 lightning strikes, and these were converted to ArcView shapefiles. Since the coordinates of these lightning strikes do not follow any obvious pattern, their distribution was considered as random.

Model validation against the Cerro Grande Fire. The wildfire behavior model had previously been partially validated against the TA-40 fire, which burned for 8 hours on March 22, 1996 (Koch et al. 2000). The model was further validated against the Cerro Grande Fire. In addition to the pre-Cerro Grande Fire fuel and topographic data layers that had been previously developed, weather data from May 1–15, 2000, were downloaded from several LANL weather towers, including Pajarito Mountain, TA-6, TA-49, and TA-54. In addition, fuel-moisture data that were collected by Bandelier National Monument and by the U.S. Forest Service immediately preceding and during the Cerro Grande Fire were also incorporated into the modeling system. Then, three segments of the Cerro Grande Fire were selected for further modeling:
1) the Sunday, May 7, segment that occurred in the upper Sierra de los Valles between Water Canyon and Pajarito Canyon, 2) the Wednesday, May 10, segment along the western portions of the Los Alamos townsite, and 3) the Thursday, May 11, segment that burned on LANL between S-Site and TA-18. Each of these segments was modeled under constant conditions except for iterations of weather data from the four weather towers.

Database revisions after the Cerro Grande Fire. The Cerro Grande Fire had profound effects on the fuel structures in the Los Alamos region and it is now desirable to revise and update the input data layers for the modeling system to reflect these changes. The revised data will allow comparisons of fire behaviors and soil-erosion potentials before and after the Cerro Grande fire, and will address the current post-fire hazards. To revise the fuels data layers, we focused on the primary first-order impacts of the Cerro Grande Fire, which were to the vegetation cover. First, we adopted the Burned Area Emergency Rehabilitation Team burn-severity maps that classified burn severities into high, moderate, low, and unburned (Interagency BAER Team 2000). Second, we incorporated data collected in the field during the summer of 2000. From preliminary analyses of these field data, we learned that areas with high-burn severity contained virtually no fuels during the first summer after the fire. In contrast, the fuel levels of areas with moderate- or low-burn severities were similar to pre-Cerro Grande fire conditions. As a result of these field observations, we set the areas that were burned at high severity during the Cerro Grande Fire to unburnable. In contrast, fuel levels of areas that were burned with low or moderate severities were left unchanged from prefire conditions.

Monte Carlo simulations of expected loss to LANL from wildfire. We performed repeated simulations of wildfires to estimate the potential or expected impacts to LANL before and after the application of thinning treatments to LANL forests. These simulations used the randomly distributed lightning strikes as starting points. Wildfires were initiated at the 122 lightning strike locations and allowed to burn from 8:00 A.M. to 8:00 P.M., a 12-hour period, under both pre-thinning and post-thinning conditions. The outputs from the pre-thinning simulations were used to calculate the average expected loss (AEL_{pre}) to LANL, and these results were combined with outputs from identical simulations under post-thinning conditions (AEL_{post}) to calculate the reduced expected loss (REL) to LANL.

For these wildfire simulations, we utilized the weather conditions that were recorded during Sunday, May 7, 2000, at the weather towers on Pajarito Mountain and at TA-6. The weather data from Pajarito Mountain were used for all mountainous terrain to the west of LANL, whereas the weather data from TA-6 were used for LANL and townsite property. From a wildfire standpoint, the weather and fuel moisture conditions recorded at these towers on May 7, 2000, were severe and similar to those experienced during the Dome Fire of 1996. In contrast, these weather conditions are not as extreme as those experienced on Wednesday, May 10, 2000.

Using the lightning-strike locations as ignition points and the weather and fuel moisture conditions recorded during the Cerro Grande Fire, in combination with the pre-Cerro Grande Fire data layers, we simulated wildfires in the LANL region and calculated the pre-treatment average expected loss (AEL_{pre}) to LANL from wildfire:

$$\mathrm{AEL_{pre}} = \frac{1}{N}\left\{\sum_{n\in N} S(n) + \sum_{n\in N}\sum_{x\in X} I_{n,x}[(F(x) + R(x)]\right\} \quad (1)$$

where, S(n) = cost of wildfire suppression activities during the nth wildfire,

$I_{n,x}$ = indicator variable of damage or severe destruction to facility x during wildfire n,

$F(x)$ = replacement value of facility x, including the value of its contents, and

$R(x)$ = burdened costs of LANL employees populating facility x.

The cost of wildfire suppression [$S(n)$] was determined by multiplying the acreage of the nth simulated wildfire by the average cost of suppression. The average cost of suppression, $125 per acre, was calculated from data reported for the time period from 1994 to 2000 by the National Interagency Fire Center (NIFC 2001). The number of facilities or buildings burned for each simulated fire was determined by superimposing the 12-hour fire perimeter output from the fire model upon the GIS data layer of burnable LANL facilities. For each of these facilities, the indicator variable of damage ($I_{n,x}$) was set to 1. Otherwise, $I_{n,x}$ remained set at 0. The replacement values of each facility [$F(x)$] and its occupancy of LANL employees were obtained from a 2001 summarization for LANL compiled by the Site and Project Planning Group (SPPG 2001). This assumes that the facility would be closed during and after the wildfire, but would be essentially undamaged by the fire itself. To calculate the cost of lost income for each facility [$R(x)$], we first assumed that facility x would be closed for one month after the fire or that the LANL employees who work in facility x would be displaced for one month before being relocated to another LANL workplace. Then, we multiplied the number of LANL employ-

ees working in facility *x* by an estimate of the average monthly burdened cost to LANL for each employee, $20 K.

To calculate the reduced expected loss (*REL*) to LANL, we adopted the GIS data layer of forested and wooded areas on LANL property that had been thinned before the Cerro Grande fire. These areas, which include a total of approximately 800 acres, had been thinned from 1997 to 2000 in accordance with the fuel-break prescription outlined in the Wildfire Hazard Reduction Program (DOE LAAO 2000). Based on field data collected in these fuel breaks, we reduced the canopy cover values by 50 percent and increased the distances between the ground fuels and the crown fuels by 25 percent. Next, we repeated the 122 simulations that had been used to calculate AEL_{pre}, with the exception that the addition of fuel breaks in previously unthinned forests during these simulations resulted in a post-treatment average expected loss (AEL_{post}) to LANL. Finally, these intermediate results, along with the cost of thinning the forest to fuel break specifications (*C*), were used to calculate the reduced expected loss (*REL*) according to

$$REL = AEL_{pre} - (AEL_{post} + C) \quad (2)$$

where AEL_{pre} = the pre-thinning average expected loss from wildfire,
AEL_{post} = the post-thinning average expected loss from wildfire, and
C = the cost of thinning the forests and woodlands to fuel break specifications.

Progress and Results

Model validation against the Cerro Grande Fire. The Pajarito Tower weather data modeled the Sunday, May 7, segment with high fidelity. In contrast, weather data from the TA-6, TA-49, and TA-54 weather towers did not faithfully model the Sunday, May 7, segment. Similarly, the Wednesday, May 10, segment was modeled most successfully with the Pajarito Tower weather data, and the Thursday, May 11, segment was modeled most successfully with the TA-49 weather data. Substitution of weather data from alternate towers for modeling of these fires produced less desirable results. In all cases, the weather data that contributed to successful modeling of individual fire segments was gathered from the weather tower closest to the starting point for that segment, less than 2 miles. Substitution of weather data from other towers, even those that were not more than 5 miles distant from the starting point, produced less desirable results. These results emphasized the importance of using locally gathered data to successful fire behavior modeling.

Monte Carlo simulations of expected loss to LANL from wildfire. Of the 122 lightning-strike ignition points, 26 occurred on bare rock, buildings, parking lots, or other unburnable locations and, therefore, did not produce a measurable simulated fire. An additional 49 simulated fires did not burn on LANL property and were eliminated from further consideration. Of the remaining 47 simulated wildfires, the average area burned per fire was 1594 acres before thinning and 914 acres after thinning (Table 1). This represents a 43 percent reduction in the average number of acres burned. Similarly, the average number of buildings affected by the 47 fires was reduced from 69 to 31, a 55 percent reduction. The number of LANL employees per fire that were displaced was also reduced from 177 to 45.

The calculated pre-thinning and post-thinning components of the AEL are shown in Table 2. In each case, the cost of burned buildings (X) is the primary contributor to the respective AEL. The costs of fire suppression (S) and income losses (R) are relatively less important.

The cost of thinning 800 acres of forests and woodlands at LANL to fuel-break specifications (C) was approximately $2.5M. Using this value and the simulated results for AEL_{pre} and AEL_{post} (Table 2), the REL calculates as follows:

$$REL = \$78.66\ M - (\$32.35\ M + \$2.50\ M) = \$43.81\ M. \quad (3)$$

Thus, after a $2.5M investment in thinning, the average cost to LANL, based on 47 wildfires that each burned for 12 hours under typical weather conditions, would be reduced by approximately $44M. This represents a more than 17-fold return on the original investment.

Table 1. *Average per-fire results of pre-thinning and post-thinning simulations (N = 47).*

Intermediate result	Pre-thinning	Post-thinning
Acreage of fires	1594	914
Number of buildings affected	69	31
Number of displaced employees	177	45

Table 2. *Cost components of AEL_{pre} and AEL_{post} in $M.*

Component	Pre-thinning	Post-thinning
Fire suppression (*S*)	$ 0.20	$ 0.11
Burned buildings (*X*)	$74.92	$31.33
Income losses (*R*)	$ 3.54	$ 0.90
AEL	$78.66	$32.35

Conclusions and Deliverables

Deliverables. As originally proposed in this project, we have produced a fully functioning, validated system for modeling wildfire behaviors and soil erosion potentials in the Los Alamos region. This modeling system was used successfully to complete Monte Carlo simulations of expected loss to LANL from wildfires. We have also applied the modeling system to comparative analyses of soil-erosion potentials before and after the Cerro Grande fire (Nyhan et al. 2001). The system will continue to be available for future research and management activities related to wildfire and soil erosion.

Assumptions and availability of data for simulations. Given the assumptions and the data available for this analysis, the results of the Monte Carlo simulations appear to be conservative. First, a total of 1035 buildings and structures burned at least once during the 47 simulated wildfires. However, replacement values for only 531 of these structures were available (Site and Project Planning Group 2001). Therefore, the values of 504 buildings and structures were not included in the AEL calculations, even though they were likely to have burned or been damaged by wildfires. Second, conservatism is introduced by the replacement values of the buildings, which do not include the values of the contents of these buildings. Third, the results are conservative if one considers that the simulations were limited to 12 hours, whereas the Cerro Grande Fire actively burned on LANL property for several days. This is consistent with the most credible wildfire scenario that assumes that catastrophic wildfires will burn for up to one week (Balice et al. 1997).

Locally collected data and robust modeling. This project demonstrates the validity of our approach that uses detailed, locally collected data for parameterizing models of wildfire behavior and soil erosion. The importance of obtaining accurate, precise, and relevant data to ensure robust modeling is supported by similar results generated elsewhere in the western United States (Keane et al. 1998, Keane et al. 2000). The disadvantages of using these kinds of data are that they can be expensive to obtain and are available to the modeling team only after extensive fieldwork and laboratory analyses are completed. Another consequence of using locally collected data is that the associated model data layers may require frequent revisions as new information becomes available, or, in our case, as post-fire environmental conditions change and as ecosystem recovery occurs within the study region of interest.

Importance of reducing fuels in fire hazard management. We also provided additional support for the importance of active and aggressive management of forests to protect LANL from wildfires. Of the three components of the fire triangle, fuel, heat and ignition, only fuels can be conveniently manipulated and managed in a typical wildfire scenario (Balice et al. 1997). At LANL, fuels are represented by trees, which can only be reduced by thinning and removal. These thinning treatments should be completed well before the onset of a wildfire season for the full benefits.

On the other hand, thinning treatments do not have to be severe to significantly reduce fire hazards. In the example of this modeling exercise, thinning 800 acres of forested land to average densities of 50 to 150 trees per acre significantly reduced the number of facilities and buildings damaged or destroyed by wildfire.

References

Air Quality Group, The LANL weather machine: raw data request form. Web page (http://weather.lanl.gov/cgi-bin/datarequest) maintained by the Air Quality Group (ESH-17), Los Alamos National Laboratory (2001).

Anderson, H.E., Aids to determining fuel models for estimating fire behavior. General Technical Report INT-122, USDA Forest Service, Intermountain Forest and Range Experiment Station, Ogden, UT (1982).

Baars, J., D. Holt, and G. Stone, "Meteorological monitoring at Los Alamos." Los Alamos National Laboratory, report LA-UR-98-2148 (1998).

Balice, R.G., "A preliminary survey of terrestrial plant communities in the Sierra de los Valles." Los Alamos National Laboratory, report LA-13523-MS (1998).

Balice, R.G., S.G. Ferran, and T.S. Foxx, "Preliminary vegetation and land cover classification for the Los Alamos Region." Los Alamos National Laboratory, report LA-UR-97-4627 (1997).

Balice, R.G., B.P. Oswald and C. Martin, "Fuels inventories in the Los Alamos National Laboratory Region: 1997." Los Alamos National Laboratory, report LA-13572-MS (1999).

Balice, R.G., S.W. Koch, P. Valerio, S. Loftin, and J. Baars, 2000a. "A wildfire behavior model for the Los Alamos Region and an evaluation of options for mitigating fire hazards." Technology, Development, Evaluation and Assessment (TDEA) FY 1999 Progress Report. Los Alamos National Laboratory,report LA-13766-PR (1999).

Balice, R.G., J.D. Miller, B.P. Oswald, C. Edminster and S.R. Yool, 2000b. "Forest surveys and wildfire assessment in the Los Alamos region, 1998-1999," Los Alamos National Laboratory, report LA-12714-MS (2000).

Balice, R.G., S.W. Koch, P. Valerio, S. Loftin, J.W. Nyhan, and G. Fenton., "A wildfire behavior model for the Los Alamos Region and an evaluation of options for mitigating fire hazards," Technology, Development, Evaluation and Assessment (TDEA) FY 2000 Progress Report. Los Alamos National Laboratory, report LA-13901-PR (2002).

Bennett, K., S.W. Koch, S. Gebhardt, M. Wright and W. Red Star, "GIS applications within the Ecology Group of LANL." Los Alamos National Laboratory, report LA-UR-01-1209 (2001).

DOE LAAO, "Environmental Assessment for the Wildfire Hazard Reduction and Forest Health Improvement Program at Los Alamos National Laboratory," Los Alamos, New Mexico. DOE-EA-1329, prepared by Department of Energy, Los Alamos Area Office, (2000).

Finney, M.A., FARSITE: Fire area simulator model development and evaluation. Research Paper RMRS-RP-4, USDA Forest Service, Rocky Mountain Research Station, Fort Collins, CO. (1998).

Interagency BAER Team, Cerro Grande Fire burned area emergency rehabilitation (BAER) plan. Prepared by the Interagency BAER Team, Los Alamos, NM. (2000).

Jacobson, A.R., K.L. Cummins, M. Carter, P. Klingner, D. Roussel-Dupré, and S.O. Knox, "FORTE radio-frequency observations of lightning strokes detected by the National Lightning Detection Network." *J. Geophys. Res.* 105 (D12), 15,653-15,662. (2000).

Keane, R.E., J.L. Garner, K.M. Schmidt, D.G. Long, J.P. Menakis, and M.A. Finney, "Development of input data layers for FARSITE fire growth model for the Selway-Bitterroot Wilderness Complex, USA," General Technical Report RMRS-GTR-3, USDA Forest Service, Rocky Mountain Research Station, Ogden, UT. (1998).

Keane, R.E., S.A. Mincemoyer, K.M. Schmidt, D.G. Long, and J.L. Garner, "Mapping vegetation and fuels for fire management on the Gila National Forest Complex, New Mexico," General Technical Report RMRS-GTR-46-CD, USDA Forest Service, Rocky Mountain Research Station, Ogden, UT. (2000).

Koch, S.W. and R.G. Balice, "Input data development for the FARSITE fire area simulator for the Los Alamos National Laboratory Region." Presented at the ESRI User Conference, San Diego, June 26, 1999.

Koch, S.W., T.K. Budge, and R.G. Balice, "Development of a land cover map for Los Alamos National Lab and vicinity." Los Alamos National Laboratory, report LA-UR-97-4628 (1997).

Koch, S.W, R.G. Balice, J.W. Nyhan, and S.R. Loftin, "Validation and sensitivity analyses of a wildfire behavior model," presented at the ESH Division Review Committee Meeting, Los Alamos National Laboratory, April 11–13, 2000.

NIFC, "Wildland Fire Statistics." Web page (http://www.nifc.gov/stats) maintained by the National Interagency Fire Center, Boise, ID (2001).

Nyhan, J.W. and L.J. Lane, "Erosion control technology: a user's guide to the use of the universal soil loss equation at waste burial facilities," Los Alamos National Laboratory, report LA-6779-MS (1986).

Nyhan, J.W., L.W. Hacker, T.E. Calhoun, and D.L. Young, "Soil survey of Los Alamos County, New Mexico." Los Alamos Scientific Laboratory, report LA-6779-MS (1978).

Nyhan, J.W., S.W. Koch, R.G. Balice, and S. Loftin, "Estimation of soil erosion in burnt forest areas of the Cerro Grande Fire in Los Alamos, New Mexico." *Catena*, submitted, in review (2001).

Smith, D.A., K.B. Eack, J. Harlin, M.J. Heavner, A.R. Jacobson, R.S. Massey, X.M. Shao, and K.C. Wiens, "The Los Alamos Sferic Array: A research tool for lightning investigations." *J. Geophys. Res.* submitted, in review, (2001).

Site and Project Planning Group (PM-1), "FY01 ten-year comprehensive site plan." Los Alamos National Laboratory, report LA-CP-01-374 (2001).

Wischmeier, W.H. and D.D. Smith, "Predicting rainfall erosion lossesæa guide to conservation planning." USDA Handbook 537, U.S. Government Printing Office, Washington, D.C. (1978).

Developing Genetic Analysis Capabilities as a Tool to Manage Large Carnivore Species at LANL in Response to the Cerro Grande Fire and Associated Impacts

Principle Investigators: James R. Biggs (ESH-20), Jon L. Longmire (B-N1), Heather Alexander, New Mexico State University/B-N1, Leslie Hansen (ESH-20)

Coinvestigators: Carey Bare, Sherri Frybarger, (ESH-20)

Other collaborating organizations: United States Forest Service, Bandelier National Monument, New Mexico Dept. of Game and Fish

Funding: FY01, $15K

Introduction

The Cerro Grande fire (CGF) of May 2000 burned approximately 45,000 acres of forest and range land on and adjacent to Los Alamos National Laboratory (LANL) property. Approximately 8,000 acres burned on LANL property. This will most likely lead to both short-term (1–3 years) and long-term alterations in the distribution and behavior of large carnivores, such as mountain lion (*Felis concolor*) and black bear (*Ursus americanus*). At present, studies for monitoring and studying population characteristics and behavior of these species on and around LANL are limited because of the cost of labor-intensive techniques. Following the CGF, funding was made available to monitor the effects of the CGF on large carnivores. However, the funding is specifically targeted for the monitoring of these species for three years only using advanced telemetry equipment; money has not been budgeted to explore alternative more efficient and cost-effective methods of monitoring these species. After completion of the three-year monitoring, the application of long-term cost-effective techniques to monitor activity and distribution will be necessary to continue studying effects of the fire as well as impacts from normal ongoing LANL operations. Issues pertaining to large carnivores include the following categories.

Potential increase in the number of encounters between large carnivores and LANL employees. Following the Cerro Grande fire, LANL personnel investigated a two- to three-fold increase in mountain lion and black bear encounters at LANL. This was attributed to several factors including loss of available habitat, the redistribution patterns of prey species, and human impacts associated with flood prevention measures. The increased sightings prompted the Laboratory to issue Lab-wide alerts about the potential dangers of encounters with mountain lions and black bears. In addition, several reports of mountain lion attacks on pets have taken place in Los Alamos County during 2001.

Also in Los Alamos County, multiple nuisance bears have been transplanted to extreme northern New Mexico. Most of these bears will either die because of territorial disputes with existing bears in the transplant site or will return to the site of capture. Animals that do return could become a nuisance again and ultimately have to be destroyed. Long-term monitoring of carnivore populations can provide data critical to developing management strategies to minimize the potential for nuisance animals. ESH-20 is collaborating with the New Mexico Department of Game and Fish (NMDGF) to provide mountain lion and black bear awareness training to LANL employees through ESH-13. The primary issues of concern voiced by LANL employees include safety while performing field work, working in areas relatively isolated from centers of activity, jogging, hiking, and current, past, and predicted future status and trends of these species due to the fire. Although we can offer awareness training, we cannot provide detailed information on distribution, behavioral patterns, areas of potentially greater risk of encounters, and potential problem individual animals. Nor can we provide information on the long-term fire effects to these species and thus cannot develop management strategies to mitigate potential problems.

Application of low-cost techniques to study population characteristics of large carnivores. Currently, studies are underway to identify distribution, habitat use, and population characteristics of elk and deer using advanced telemetry systems. Telemetry systems can be deployed on these species relatively quickly and inexpensively because of the ease of capturing these species. However, capturing and collaring of large carnivore species, such as mountain lion and black bear, can be difficult, costly, time consuming, as well as posing a risk to the animal. Telemetry techniques applied to large carnivores can be cost effective and provide important data at the onset of a study, but can become too costly and labor intensive to continue for extended periods of time. The development of alternative methods to study the behavior, distribution, movement patterns, and population characteristics of large predators is imperative to the long-term management of such species. Recent advancements in genetic analysis may offer a more innovative low-cost technique to obtain the information necessary to develop and implement management strategies for large carnivores. Genetic analysis of hair samples has been applied to wildlife studies (Foran et al. 1997) but further refinements in techniques to collect hair and scat samples are necessary. Scat (fecal material) is one of the most easily obtainable, low-cost sources of information on population characteristics of animals available (Kohn and

Wayne 1997) and can provide data on animal distribution, abundance, spatial-temporal movement, diet, and disease (Putnam 1984). The further refinement and application of genetic analysis of animal scat that is both cost-efficient and effective would aid in significant cost-savings to LANL projects. Cost estimates to implement a study utilizing telemetry techniques would be about $100K per year versus an estimated $35–40K per year using genetic analysis (assumes 6–10 individuals of each species [lion, bear] are radio collared with GPS radio collars).

Effects of the Cerro Grande fire on the distribution and movements of large carnivores at LANL. Deer and elk are primary prey items for mountain lions in this area. Black bear readily feed on deer and elk as carrion. Black bear will also feed on the young of these species. Several vegetation monitoring studies were initiated in CY00 and CY01; results indicate that the production of extensive foraging range on and around LANL for deer, elk, and bear is taking place in the CGF burn area. In turn, the Laboratory may observe a significant increase in the use and distribution of these species on LANL property. The increase in prey species may result in an increase in the number of large carnivore species inhabiting and/or feeding in this area. LANL mitigation measures to reduce the adverse impacts from the fire (e.g., flood retention structures) may not only effect the movement patterns of large ranging carnivores, but also the long-term distribution patterns associated with the increase and distribution of prey species.

Collaborative efforts including Bandelier National Monument (BNM), Santa Fe National Forest (SFNF), NMDGF, and area pueblos are underway to address issues related to the long-term management of game species across the Jemez Mountains. Efforts have been stepped up because of the CGF and associated mitigation measures. In many instances, individual mountain lions and black bears will utilize each of these lands as part of their territory or home range thus necessitating a region-wide approach to management. The primary factor most limiting to implementing a wide-scale study on large carnivores is cost and sampling consistency across the region. LANL may implement limited radio collaring efforts as part of project specific needs. However, most adjoining entities and landowners are unable to implement such studies because of cost and available resources. Thus,` collected data is inadequate to develop and implement region-wide management strategies. The use of fecal and hair genetic analysis could offer a sampling and analysis technique that would not be cost prohibitive and will provide the data necessary to implement wide-scale management strategies. The application of these techniques can be easily applied to studying distribution and population trends of large carnivores in this area.

Techniques for collecting genetic-analysis samples have been limited to blood and/or tissue samples from captured, radio collared animals as part of project-specific needs (Biggs et al. 1999). These projects have focused primarily on elk and deer because of the cost-prohibitive nature of capturing large carnivores. Genetic-analysis sampling results help establish a genetic baseline of prey for mountain lion and black bear on LANL property. For application to management of large carnivores, a method needs to be rapid, relatively inexpensive, easy-to-learn, and definitive in its results (Foran et al. 1997). The method cannot vary with time, diet, or other factors. Genetic markers of individual animals do not change over time nor do they change with differing diets or other factors (Foran et al. 1997). Because of the behavioral characteristics of large carnivores, the collection of tissue and blood samples is problematic. Mountain lions and black bears are difficult to capture, elusive, and secretive; therefore, the collection and analysis of scat or hair is often one of the best noninvasive methods for monitoring their populations (Foran et al. 1997). Although several technical problems prevent the widespread large-scale application of fecal genetic analysis, some studies have provided information on population characteristics, food habits, and reproduction characteristics of wildlife species (Kohn et al 1995, Reed et al. 1997, Ernest et al. 2000). Fecal DNA analysis is an effective method for detecting and identifying individual mountain lions (Ernest et al 2000). Comprehensive sampling of an area for feces or systematic fecal transects of populations may allow estimates of home range, territory dimensions, core-use areas, reproductive patterns, and population size (Kohn and Wayne 1997). The same analytical methods used to deduce core areas and home range from radio telemetry could be applied to these kinds of data from fecal samples.

The primary objectives of this study are the following:

1. Provide distribution, behavioral, and population data on large carnivores to develop management strategies.
2. Further develop and refine genetic analysis of fecal material for the study of large carnivores.
3. Further refine methods of collecting scat and hair samples at LANL for genetic analysis.
4. Provide a technique to study the long-term effects of the Cerro Grande fire on large carnivores.

Methods

Line transects and sampling stations to collect hair were established and evaluated during FY01 and are discussed further in the next section (Progress and Results). Additional sampling stations and transects will be established throughout the study area to collect hair and scat and to characterize carnivore population parameters (i.e., population size, sex ratios, distribution). When possible, blood and tissue samples will be collected from radio-collared animals from other project-specific studies and roadkill animals for comparison to fecal and hair analysis results. Once fully implemented, sample collection sites will be plotted, individual animals identified via genetic analysis, and distribution coverages developed with the GIS.

The technology to identify and monitor individual lions and bears is based on the analysis of microsatellites. Microsatellites are short, tandemly repeated DNA sequences found within the genomes of organisms. Microsatellite characteristics that make them "the system of choice" for modern genetic analyses are that they are highly variable (polymorphic) and they are easily analyzed using the polymerase chain reaction (PCR) (Weber and May, 1989; Epplen, 1991; Tautz and Renz, 1984). Short oligonucleotide primers (approximately 20 nucleotides each) are developed to complement sequences that directly flank both sides of specific microsatellite repeat clusters (loci). These primer pairs, together with the PCR reaction, allow amplification of the microsatellite loci from small amounts of target DNA. The amplification products are florescently labeled and their length is determined using an automated DNA sequencing machine and DNA standards of known size. Variability at microsatellite loci is observed when different length amplification products are generated due to differing numbers of basic repeating units within the microsatellite clusters. The level of allelic variation that is seen at a series of specific microsatellite loci is generally sufficient for true genetic differentiation (or DNA profiling) of all individuals within a population (Weber and May, 1989).

Progress and results

Proposed for FY01. As part of the FY01 objectives, a sampling design for collection of fecal and hair material would be developed at the onset of the study; this was accomplished by July 2001. Also in FY01, fecal samples were to be collected through systematic area sampling when techniques for the collection of samples and the genetic analysis would be refined. Line transects would be established within plots that have been located via a stratified random approach across LANL property. When possible, blood and tissue samples would be collected from radio-collared animals, other project-specific studies, and roadkill animals for comparison to fecal and hair analysis results. Hair traps of different designs would be developed, deployed, and evaluated for effectiveness in collecting hair samples from target species.

Progress to Date. Line transects for collecting fecal samples were established in three canyons (Cañada del Buey, Los Alamos Canyon, and Ancho Canyon) and along one mesa top (Ancho Mesa). Samples were collected using a standardized protocol developed during FY01. The transects will be extended throughout the Lab and in surrounding areas (USFS, BNM) during FY02. All line transects will have Global Positioning System (GPS) coordinates taken to establish exact location of the line transects. During the FY01 sampling period, twenty-four scat samples were collected and included bear (most samples), bobcat, and coyote. All samples have been stored for genetic analysis to be performed during FY02. Also during the summer FY01, different hair-snare designs were tested for efficacy in collecting hair samples of high enough quality and quantity for performing genetic analysis (Fig. 1). Several snares of different designs were established at eight locations near the same locations as the line transects. At each location, cameras were set to take pictures of animals visiting the snares for confirmation of species (Figs. 2 and 3). Hair was placed in a small envelope, sealed, and labeled with date, location of sample, type of snare used, and identification of animal if possible. The samples were then placed in a freezer until needed for DNA analysis. Preliminary results of the hair snares are reported in Quintana and Alexander (2001).

During FY01, we proposed evaluating two approaches for designing the primer pairs needed to conduct the genetic work on mountain lion and black bear. The first approach uses microsatellite primer pairs developed for other cat species. The other approach involves developing new microsatellite markers by cloning and sequencing microsatellite loci directly from lion DNA as has been done for other species (Longmire et al. 1999; Longmire et al. in press, White et al. 1999). This approach could require a year or more of development time and would be used only if we require additional resolving power to achieve full genetic differentiation of all individuals. As a result of FY01 efforts, it appears existing microsatellite primer pairs will work effectively for both black bear and mountain lion.

DNA isolation from scat. We have compiled information about benefits and limitations of how scat and hair samples have been used in the past. Different protocols used to isolate DNA from samples were also tested. During FY01, we began testing the QIAamp DNA Stool Mini Kit, which offered a quick and easy system to isolate DNA from scat. This kit is ideal because it not only eliminates inhibitors present in the sample, but also it isolates DNA with minimal use of hazardous organic compounds, such as phenol and chloroform. Using the kit's protocols, we have been able to isolate DNA from the scat; however, when PCR was performed, the primer sets were unable to amplify the microsatellites. The problem with isolating genomic DNA from scat is an incredibly high amount of bacterial DNA present, which makes it difficult to pull out the genomic DNA from the specific animal. In order to get amplification of the microsatellites, we added a phenol extraction into the kit's protocol along with increasing the number of cycles performed in PCR. These changes allowed us to successfully amplify the microsatellites we were looking for. During FY02, we will continue to use this kit with a larger number of different dog scat samples to determine the kit's consistency. We will also look at the environmental influences on the degradation of DNA in scat samples by looking at the success rate of isolating genomic DNA in a set period of time. Once the protocol is refined, DNA will be isolated from samples collected out in the field, and species identification along with individual animal profiling will be performed. Once individuals are identified, the samples from these individuals will be located on a map and

Figure 1. *Two types of hair snares are shown. The cubby snare (right) grabs hair samples from animals entering the snare to investigate scents that are placed on the tree. Hair is taken from animals using a series of brushes placed along the two timbers. The barbed wire snare (left) grabs hair samples from animals entering the enclosed area (scents are placed at the center of the area to attract animals). The barbs are long enough to grab hair without injuring the animal.*

Figure 2. *Picture of a coyote entering the sampling station. In addition to mountain lions and black bears, this system can monitor other carnivore species such as coyote and bobcat.*

Figure 3. *An up-close picture of a young black bear investigating the camera unit at the sampling station with the barbed wire snare in the background. The pictures help verify animal species tracks, hair, and scat samples collected at the station.*

distribution will be determined along with overall population size.

DNA isolation from hair. Hair samples have been collected out in the field via the hair snares and trapping live bears. These samples are stored in a freezer until the protocol for DNA isolation from hair is tested. To test the protocol (obtained from LANL's Bioscience Division), dog hair from a number of individuals will be used. Once the protocol is refined for use on mountain lion and black bear hair, we will begin isolating DNA from samples collected in the field and from live trapping for species identification (if needed). The plotted sample locations will be combined with the DNA analysis to determine distribution and overall population size.

Use of buccal swabs for collection of DNA. In July 2001, we tested a method for collecting buccal cells using cytobrushes to swab the inside of the animal's mouth. DNA is easily isolated by heating the cells to 100°C, which causes the cells to lyse. The buccal swabs yielded a high amount of DNA, so this technique will be added to the sample collection with black bears and mountain lions being trapped. These mouth swabs will be used as positive controls for individual identifications and comparisons to samples collected in the field. In August 2001, project personnel contacted the NMDGF to request that field officers collect mouth swab samples from nuisance bears captured throughout northern New Mexico. As a result, officers have been supplied with 40 kits to collect the swab samples and hair samples.

Primer sets for mountain lion and black bear. All current genetic studies of mountain lions use primer sets found for dinucleotide repeats in the domestic cat. No testing of primer sets for tetranucleotide repeats has been performed. There are many benefits to amplifying tetranucleotide repeats rather than dinucleotide repeats, mainly the ability to distinguish between two different alleles located close to one another. This increases the ability to

identify individuals. So far, 18 tetranucleotide repeats in the domestic cat have been identified. All primer sets for these repeats will be tested with mountain lion samples obtained from Northern Arizona University to determine success in amplifying microsatellites (Fig. 4). Based on the findings from these tests, a primer note will be prepared and submitted to a peer-reviewed journal. Primer sets for black bear have been ordered and will be tested for their success in amplifying microsatellites. By the end of CY01, a set of primers will be selected for the study.

Conclusion and deliverables

The development and application of a noninvasive technique, such as fecal genetic analysis, would be cost-effective and would provide biological data specific to target species. Using fecal and hair analysis, population characteristics such as population size and trends, sex ratios, and distribution patterns could be effectively monitored through time and in relation to large scale perturbations (i.e., wildfire) once sampling and analysis issues have been addressed. Using genetic analysis of hair and scat from within and near the Laboratory could ultimately minimize the number of collars deployed on these species or other invasive techniques to gather similar information. Genetically fingerprinting individuals within populations can also address questions related to reproduction and dispersal patterns of each species. During the first year of this study, we have successfully isolated DNA from animal scat samples using existing protocols, eliminating the need to further develop certain techniques. However, further refinements in sample collection and processing are needed and will be addressed during FY02. Furthermore, sampling efforts will be expanded from LANL property to the adjacent burned areas and other properties to gain more accurate baseline information on carnivore populations in this region.

During FY02, a report will be prepared discussing current techniques for genetic analysis of carnivore scat and hair and limitations for application to the management of these species, an assessment of the necessary refinements and/or improvements to the genetic analysis, and results of sampling efforts. The report will discuss a final evaluation of hair snares to collect quality samples. A primer note discussing the use of tetranucleotide repeats applied to mountain lion samples will be submitted by January 2002.

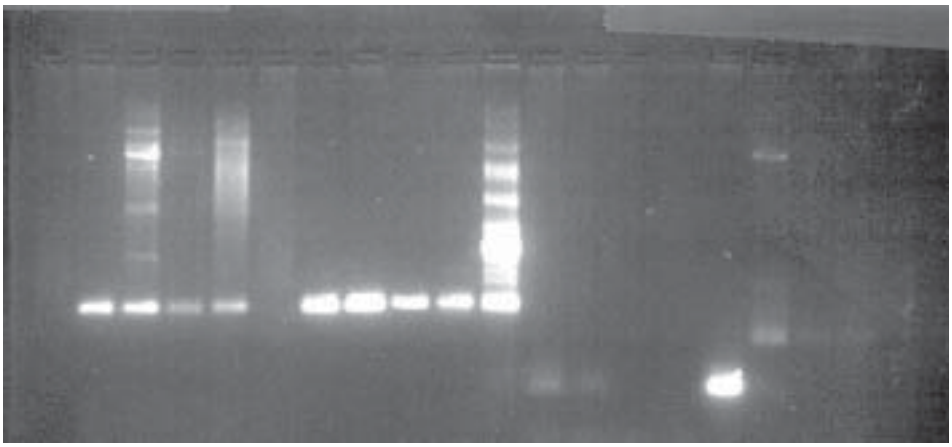

Figure 4. *Picture of primers established for tetranucleotide repeats in the domestic cat, tested with five mountain lion DNA samples. Bands lit up in the gel represent amplified alleles. The allele sizes amplified in the mountain lion samples correspond to allele sizes in the domestic cat.*

References

Biggs, J., K. Bennett, and P.R. Fresquez, "Resource use, activity patterns, and disease analysis of Rocky Mountain elk (*Cervus elaphus nelsoni*) at the Los Alamos National Laboratory," Los Alamos National Laboratory report LA-13536-MS (1999).

Epplen, J.T., "On simple repeated GAT/CA sequences in animal genomes: A critical reappraisal," *Journal of Heredity* **79**: 409–417 (1991).

Ernest, H.B., M.C. Penedo, B.P. May, M. Syvanen, and W.M. Boyce, "Molecular tracking of mountain lions in the Yosemite Valley region in California: genetic analysis using microsatellites and fecal DNA," *Mol. Ecology* **9**(4):433–441 (2000).

Foran, D.R., K.R. Crooks, and S.C. Minta, "Species identification from scat: an unambiguous genetic method," *Wildl. Soc. Bull.* **25**(4):835–839 (1997).

Kohn, M.H., F. Knauer, A. Stoffella, W. Schroder, and S. Paabo, "Conservation genetics of the European brown bear: a study using excremental PCR of nuclear and mitochondrial sequences," *Mol. Ecology* **4**(1):95–103 (1995).

Kohn, M.H. and R.K. Wayne, "Facts from feces revisited," *Trends Ecol. and Evol.* **12**(6):223–227 (1997).

Longmire, J. L., D.C. Hahn, and J.L. Roach, "Low abundance of microsatellite repeats in the genome of the brown-headed cowbird (*Molothrus ater*)," *Journal of Heredity* **90**: 574–578 (1999).

Longmire, J.L., J.L. Roach, M. Maltbie, P.S. White, O.L. Tatum, K.D. Makova, and D.C. Hahn, "Tetranucleotide microsatellite markers for the brown headed cowbird (*Molothrus ater*)," In press: *Journal of Avian Biology*.

Tautz, D., and Renz, M., "Simple sequences are ubiquitous repetitive components of eukariotic genomes," *Nucleic Acids Res.* **12**: 4127–4136 (1984).

Putnam, R., "Facts from feces," *Mammal Rev.* **14**:79–97 (1984).

Quintana, E. and H. Alexander, "The evaluation of techniques to collect hair and scat samples from free-ranging carnivores." Los Alamos National Laboratory report LA-UR-01-3845 (2001).

Reed, J.Z., D.J. Tollit, P.M. Thompson, and W. Amos, "Molecular scatology: the use of molecular genetic analysis to assign species, sex, and individual identity to seal feces," *Mol. Ecology* **6**(3):225–234 (1997).

Weber, J.L. and P.E. May, "Abundant class of human DNA polymorphisms which can be typed using the polymerase chain reaction," *Am. J. of Human Genetics* **44**: 388–396 (1989).

White, P.S., O.L. Tatum, L.L. Deaven, and J.L. Longmire, "New, male-specific microsatellite markers from the human Y chromosome," *Genomics* **57**: 433–437 (1999).

The Effects of Depleted Uranium on Amphibian Health

Principle Investigator: Gilbert J. Gonzales, Ecologist, Contaminant Monitoring Team, Ecology Group (ESH-20)

Coinvestigators: Colleen A. Caldwell, Aquatic Toxicologist, United States Geological Survey, Biological Resources Division and Department of Fishery and Wildlife Sciences, New Mexico State University; Sarah Mitchell, Graduate Research Assistant, New Mexico State University, Department of Fishery and Wildlife Sciences; and William R. Gould, New Mexico State University Experimental Statistics Center

Funding: FY00 $15K; NMSU Cost Share, $30K; Ecology Group (ESH-20), $29K; FY01 $52K; NMSU Cost Share, $30K

Introduction

The Los Alamos National Laboratory (LANL) is located on the Pajarito Plateau on the east side of the Jemez Mountains. The plateau is a series of finger-like mesas transected by a series of canyons, which serve as the primary drainage from LANL. The canyons contain ephemeral, intermittent, and interrupted reaches of streams that feed into the Rio Grande Basin. The Laboratory's Environmental Surveillance Program routinely collects water, soil, vegetation, and biota to evaluate the uptake and distribution of radionuclides within and outside LANL boundaries. Amphibians, which are known to exhibit hypersensitivity to environmental contaminants, are present in some of the canyons that traverse LANL.

Characteristics and Use of Depleted Uranium. Depleted uranium (DU) is the by-product of an enrichment process to increase the percentage of the isotope ^{235}U in natural uranium ore to make it suitable for use as nuclear fuel and in nuclear weapons. Compared to natural uranium, the physical properties of DU have resulted in widespread use in military and civilian applications. These properties include a density of 1.9 g/cm^3 (1.7 times greater than lead) and a pyrophoric or ignitable nature (Eckelmeyer 1990; AEPI 1995). Since the early 1940s, the Department of Energy (DOE) and Department of Defense have tested and used DU in weapons systems and in armor plating of military vehicles (Ebinger et al. 1990; AEPI 1995). Weapons systems containing DU were successfully used during the Gulf War in Operation Desert Shield/Desert Storm, resulting in a renewed interest by other countries throughout the world and the concern for elevated levels of DU in the environment. In their 1994 Summary Report to Congress, the Army Environmental Policy Institute (AEPI) recognized the long-term environmental consequences of using DU on the battlefield and in test ranges. As a result of our limited understanding of its toxicity, the report recommended an evaluation of the environmental fate and effect of DU (AEPI 1995).

Environmental Release, Transport, and Fate of Depleted Uranium. The primary release of DU to the environment occurs when weapon components or munitions are explosively detonated or impacted against a target. Upon impact, DU particles and aerosols are formed and, depending on their size, can spread throughout a large geographic area (AEPI 1995; Becker 1992). Since DU is depleted in isotopes ^{234}U and ^{235}U, it is nearly 40–60% less radioactive than natural uranium. Therefore, the environmental concerns are based on its chemical properties and toxicity rather than its radioactivity. This is also in agreement with the principle that chemical effects of radionuclides on nonhuman biota are greater than the effects of the radioactivity (Whicker and Schultz 1982). Numerous studies at LANL have also implied this (Gonzales et al. 1998, Gonzales et al. 1997, Ferenbaugh et al. 1996). Impact to the environment from DU metal was thought to be low because of the overall low solubility of uranium and because DU metal was alloyed with other heavy metals, such as titanium, that also have a low solubility. However, high temperatures and fire associated with explosion and impact can affect the surface of the DU metal. Over time, exposure to environmental conditions (e.g., photo-oxidation) alters the chemical state of DU increasing its solubility and potential for transport through the environment. The most effective transport of DU in the environment is by aqueous processes associated with erosion, surface runoff, and ground water (Hanson and Miera 1976; Ebinger et al. 1990). The low solubility of alloyed heavy metals has led researchers to consider DU in soil as more of a terrestrial hazard than an aquatic one. However, a study investigating the movement of uranium from firing sites at LANL reported average concentrations in soil runoff and stream sediments of 51.1 μg/g and 42.2 μg/g, respectively (Becker 1992). Soil surveys close to the impact area of an active firing site on LANL showed concentrations of total uranium ranging from 0.8 μg/g to 13,300 μg/g, which was an outlier. Uranium occurs naturally in the Bandelier Tuff at relatively high concentrations (~3.4 μg/g, Fresquez et al. 1994).

Potential Health Effects of Depleted Uranium on Amphibians. Amphibian population declines have been reported throughout the world. The decline appears to be complex and includes factors, such as normal population fluctuations caused by climatological factors, habitat destruction because of urbanization and drainage of wetlands, higher levels of UV radiation, acid precipitation, toxic substances, and increased susceptibility to disease. Amphibians have become an important indicator species of global health as a result of their biphasic life cycle, more frequent contact with soil, sediment, and

water, and permeable skin which exposes the aquatic larvae and terrestrial adults to water-borne and terrestrial-borne toxicants. Reproduction and early life stages are an extremely vulnerable time in the life cycle of amphibians. Environmental toxicants can interfere with embryological development and larval growth by increasing susceptibility of eggs to pathogens and disease, retarding growth and development, and/or inhibiting the larvae's ability to avoid predators (Carey and Bryant 1995). The application of aquatic toxicity tests using amphibians as test models has become an acceptable approach for identifying factors that might be related to their decline. Specialized acute and chronic toxicity tests have been developed, standardized, and adopted to identify the reasons for the worldwide disappearance of amphibians (ASTM 1991).

Previous research on the effects of DU on *Ceriodaphnia dubia* (water flea) has shown significant effects of DU on water flea reproduction at concentrations as low as 3.91 μg/L (Kuhne 2000). Concentration-responses were observed in the number of offspring produced and the adults were reduced in size at greater concentrations. In chronic tests, statistical analysis show significant effects of DU on *C. dubia* survival in concentrations ranging from 14.0 to 63.8 μg/L. Metals of toxicological concern such as Cd and Pb were below concentrations reported to affect reproduction for a similar organism (water flea, *Daphnia magna*) (Eisler 1985; 1988). Metal concentrations in test water indicated that toxicity most likely resulted from uranium with concentrations 14,500 times greater than Pb and 11,724 times greater than Cd.

Benefit. This investigation is designed to increase the ability to meet technical objectives of the Laboratory's environmental health programs (e.g., the Environmental Surveillance Program). More specifically, the short-term goals of this research project will identify (1) health effects of DU from LANL soil on amphibian models and (2) contribute data to aid in the construction of a database, where none currently exist, on the effects of DU in an aquatic animal model. While not every organism nor class of organisms at the Laboratory can be monitored to ensure environmental quality, amphibians constitute a major class of animal that have been proven to be exceptionally sensitive to contaminants (Ulsh et al. 1999). However, before field measurement of contaminant levels in amphibia can be interpreted, dose-response toxicity on a number of measurement endpoints must first be established. This work will establish the toxicity of DU on amphibians. Results may also prove useful in monitoring the effects of the recent Cerro Grande fire.

The long-term benefits of this research project will be the provision of data needed in developing ecological risk assessments for amphibia such as the Jemez Mountains salamander (*Plethodon neomexicanus*), which is endemic only to the Jemez Mountains in north-central New Mexico and listed by New Mexico Department of Game and Fish as endangered. Another long-term benefit is the contribution of information that can be used by regulatory agencies to develop state and national water quality criteria for uranium in amphibia. Currently, fish are the standard aquatic test organisms in developing water quality criteria. However, mounting evidence indicates the embryonic and juvenile stage of amphibians (tadpoles) may be more susceptible to contaminant effects than fish.

Objectives. The objective of the proposed work is to develop DU/amphibian toxicity benchmarks through acute and chronic testing of embryonic development and growth of a standard amphibian model, the South African clawed frog (*Xenopus laevis)* and the western chorus frog (*Pseudacris triseriata*), a species native and common to LANL (Fig. 1). The results from the clawed frog toxicity assays will allow direct comparison with results of toxicity assays using the western chorus frog collected from lands adjacent to LANL. Corollary field studies on the chorus frog will ultimately provide the needed complement to this study.

Methods

Amphibia Collection and Rearing. In April and May of 1999 several aquatic habitat sites in northern and north-central New Mexico were visited and surveyed for chorus frogs. Standing collection by netting was used at a site where chorus frogs were present to capture frogs for transport to New Mexico State University (NMSU) for the development of a captive breeding capability in June 2000.

Test Solutions. A Memorandum of Agreement between the Regents of NMSU and the Regents of the University of California established mutual commitments between the two universities to collect surface soil containing DU from LANL and its delivery to NMSU. Approximately 50 pounds (23 kg) of DU-containing soil was collected, sieved, homogenized, and analyzed for total uranium and 33 additional metals by mass spectrometry at the NMSU Carlsbad Environmental Monitoring and Research Center (CEMRC) in Carlsbad, NM. The purpose of the analyses of the additional constituents is to determine whether the study is confounded by toxicants other than uranium, i.e., whether any observed effects on amphibia are the result of metals other than uranium. The analytical results of the supernatant test water are shown in Table 1.

Figure 1. *Adult chorus frog at the NMSU aquatic toxicology lab. (Photo taken by Gil Gonzales, LANL.)*

Table 1. *Concentration (μg/L) of metals in treatment and control test solutions.*

Medium	Ba	Be	Cd	Cu	Fe	Mg	Mn	Mo	Na	Pb	Sb	Sr	Ti	U	Zn
FETAX Solution[1]	0.7	0.1	0.1	0.8	115	12137	0.2	-0.5	2.5E+05	0.2	-0.1	11.9	16.8	21.4	6.3
Reference Water[2]	518	0.3	0.0	0.4	413	11194	63	1.2	3.2E+04	0.8	-0.1	508	55.6	2.3	21.0
Well Water (negative control)[3]	63	0.1	0.1	0.1	226	10144	8.8	2.5	4.3E+04	-0.7	-0.1	706	38.1	8.7	0.8
Positive Control[4]	0.7	0.1	0.0	2.7	67	11161	-0.4	-0.4	2.5E+05	0.1	-0.1	12.1	17.2	0.3	7.0
100% test water	1283	1.1	10.3	44.7	312	7888	0.3	47.8	3.9E+04	8.5	64.0	464	57.2	5309	13.6
50% test water	612	0.9	5.5	47.5	212	9449	5.1	21.7	1.8E+05	7.5	28.8	216	37.3	2997	15.2
25% test water	295	0.4	1.0	33.8	155	10368	2.8	10.3	2.5E+05	5.5	13.8	113	28.1	1711	14.7
12.5% test water	150	0.5	1.6	20.1	123	10580	1.2	4.8	2.7E+05	3.6	7.1	62	22.6	1342	12.0
Min Detection Level	3.1	0.5	0.5	6.5	150	103	1.1	1	3.8E+02	1.7	1.4	5.1	2.4	0.03	13

[1]The FETAX solution is a balanced nutrient salt solution standard that allows the production of data that are repeatable, reliable, and comparable to other FETAX research results.
[2]Reference water, one of the four control solutions, is water that was aged with soil collected from the reference site outside of LANL and is expected to be relatively free of DU, but also is expected to have natural deposits of the naturally occurring heavy and trace metals.
[3]The negative control consists of well water, which is expected to be relatively free of the metals of toxicological concern and is used in preparation of the test solutions and the reference water.
[4]The positive control consists of 6-aminonicatinamide, which is used as a reference toxicant. With a known EC_{50} for malformation in tadpoles, the target response rate to this control must be achieved for experimental validation.

Acute and Chronic Depleted Uranium Exposures. DU-aged test solutions were prepared from the aging of water with the DU-contaminated soil. Corresponding reference solutions (free of DU contamination) were also produced. The Frog Embryonic Teratogenic Assays-Xenopus (FETAX) acute toxicity tests are being conducted to determine the effects of DU on embryonic amphibian development when, during the developmental stage, unique cellular and molecular processes operate to form a complex multicellular organism. During this stage, the processes are easily perturbed by chemicals. The FETAX acute toxicity assay results in standard endpoints of concentration-response mortality, and malformation curves are generated using probit analysis (Bantle 1995). Embryo death is being measured by the 96-h LC_{50}. Embryo malformation is being measured by 96-h EC_{50}. A teratogenic index (TI) is then calculated as a measure of developmental hazard (TI = 96-h LC_{50}/96-h EC_{50}). This value can then be used to rank toxicants according to their teratogenic hazard. The minimum concentration to inhibit growth is being calculated by measuring body length at the end of the acute toxicity tests.

The chronic toxicity tests will be conducted on both amphibian species beginning at the tadpole stage to determine the effects of DU on hind-limb formation and tail resorption. The effects on hind-limb formation will be evaluated by exposing young larvae to DU-aged water for approximately 21 days. At the end of the test, the rate of development of the hind-limbs and any malformations will be evaluated. The rate of tail resorption will be monitored by exposing 50-day-old tadpoles to DU-aged water (Fort et al. 1999).

Chemical and Statistical Analyses. The acute and chronic toxicity tests will result in two matrices requiring analysis of DU concentrations: test water and whole organisms (embryos and tadpoles) collected before and during the toxicity tests. Total uranium will be analyzed using trace metal analysis at the CEMRC in Carlsbad, NM. The CEMRC is a state-of-the-art facility designed to monitor a wide range of chemicals, including radionuclides. Trace metal analysis at CEMRC meets the U.S. Environmental Protection Agency level-4 requirements where the minimum detection limits are determined as three times the standard deviation of the method blanks. The analyses are conducted with a Perkin–Elmer ELAN-6000 Inductively Coupled Plasma-Mass Spectrometer, allowing for analysis of up to 39 metals with a short turnaround time (2 to 3 weeks).

FETAX will provide information on the developmental toxicity of DU on two amphibian species. Concentration-response data for mortality and growth will be collected and compared with a reference soil. A nonlinear relationship will be observed between concentration and developmental toxicity responses from which a nonlinear model will be employed with the assistance of Dr. William Gould of the NMSU Experimental Statistics Center.

Progress and Results

Collection, Rearing, and Maintenance of Test Amphibians. Breeding adults of the clawed frog have been purchased from commercial suppliers and are currently being grown at the coinvestigator's research facilities at NMSU. The clawed frogs have been put on a breeding rotation and are injected with hormone (human chorionic gonadotropin) every 60 days to maintain the viabilty of the eggs.

In May 2000, approximately 25 chorus frogs were collected and an additional 15 were collected in June of 2001 in the Canjilon area (Fig. 2) (off DOE LANL property) of the Carson National Forest in northern New Mexico. The frogs are currently housed at the co-investigators research facilities at NMSU where they are being studied to develop a captive breeding capability in the laboratory.

Figure 2. *Aquatic habitat in Canjilon area of northern New Mexico where adult chorus frogs were captured.*

Optimal rearing environmental factors (i.e., photoperiod, temperature, humidity) and breeding techniques are being developed and evaluated to induce breeding in a laboratory setting. This information is being used to develop a program for the environmental chamber to simulate natural climatic conditions that will, in turn, induce breeding in the chorus frog.

Experimental Batch Solutions. Experimental DU batch treatment solutions and control soultions were prepared. Table 1 shows the analytical results for 15 metals in treatment and control test solutions. A small subsample was also screened for gross alpha (2 nCi/g), beta (7 nCi/g), and gamma (1.5 nCi/g) radioactivity.

Acute Exposure Pilot and Range Finding Tests. With the use of the human chorionic gonadotropin to induce amplexus, clawed frogs have been successfully bred and used in a series of pilot studies to develop and refine the techniques in the FETAX protocol. Several range finding tests have also been conducted whereby clawed frog larvae have been acutely exposed to DU using DU-aged water.

Acute Toxicity Tests. Three pairs of adult clawed frogs were bred and the eggs were harvested. These eggs were then used in the four-day toxicity tests. Three separate tests were run simultaneously. Each test used eggs from only one pair of frogs. The average percent mortality for the FETAX controls in one of the three tests was above 10%; as a result, that test was eliminated in the summation of the results. Therefore, the results represent an average of the remaining two tests. Test water concentrations ranging from 6.0 to 96.5 μg/L showed no concentration-response for mortality or for malformations (Table 2).

Table 2. *Percent cumulative mortality of Xenopus laevis in a 96-h exposure to test water containing DU.*

Medium	Cumulative Mortality (%)
Control	4
Reference	0
Positive Control	100
Test Solution (% Dilution)	
6.25	0
12.50	0
25.00	8
50.00	2
100.00	2

Chronic toxicity tests. Pilot studies for the 21-day hind limb formation test have been conducted. Early results indicated a problem with the rate of development in all the tadpoles, including the controls. Further tests are being conducted to determine the role of food, control water (FETAX solution), and amount of test water.

References

AEPI (Army Environmental Policy Institute), "Health and environmental consequences of depleted uranium use in the U.S. Army: technical report," Georgia Institute of Technology, Atlanta, GA (1995).

ASTM (American Society for Testing and Materials), "Standard guide for conducting embryo teratogenesis assay-Xenopus (FETAX), E 1439-91, Philadelphia, PA 825–835 (1991).

Bantle, J.A., "FETAX- A developmental toxicity assay using frog embryos," in *Fundamentals of Aquatic Toxicology: Effects, Environmental Fate, and Risk Assessment*, G.M. Rand (editor), Taylor and Francis Publishers, Washington, DC, 207–230 (1995).

Becker, N.M., "Quantification of uranium transport away from firing sites at Los Alamos National Laboratory— A mass balance approach," in *Proceedings of the Symposium on Waste Management: Technology and Programs for Radioactive Waste Management and Environmental Restoration*, E.G. Post (Editor), March 1–5, 1992; Tucson, AZ (1992).

Carey, C. and C.J. Bryant, "Possible interrelations among environmental toxicants, amphibian development, and decline of amphibain populations," *Environmental Health Perspectives*, Vol. 103 Supplement 4, 13–17 (1995).

Ebinger, M.H, E.H. Essington, E.S. Gladney, B.D. Newman, and C.L. Reynolds, "Long-term fate of depleted uranium at Aberdeen and Yuma proving grounds," Los Alamos National Laboratory report LA-11790-MS (1990).

Eckelmeyer, K.H, "Uranium and uranium alloys," in *ASM International Handbook Committee, Metals Handbook, Vol. 2. Properties and Selection, Nonferrous Alloys and Special Purpose Materials*, American Society of Metals, International Materials Park, OH, 670–681 (1990).

Eisler, R., "Cadmium hazards to fish, wildlife, and invertebrates: A synoptic review," U.S. Fish and Wildlife Service, Contaminant Hazard Reviews Report No. 2, Biological Report No. 85 (1.2) (1985).

Eisler, R., "Lead hazards to fish, wildlife, and invertebrates: A synoptic review," U.S. Fish and Wildlife Service, Contaminant Hazard Reviews Report No. 14, Biological Report No. 85 (1.14) (1988).

Ferenbaugh R., O. Meyers, M. Ebinger, A. Gallegos, and D. Breshears, "Ecological risk assessment approach for Los Alamos National Laboratory," Los Alamos National Laboratory report LA-UR-96-766 (1996).

Fort, D.J., T.L. Propst, E.L. Stover, J.C. Helgen, R.B. Levey, K. Gallagher, and J.G. Burkhart, "Effects of pond water, sediment, and sediment extracts from Minnesota and Vermont, USA, on early development and metamorphosis of Xenopus," *Environmental Toxicology and Chemistry* 18:2305–2315 (1999).

Fresquez, P., D.R. Armstrong, and J.G. Salazar, "Radionuclide concentrations in game and non-game fish upstream and downstream of Los Alamos National Laboratory: 1981 to 1993," Los Alamos National Laboratory report LA-12818-MS (1994).

Gallegos, A.F., G.J. Gonzales, K.D. Bennett, L.E. Pratt, and D.S. Cram, "A spatially-dynamic preliminary risk assessment of the American peregrine falcon at the Los Alamos National Laboratory," Los Alamos National Laboratory report LA-13321-MS (1997).

Gonzales G.J., A.F. Gallegos, M.A. Mullen, K.D. Bennett, and T.S. Foxx, "Preliminary risk assessment of the southwestern willow flycatcher (*Empidonax traillii extimus*) at the Los Alamos National Laboratory," Los Alamos National Laboratory report LA-13508-MS (1998).

Hanson, W.C. and F.R. Miera, Jr., "Long-term ecological effects of exposure to uranium," Los Alamos Scientific Laboratory report LA-6269-MS (1976).

Kuhne, W.W., "Effects of depleted uranium on the survival and health of *Ceriadaphnia dubia* and *Hyalella azteca*," Master of Science Thesis, New Mexico State University (2000).

Ulsh, B., M. Muhlman-Diaz, F.W. Whicker, J. Bedford, T. Hinton, and J. Congdon. 1999. Reptilian and amphibian evaluation methods. Proceedings of the Wildlife Applications to Remediation Decision-Making Conference, 17–19 Aug., Denver, CO.

Whicker, W.F., and V. Schultz. 1982. *Radioecology: Nuclear Energy and the Environment*, CRC Press, Inc., Boca Raton, FL.

Modification of the Los Alamos/Canberra Environmental Continuous Air Monitor (ECAM) Inlet for Enhanced Performance by Removal of Fine Particles

Principle Investigator: John C. Rodgers (ESH-4)

Collaborators: Suilou Huang, Atmospheric Radioactivity Group, New Mexico Institute of Mining and Technology, Socorro, New Mexico

Funding: FY01, $15K plus $8K supplemental ($23K).

Introduction

In the post-fire assessments and discussions of the Cerro Grande fire, a number of challenging questions have been raised in regard to the sources and radionuclide identities associated with gross-alpha and gross-beta activity in the smoke plumes. One particular concern is that apparently Los Alamos National Laboratory (LANL, the Laboratory) had no way to rapidly monitor the smoke plumes generated on-site to determine if there were significant quantities of man-made alpha-emitting radionuclides being released into the air. Although there were good grounds for believing that the increased alpha activity in the smoke from this fire was derived from naturally occurring radon progeny, especially ^{210}Po, released from burning vegetation and forest floor litter (M.F. LeCloarec et al 1995; Nho et. al. 1996), it was difficult to quickly confirm this because of sample size and analysis requirements.

Generally, in the absence of fire conditions on-site, it is advantageous to be able to continuously monitor for alpha-emitting radionuclides under ambient conditions with sufficient sensitivity to address worker safety concerns. Such monitoring would require a continuous air-monitoring instrument with a high-volumetric sampling rate to quickly acquire a detectable quantity of alpha radionuclides from elevated concentrations in the air, but also an accurate means for correcting the gross alpha count for the interference effects of radon progeny collected in the sample. The alpha energy of certain of the radon progeny is close to the emission energy of plutonium and americium, and thus activity in their low-energy tails overlap with the energy levels of these transuranics, creating interference (e.g., $^{239}Pu_a$ = 5.15 MeV, $^{241}Am_a$ = 5.49 MeV, $^{218}Po_a$ = 6.0 MeV, $^{214}Po_a$ = 7.69 MeV).

The short-lived radon progeny occur in the air at levels in the range of tenths of pCi/l, depending on time of day, conditions of the atmosphere, and other factors. At these concentrations, backgrounds of natural alpha emitters create serious interference with the detection of levels of man-made alpha emitters, which would be of concern. These interference effects can be partially corrected by alpha spectroscopy-based spectral analysis and removal of overlapping sources of counts. By a combined process of such background correction to reduce the degree of interference, and increased sampling rate to accumulate larger quantities of particulate radionuclides of concern, real-time monitoring can offer useful ambient monitoring results in applications on-site.

Concept Over the past several years, the Laboratory has developed (and an industrial partner, Canberra Industries, has commercialized) an environmental continuous air monitor for alpha-emitting radionuclides (alpha-ECAM). ECAM has special environmental inlet and weather-tight enclosure, capable of higher sampling rates (over 3 CFM), and incorporating alpha-spectroscopy based background interference correction algorithms.

The instrument was designed to provide accident-response air monitoring for responder protection in the vicinity of spills or accidents to which the Accident Response Group (ARG) might be called. The design of the ECAM inlet and the sampling train are such that attained levels of sensitivity and periods of sampling without filter change are suitable for the worker protection mission in most conditions. However, were the sampling rate through this inlet to be simply increased (tripled or quadrupled) in an attempt to increase sensitivity, quantities of radon progeny collected would correspondingly increase, along with the rate of dust loading and rapidity of filter clogging leading to frequent filter changes. Clogging would be made worse by the presence of smoke in the air.

As shown in Figure 1, wood smoke rapidly clogs CAM filters. At an initial sampling rate of about 3 CFM, the filter clogs in about 30 minutes. At 10 CFM, the time to failure would be even shorter. Smoke particles generated by burning wood are generally in the 0.01 μm – 1.0 μm size range. Both theoretical and experimental studies indicate this is the size responsible for the most rapid clogging of filters (Brown 1993). The particle size associations of the radon progeny in the environment are also small: George (1972) found that the activity median aerodynamic diameter (AMAD) of radon progeny in rural outdoor air is approximately 0.3 μm. In contrast, in a survey of published measurements of the AMAD of environmental samples of radioactive particulates (Dorian 1997) found that while fallout aerosols and natural radioactive aerosols are found in a size mode about 1 μm, for the case of resuspended man-made radionuclide aerosols in the environment, an AMAD of about 6 μm was reported. There is, then, an opportunity to address the problem of interference and clogging by size-selective sampling. If the fine component

(D_p < 1 μm) of a polydisperse environmental particulate aerosol could be reasonably efficiently separated from the large components in the inlet stage of an ECAM, before filtration, while the larger particle components are captured, then it would be possible to greatly increase the sampling rate (and thereby the sample size of the transuranics). The increased sampling rate would not fully incur the penalties of increased collection of radon progeny that interfere with alpha detection of transuranics, and increased filter loading by fine particles that contribute most to rapid clogging. While clogging could eventually occur (complete separation is not practical), it would be at a much lower rate than would be expected at the elevated sampling rate of, say, 10 CFM.

Objectives The objective of the project is to design a modified inlet for the ECAM that would achieve just such a separation and support much higher sampling rates. The technique under investigation is an application of size selective sampling using a virtual impactor to achieve separation.

In virtual impactor sampler design, particle laden air passing into the inlet is first accelerated through a jet forming *accelerator* nozzle.The jet of air impacts into a co-axially aligned *receiver* nozzle of slightly larger diameter. Flow drawn into the receiver nozzle is at a rate typically 1/10th or less of the accelerator jet flow. As a result, the slowly moving air of the receiver nozzle acts as a 'virtual' surface. The surface abruptly deflects most of the sampled air away from and around the receiver, where it is collected and discharged as the *major flow* component of the sample. Larger size particles, due to their inertia, cross the deflected streamlines, go into the receiver nozzle, and are carried to the sample filter in the *minor flow*.

A schematic cross section drawing of how a virtual impactor stage acts to separate small and large particles is shown in Figure 2. With proper design, it should be possible to construct a virtual impactor-separator having a sharp D_{50} cut-point diameter (that particle diameter at which 50% of the particles are collected in the major flow and 50% in the minor flow). The results of the first year's studies of this concept have generally confirmed the expectation that the goal of efficient separation of components of the sample can be achieved. Results have also shown that scaling from single nozzle configurations to multinozzle, high-sampling rate systems is challenging and requires careful design and meticulous construction for success.

Impact Success with the design of a modified alpha-ECAM inlet capable of operation at sampling rates 3 or 4 times the rate of a laboratory CAM, with comparable increases in sensitivity, could help address public concerns about Laboratory capabilities for rapidly determining if large concentrations of man-made alpha-emitting radionuclides are present in ambient smoke or dust generated on site. Even discussions about possibly including the present ARG alpha-ECAM in the Laboratory air surveillance network has been favorably received by the community press (Snodgrass 2001). While ECAM deployment will never achieve the level of sensitivity required for perimeter monitoring, it could play a supporting role in the Laboratory and University of California (UC) efforts to provide continuing community feedback on incidents that might be perceived to have public impacts. Furthermore, if improved performance of the ARG ECAM could be

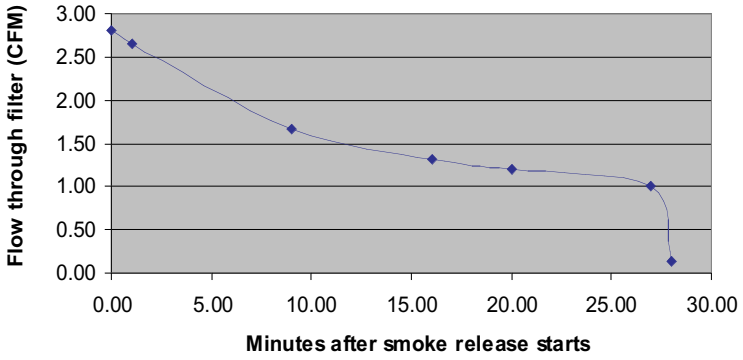

Figure 1. *Effects of wood smoke on the sample flow rate through an ECAM filter: Flow rate (CFM), is plotted over time from the beginning of smoke release. Decline in flow is a near-exponential function of the mass of small particles collected.*

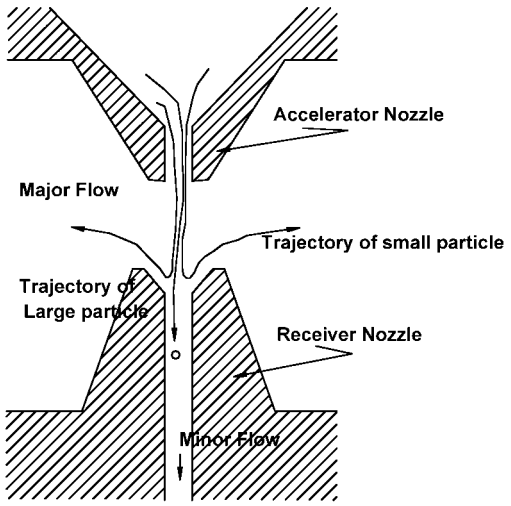

Figure 2. *Schematic cross section of a virtual impactor. A high-velocity jet air is formed in the accelerator nozzle directed at the receiver nozzle of slightly larger diameter. Small particle trajectories are shown first entering and then exiting the receiver nozzle in deflected major flow. The large particle trajectories continue down into the receiver nozzle and are transported to a sample filter in the minor flow.*

achieved, Laboratory emergency responders could be provided with enhanced real-time air monitoring of ambient conditions if they are called out where suspect emissions are occurring. This would help managers track exposure conditions and assure that appropriate levels of personal protective equipment (PPE) are being used.

Methods

Our approach to the development of a suitable virtual impactor separator stage as a modification to the ECAM inlet has included both theoretical and experimental aspects. An initial design effort was based on predictive equations reported in the technical literature that are expected to result in successful designs (Marple and Chein 1980, Marple et.al. 1993, Loo and Cork 1988), and recent design enhancements reported by Kim and Lee. The experimental studies began with an evaluation of a test-bed single nozzle virtual impactor design with a predicted D_{50} cut-point diameter of 2.5 μm. As shown in Figure 3., this test unit consists of a single accelerator jet nozzle positioned in the body section opposite the receiver nozzle. The unit is designed for easy disassembly for study. Size-separation efficiency tests were conducted in the Atmospheric Radioactivity Laboratory at New Mexico Institute of Mining and Technology (NMIMT) using a technique developed for CAM studies that involve the labeling of inert test particles with high enough levels of radon progeny to allow measurement by alpha-counting.

Figure 4 illustrates the radon progeny labeling step. The radon progeny are injected in an air stream flowing over the particles spread on a filter and are deposited on the particles by electrostatic deposition induced by a high-voltage field. (Huang et al. 2001) The labeled aerosols are then dispersed in a mixing chamber and applied to the test instrument via a transport line (Figure 5) Filters collected from the instrument and reference samplers are then simultaneously counted in an alpha-counter array (Figure. 6). To test particle size selective sampling efficiencies, mixtures of radon-progeny labeled smoke particles and particles of iron oxide (0.3–0.8 μm), glass bead particles (3.0–10.0 μm), or gold particles (5.0 μm), representing the large diameter target species were prepared. These mixtures were sampled from the mixing chamber through the test virtual impactor, and later, through a multinozzle impactor array in a modified ECAM inlet. In the test unit, separate pumps were used to establish the major flow at 1.45 CFM, shunting aside most of the small particles in the sample, and to establish the minor flow of 0.15 CFM (i.e., 10:1 ratio) through the receiver

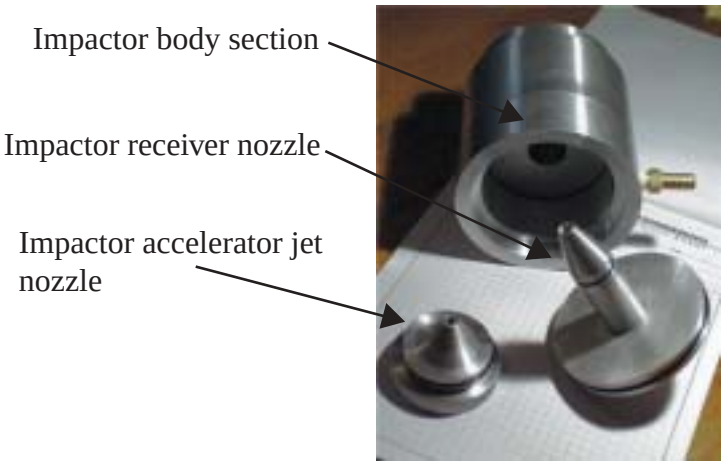

Figure 3. *The test-bed virtual impactor system: a single nozzle accelerator and receiver setup. The major flow is extracted through the hose barb on the right side of the body section. The minor flow is withdrawn from the base of the receiver nozzle (bottm right), shown still attached to the base manifold. Flow into this virtual impactor feeds into the accelerator nozzle (left), which mounts through a top manifold plate (not shown here) on the top of the body section.*

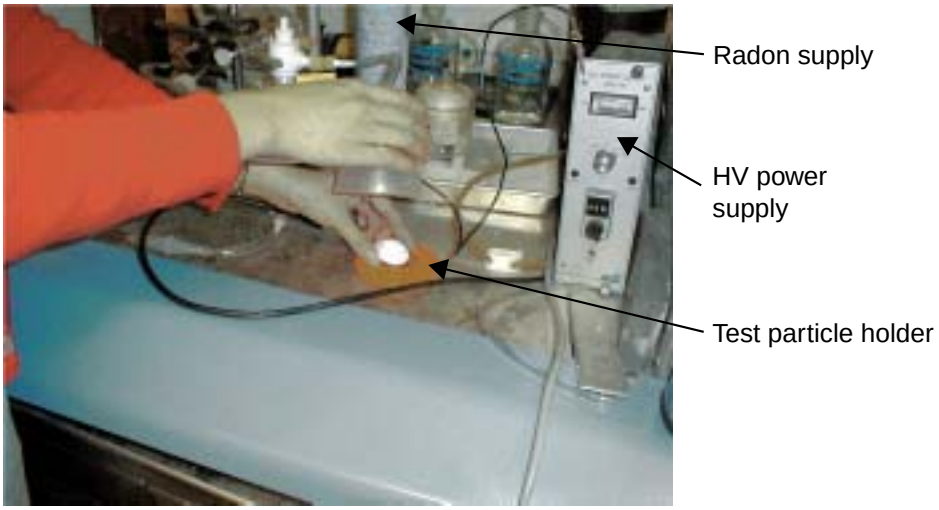

Figure 4. *Labeling test particles with radon progeny: Test particles are mounted on a filter and exposed to radon progeny in a small chamber where a high-voltage field is applied, causing electrostatic deposition onto the particles.*

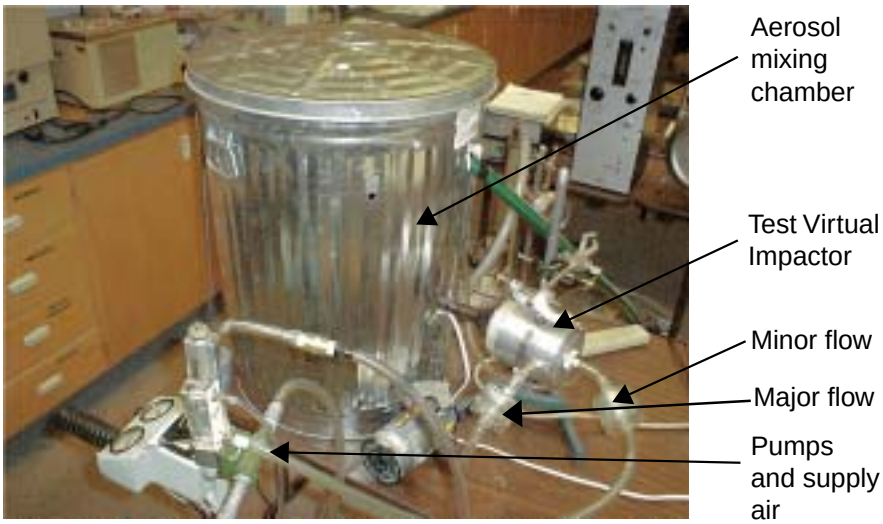

Figure 5. *Mixing chamber and test fixtures: Particles labeled with radon progeny are introduced into a large volume of air in the mixing chamber. The aerosol is drawn into the test virtual impactor (bottom right) through the accelerator. Flow then splits, with the major flow (1.45 CFM) drawn off with a separate pump. The minor flow (0.15 CFM) is extracted out of the base of the receiver. Filter cartriges in these separate flows collect radioactive labeled particles for later counting.*

Figure 6. *Multiple alpha detector and scalar array: The sample and reference filters containing radon-progeny labeled particles collected in tests of the virtual impactor are simultaneously counted in an array of ZnS(Ag) alpha-scintillation detector/scalar counters.*

nozzle to capture the separated large particles along with a portion of the small particles.

Progress and Results

Test Virtual Impactor. Studies with the test-bed impactor demonstrated that the predicted cut-point based on accelerator nozzle diameter was approximately reached (observed D_{50} ~ 2.8 μm). See Figure 7. Tests with the gold particles showed that 94% of these particles followed the minor flow path as predicted. However, internal losses on the receiver tip and other surfaces proved to be larger than expected. Literature values for expected losses range from less than 1% to over 40% depending on design, particle size, and other factors. We anticipated that losses could be held to about 20%. Experimentally, losses were found to be as much as 39% instead. At the same time, there was nearly 6 times the amount of the large particles collected on the impactor filter as collected by a reference sample filter having the same flow rate. This fact demonstrates the enormous potential for large particle enrichment in the low flow (here, 0.15 CFM) stream of a virtual impactor operating at considerably higher total flow rate (here, 1.6 CFM).

The large internal deposition observed prompted a trial of a modified receiver design based on the work of Kim and Lee. In their work, the entrance section (they call it a “flow guide” section) is flared out at a 30º angle, and the bore through the center expands from 0.64 cm near the tip into a larger diameter 0.94 cm bore through the rest of the receiver. We constructed a test receiver based on this design, as shown in the photograph, Figure 8a. The base of the new test receiver was designed with a threaded section so that the gap space between the accelerator and receiver could be adjusted in tests to determine if this were a critical design factor. A repeat of labeled particle tests with the modified receiver design showed that although the D_{50} cut-point was shifted down (to 2 μm), the interstage losses were at least as large or larger, so that the cut point is not as sharply defined. At this point in the study

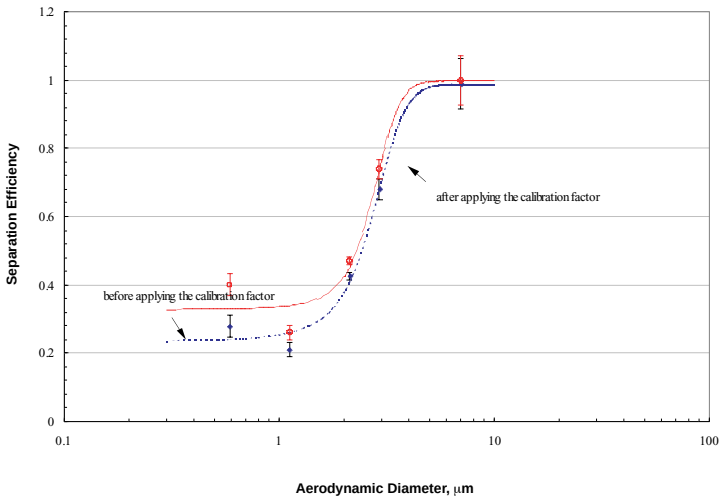

Figure 7. *Speration efficiency as a function of particle size in the test unit: It is defined as the ratio of radioactivity in the minor flow to the sum radioactivity of the minor flows. The error bars are the measurement uncertainties. Also shown is a fitting line of an exponential function. The cutoff aerodynamic diameter for the virtual impactor is 2.8 mm. The fraction of fine particles being captured along with the large particle flow is only approximately 20%, while the large particle fraction is nearly quantitative.*

(a)

(b)

Figure 8. *Modified receiver nozzle design: A receiver nozzle with the "flow guide" modification is shown mounted in the test-bed virtual impactor (a). The accelerator and receiver bore diameters were not adjusted in this stage of the design. A 5-nozzle array of these receivers was designed for a full-scale test in a prototype ECAM.*
The design (b) has as circular array of receivers mounted between two manifold plates defining a volume that accumulates the major flow passing from the top plate through small holes shown. The major flow is drawn into a plenum and discharges by the major flow pump. The minor flow exits through the bore of the receivers and passes down through the CAM head to the sample collection filter at the base.

we decided, based on time constraints for design, construction, and testing of a high-volume configuration, to proceed with the modified receiver design and apply it to a multinozzle design mounted in a test ECAM capable of larger total sampling rates, as shown in the CAD drawing of Figure 8b.

Multinozzle ECAM inlet Each element of the multinozzle array of 5 virtual impactors was designed to be about equivalent to the single nozzle design, with a total flow of approximately 11.1 CFM , composed of a major flow of 8.6 CFM and a minor flow of 1.09 CFM, together with a reference sample flow extracted out of the major flow of 1.41 CFM. A second reference sample of the total flow contents was obtained from the feed line between the mixing chamber and the test ECAM. The 5 elements, in a circular array, were designed to retrofit into the inlet section of a prototype ECAM design that had been previously built for test and evaluation in the LANL /Canberra ECAM CRADA (Figure 9a). A characteristic of the prototype design that made this possible is a space between the outer case and an inner wall surrounding the CAM head component that could be isolated by sealing rings to create a major flow manifold, as seen the photograph of the completed modification (Figure 9b). The minor flow path from the outlets of the receivers (Figure 9c) remains the same as the normal ECAM through the CAM head to the filter cartridge in the base. The sealing rings can be seen top and bottom (9b), and also ports on the sidewall through which the major flow is drawn. The top closure and inlet tube to the monitor has been removed for these views. The results of preliminary tests with the multinozzle array indicate that the D_{50} cut-point shifted back up to about 2.8 μm, which is not unacceptable for a test unit. But the internal losses actually became worse for the larger particle sizes, approaching nearly all the particles at 10 μm. Clearly, in the confined space available in the existing prototype ECAM, the potential for unwanted flow impingements has gone up. A similar increased percentage loss of large particles when scaling up from a single

nozzle to a multiple nozzle, high-volume virtual impactor array was reported by Yule (1978) in his design of a virtual impactor for alpha-air monitoring. A critical design issue is that the accelerator nozzle dimensionless Reynolds number (a function of jet diameter and velocity), at a flow rate of 1.72 CFM, is in excess of 14,000, which puts it outside many design recommendations for impactors (Re = 3,000 – 10,000), but approximately the same as the Yule design. One effect of such high-jet velocities is greater turbulence and less penetration of the jet flow into the receiver nozzle tip, with potentially greater large particle losses in this critical region. In FY02, further testing is planned using liquid particles and a fluorescent tracer to allow wiping of surfaces to recover deposited particles. Recovery and counting of deposition losses could not be done with the radioactive labels. Pinpointing the sites of major deposition losses will allow the redesign of the accelerator/receiver system to achieve better transport efficiency. An entirely new design approach will be taken in developing a second generation high-volume virtual impactor, one that will increase the effective area of accelerator nozzle and bring down the jet velocity and Reynolds number of the flow.

Conclusions and Deliverables

The investigations to date have shown that the use of a virtual impactor stage in the inlet of an ECAM has considerable potential for allowing sampling rates to be increased significantly while at the same time, by removal of most of the fine particles and radon progeny and retaining the larger particle mode, radon progeny background is kept low, and early clogging of the filter is prevented. One issue, which emerged from the first attempt at designing a high-volume, multinozzle virtual impactor array, is that within the geometrical confines of an ECAM inlet, there are possibly turbulent interactions between flows from adjacent nozzles and between flows and the side walls of the ECAM, leading to additional patterns of loss. The design and placement of multiple accelerator and receiver nozzles needs further investigation to determine major sites of deposition and to develop alternative designs. Another concern is the high velocities generated in the accelerator nozzles of the present design contribute to larger deposition losses on the receivers. We are pursuing an alternative design, which would allow for a larger jet forming accelerator, and better placement in the ECAM inlet in the continuing investigations. Among the deliverables of the first year are the following:

1) the application of radon progeny labeling of solid test particles to virtual impactor testing;
2) the design, construction, and testing of a single nozzle virtual impactor utilizing both the standard receiver nozzle and the Kim and Lee “flow guide” concept, and

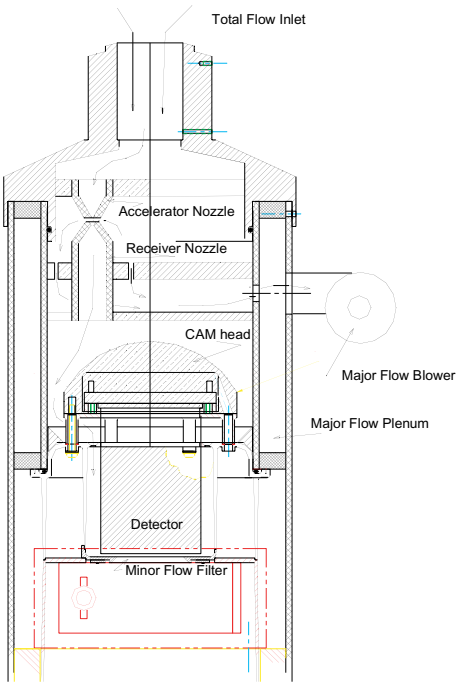

(a)

(b)

(c)

Figure 9. *Cross section drawing and photos of modified prototype ECAM: A 5-nozzle array of virtual impactors fitted to the inlet section of a Los Alamos/Canberra protorype alpha-ECAM is shown in cross section (a). Minor flow out of the receiver nozzles passes over the top of the enclosed preamp/detector chassis and down to the sample filter. A major flow plenum is created between the inner and outer walls of the ECAM body. The top and outer case have been removed in photo (b) to show the accelerators and major flow plenum. The receiver array is shown in photo (c). A portion of the inner CAM head can be seen in (b) with the filter-cartridge drawer open.*

3.) the design, construction, and testing of a full scale, 5-nozzle, retrofit virtual impactor in the inlet of a prototype ECAM.

References:

Le Cloarec, M.F., Ardouin, B., Cachier, H., Liousse, C., Neveu, S., and Nho, E.Y. (1995) ^{210}Po in savanna burning plumes. *J. Atmos. Chem.* 22, 111-122.

Nho, E.Y., Ardouin, B., LeCloarec, M.F., and Ramonet, M. Origins of ^{210}Po in the atmosphere at Lamto, Ivory Coast: biomass burning and Saharan dusts. (1996) *Atmos. Environment* **30:22** 3705-3714.

Brown, R.C. (1993) Air Filtration, Pergamon Press, Oxford.

George, A.C. (1972) Indoor and Outdoor Measurements of Natural Radon and Radon Decay Products in New York City Air. In: The Natural Radiation Environment II, J.A.S. Adams, W. M. Lowder, and T.E. Gesell, Eds., CONF-720805, 741-750. NTIS, Springfield, VA.

Dorian, M.D. (1997) Particle size distributions of radioactive aerosols in the environment. *Rad. Prot. Dosimetry* 69:2 117-132.

Snodgrass, R. (2001) "New Technology Available for Air Monitoring: Rise in Depleted Uranium Counts Not Considered Worrisome". *Los Alamos Monitor* (newspaper), August 24.

Marple, V.A., and Chien, C.M., "Virtual impactors: A theoretical study," *Environ. Sci. and Technology* 14:8 976 –985 (1980).

Marple, V.A., Rubow, K.I., and Olsen, B.A., "Inertial, Gravitational, Centrifugal, and Thermal Collection Techniques," Aerosol Measurement, K. Willeke and P.A. Baron, Eds., Van Nostrand Reinhold, New York (1993).

Loo, B.W., and Cork, C.P., "Development of high efficiency virtual impactors. *Aero. Sci. and Technology* **9**: 167–176 (1988).

Huang, S., Schery, S.D., Alcantara, R. E., Dale, N. V., and Rodgers, J.C., "Micrometer-sized short-lived radioactive aerosol particles for convenient use in laboratory measurements," *Health Physics (in press, submitted April 2001*); LA-UR-01-5464.

Kim, M.C., and Lee, K.W, "Design modifications of virtual impactor for enhancing particle concentration performance," *Aero. Sci. and Tech.* **32:3** 233–242 (2000).

Yule, T., "An on-line monitor for alpha-emitting aerosols," *IEEE Trans. Nucl. Sci.* NS-**25:1** 762-766 (1978).

Wildfire Effects on Contaminant Transport through Wind Erosion

Principle Investigator: Jeff J. Whicker (ESH-4)

Coinvestigators: John Rodgers (ESH-4), John Pinder, Colorado State University, F. Ward Whicker, Colorado State University, David D. Breshears (EES-10), and Craig Eberhart (ESH-17)

Funding: FY01, $39K

Additional Funding: FY01, $50K for resuspension measurements at Area-G
$25K for preliminary pathway study at Yucca Mountain

Summary

Redistribution of soil, nutrients, and contaminants is often driven by wind erosion, and is especially pronounced during episodic high-velocity winds. In addition, vegetation cover, which moderates wind erosion, can be reduced rapidly and dramatically by wildfire. However, few studies have evaluated key spatial and temporal aspects of wind erosion with respect to: 1) wind erosion rates on burned forest sites compared to unburned forest sites; 2) erosion rates as related to canopy and ground cover as well as episodic high-velocity winds; and 3) quantified resuspension rates for contaminated soils in burned forest areas. For this study, measurements of vertical and horizontal soil flux, forest canopy cover, ground cover, and key meteorological metrics, are being made in unburned, severely burned, and moderately burned areas at Los Alamos National Laboratory (LANL). Combined, the preliminary data suggest that 1) wind erosion rates at LANL have been significantly increased by Cerro Grande fire, 2) dust concentrations show considerable temporal variation and appear to be strongly correlated to episodic high-velocity winds, and 3) distributions of weekly vertical soil flux can be applied to estimate the mean and associated variation in resuspension rates for contaminants of interest from LANL sites.

Introduction

Wind erosion suspends soil particles and any associated contaminants from surfaces and lifts them into the atmosphere, which can result in long-distance transport and, thus, have the potential to impact human and ecological health. The resuspended particulate can impact human and ecological health through 1) direct inhalation of contaminated soil and 2) deposition onto lands where contaminants may ultimately enter food pathways. Therefore, understanding wind-driven resuspension of contaminated soils at LANL is critically important for predicting the human and ecological risk presented by such contaminated sites. In addition, the ability to accurately predict wind resuspension under possible extreme conditions, such as those created by wildfires or other major disturbances, is necessary for managing environmental restoration activities and for long-term stewardship of Department of Energy (DOE) lands.

Rates of wind erosion fundamentally depend on the characteristics of wind and vegetation cover in a complex fashion (Bagnold 1941). For example, Fryrear (1985) showed that wind erosion rates increased exponentially with loss in vegetation. Further, wind-erosion shows a threshold type response to wind velocities (Gillette et al. 1980). That is, there is essentially little erosion until the wind velocity exceeds the threshold velocity, but above this threshold wind-erosion rates increase dramatically as a power function of velocity (Woodruff and Siddoway, 1965; Anspaugh et al. 1975). Importantly, this threshold velocity can be significantly lowered by loss of vegetation, e.g., from wildfire, and by disturbances to soil cover, e.g., from vehicles, (Gillette et al. 1980; Belnap and Gillette 1998). Also, the affected areas can be slow to recover (Okin et al. 2001). Moreover, because of these highly nonlinear relationships, wind erosion may occur primarily during episodic high-wind events (Cahill et al. 1996; Goossens and Offer, 1997; Stout, 2001). Therefore, the loss of vegetation from the fire, or from other disturbances such as vehicle traffic across the landscape, could dramatically increase wind erosion and resuspension of contaminated soil, especially during high-wind events. However, there are few relevant studies that have evaluated the long-term effects of fire or other disturbances on episodic wind erosion, and how erosion rates might change as the forest recovers.

Given the dramatic removal of vegetation resulting from the Cerro Grande fire, it is possible that there will be significant increases in transport rates and concentrations of contaminated soils to offsite locations. The Cerro Grande fire burned over significant portions of LANL property (Figure 1), and these areas contained many sites with possible soil contamination (potential release sites [PRS]). The rapid removal of vegetation by fire has been shown to result in increased water and wind erosion at other DOE semiarid sites (Johansen et al. 2001a; Johnson et al. 2000; Whicker et al. 2002). At LANL, Johansen et al. (2001b) found water erosion rates for plots burned by the Cerro Grande fire were an order-of-magnitude greater than unburned plots. Despite the critical role fire could have on wind erosion and contaminant transport, there have been only a couple of studies of the effects of fire on wind erosion. Moreover, these studies have been focused on ecosystems that are very different from that found at LANL. Zobeck et al. (1989) studied the effects of fire on wind erosion in Texas rangeland, and Whicker et al. (2002) studied fire effects in shrublands in southern New Mexico. Both studies

showed that fire, through its effects on vegetation, significantly increased wind erosion; however, extrapolating the quantitative results of these studies to LANL may underestimate effects because the mass and vertical structure of the forest vegetation is greater than that in rangeland and shrubland. It is important to consider the possible moderating effect of the extensive remediation done on LANL burned areas on wind erosion, but the level of effectiveness of these efforts to stabilize the soil remains unknown. It is also important to remember that these remediation efforts were 1) generally designed to reduce water erosion and are not necessarily effective for wind erosion, and 2) these remediation efforts were designed to reduce and not prevent erosion. Thus, understanding and quantifying the effects of the Cerro Grande fire and follow-up remediation efforts on wind erosion is essential for accurate human and ecological risk assessment, which are required for long-term stewardship of DOE owned lands.

Objectives. Because fire may affect wind resuspension in LANL ecosystems by 1) removing tree canopies, thus increasing wind velocities at the ground surface and 2) removing ground vegetation and litter cover, thus exposing the soil particles (i.e., reducing wind-erosion thresholds), studies are being performed at three levels of burn effects. These are: 1) severely burned areas where most of the trees were killed and almost all of the needle and ground litter was consumed by the fire, 2) moderately burned areas where the fire was confined largely to the ground vegetation and litter cover and the damage to the canopy was primarily the scorching of needles on the lower branches, and 3) unburned areas where there was no evidence of fire effects. The general objective of this project is to investigate resuspension of soils as affected by these different types of effects from the Cerro Grande fire.

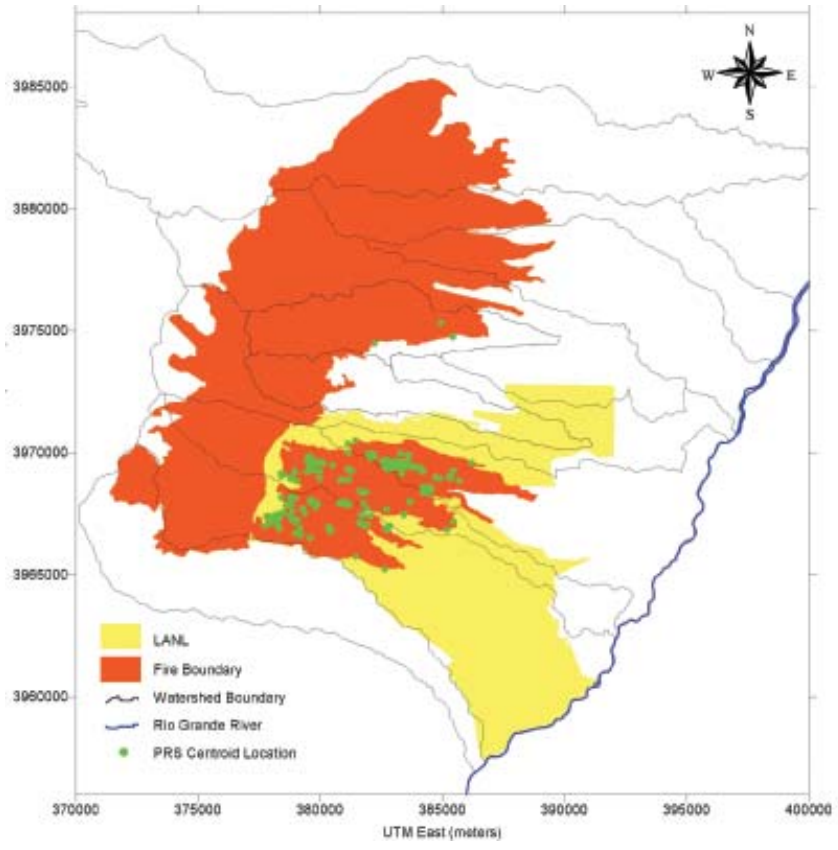

Figure 1. *Outline of Cerro Grande fire (in orange) across the LANL site (in yellow) with potential release sites (in green).*

Specifically, we: 1) measure and compare wind erosion at replicate sites in areas that were severely burned, moderately burned, and unburned; 2) relate wind erosion (by particle size for some measurements) to locally measured parameters of meteorology, vegetation, and soil conditions in these burned and unburned areas; and 3) quantify resuspension rates, especially during periods of extreme wind events, to obtain more accurate prediction of human risk. This report covers progress for the first of a three-year proposed project.

Methods

Effects of fire on soil resuspension. For this study, two replicate sites, termed primary and secondary sites, were selected for each burn type. Sampling and data collection are being performed at both primary and secondary sites in severely burned, moderately burned, and unburned areas (Figure 2). To quantify wind-erosion rates in the different burned and unburned sites, we are using numerous Big Springs Number Eight (BSNE) samplers. These BSNE field dust collectors (Figure 3) have been extensively tested and show good sampling efficiency for soils with higher fractions of sand and silt (Fryrear 1986; Goossens and Offer 2000) such as those which are abundant at LANL (Nyhan et al. 1978). These samplers are passive collectors of airborne dust that do not require electricity and are easy and inexpensive to assemble from interchangeable parts. Numerous samplers can be employed with great flexibility in their placement. This allows us to make continuous measurements using multiple samplers at multiple sites. As shown in Figure 3, a BSNE sampling station consists of three BSNE samplers at heights of 0.25 m, 0.5 m, and 1 m. The BSNE samplers provide measures of integrated resuspension collected over sampling intervals of normally one to two weeks. The BSNE sampling stations are arranged in line transects at intervals of 30 m with three sampling stations at the primary sites and two sampling stations at the secondary sites. To ensure comparability with previous studies, comparative data are

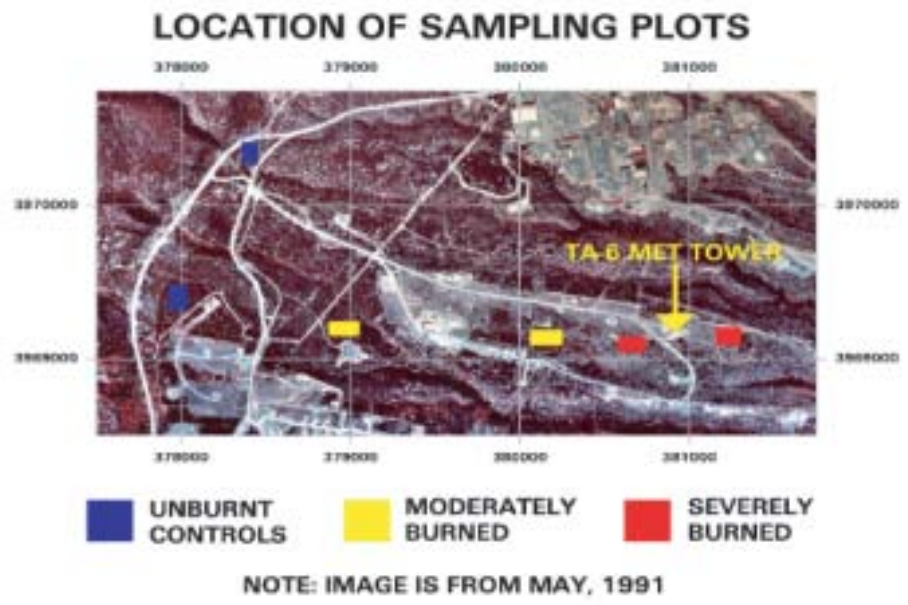

Figure 2. *Aerial photograph with overlay of sampling plots.*

Figure 3. *Photograph of a BSNE sampling station in the primary severely burned area.*

being collected at several sites using the older, less flexible Bagnold-type dust collectors used in previous studies.

Wind erosion relationships to meteorological conditions and vegetation cover. Meteorological data-collection stations are installed at primary sites to obtain data on wind velocity, temperature, relative humidity, and rainfall at 1-minute intervals. These data may be integrated over longer time intervals for comparison to the data from the BSNE samplers. The data can also be related more directly to short-term measures of resuspension being collected by 1) the TSI DustTrak monitor which provides minute-by-minute PM-10 concentration measurements and 2) the ESH-17 TEOM (Tapered Element Oscillating Microbalance) monitor, which provides PM-10 concentration averages every 15 minutes. These combined measurements will be used to establish critical conditions for enhanced resuspension, such as threshold velocities, by correlating particle concentration measurements to the local meteorological conditions (e.g., wind velocity). In addition, the meteorological tower at Technical Area (TA) 6 is providing additional data on friction velocities and soil moisture. These local meteorological measurements include relatively short-term averaging (1–15 minute averages) to provide finer time scales.

In addition to measurement of meteorological conditions, measurements were made to characterize tree-canopy cover and ground-level cover at both the primary and secondary sites for each burn type area. Measurements of the tree-canopy cover have been estimated using a spherical densiometer (and limited aerial photography analysis). Ground-cover measurements were made using 1-m sampling plots randomly positioned in the sampling areas. Digital pictures of the ground cover within the 1-m squares are being analyzed for percent cover and categorized by type (i.e., bare, live vegetation, pine needles). The ground-cover measurements were made toward the middle and the end of the summer growing season (June and September 2001), and next year we plan to make similar measurements at the beginning of the growing season (i.e., April/May).

Obtain distribution of resuspension rates at a burned area. Resuspension rates will be made using the meteorological flux gradient method (Stull 1988). For this method, the mass flux (F) is the product of the eddy diffusivity coefficient (K_z) and the mass air concentration (x) gradient with height (z):

$$F = K_z \frac{dx}{dz} \qquad (1)$$

The eddy diffusivity coefficient is a linear function of the friction velocity (u_*). The friction velocity is a measure of the boundary shear created as winds pass over vegetation and soils. The friction velocity for a given terrain and wind-velocity can be measured by

measuring the wind velocity profile with height (Bagnold 1941) or it can be determined using high-frequency three-dimensional measurements of wind velocities (Stull 1988) using Equation 2.

$$u_* = \left[\overline{u'w'}^2 + \overline{v'w'}^2\right]^{\frac{1}{2}} \quad (2)$$

where u', v', w' are the instantaneous wind-velocity components in the x, y, (horizontal) and z (vertical) directions. The instantaneous wind-velocity components will be measured using a sonic anemometer. Data for the wind profiles with height (as well as other meteorological conditions) will be obtained from the existing four 100 m meteorological towers on LANL property. Once F is determined, the resuspension rate is determined by the mass flux divided by the density of the local soil and the depth of the resuspendable soil (i.e., 3 mm [Webb et al. 1997]).

To determine the concentration gradient with height (dx/dz), which is needed for resuspension rate measurements, total suspended particulate (TSP) measurements will be collected weekly. These samplers will be placed at two heights (1 and 3 m) to allow measurement of the concentration gradients. The TSP air samples to be used have a sampling inlet that was slightly modified from a sampler of that described in Liu and Pui (1981). This sampling inlet has the advantage of sampling without directional dependence and appears to provide accurate sampling at typical wind velocities and for predominant particle sizes expected at LANL. Liu and Pui (1981) tested the sampling inlet in a wind tunnel and found aspiration efficiencies for particles of aerodynamic diameters of 8.5 and 11 μm was 100% ± 10% at wind speeds up to 2.5 m s^{-1} (typical velocities measured at LANL). However, measurement of resuspension at velocities higher than this was also needed because during these higher-wind velocities, resuspension is increased. The original Liu and Pui inlet design was for a PM 10 sampler, so modification to this inlet was required for collection of all particle sizes, not just those less than 10 μm.

The modifications of the Liu and Pui design included placement of the filter close to the bottom plate and the addition of a coarse wire screen to keep insects out of the filter. Because of the modifications to the inlet and the need to determine sampling efficiencies at higher wind velocities, Rodgers et al (2000) tested the sampler at velocities 12, 15, and 17 m s^{-1} and for particle aerodynamic sizes of 5, 10, and 30 μm. Results of this study suggest that collection efficiency for the used inlet was most affected by particle size and less affected by wind velocity. Collection efficiencies for the 5 μm particles was about 120% (20% over sampling on average), and dropped to around 50% for both the 10 μm and 30 μm particles.

Progress and Results

Effects of fire on soil resuspension. Figure 4 shows mean collection rates at each of the areas (severely burned, moderately burned, and unburned forest). Each of the three graphs represent data from the three different collection heights (0.25, 0.5 and 1 m). All three graphs show that collection rates were greater in the severely burned area compared to the other two areas, and the collection rates for each burn category decreased with increasing collection height.

Also, we have noticed evidence of deposited soil on the BSNE surfaces from rainsplash on the lower two samplers after rains, especially for the 0.25-m sampler. Because these graphs represent data collected from May through August of 2001, which includes the monsoon season where significant rainstorms occur, some of the differences between burn areas at the 0.25-m height and, to a lesser extent, the 0.5-m height are likely due to rainsplash. We found no evidence of rainsplash at the 1-m sampling height. Rainsplash can be an important mechanism for contaminant mobility because the water droplets can entrain soil particles and inject them into the air where they can deposit and dry on foliage and branches, becoming a secondary source for plant uptake and ingestion (Dreicer et al. 1984) or for resuspension (Giess et al. 1997). Therefore, finding increased rainsplash in the severely burned areas does have additional implications for contaminant transport. Landscape fabric was placed directly under the BSNE samplers in June to minimize rainsplash, and we believe this was partially successful. We plan to investigate the possible use of rain hoods

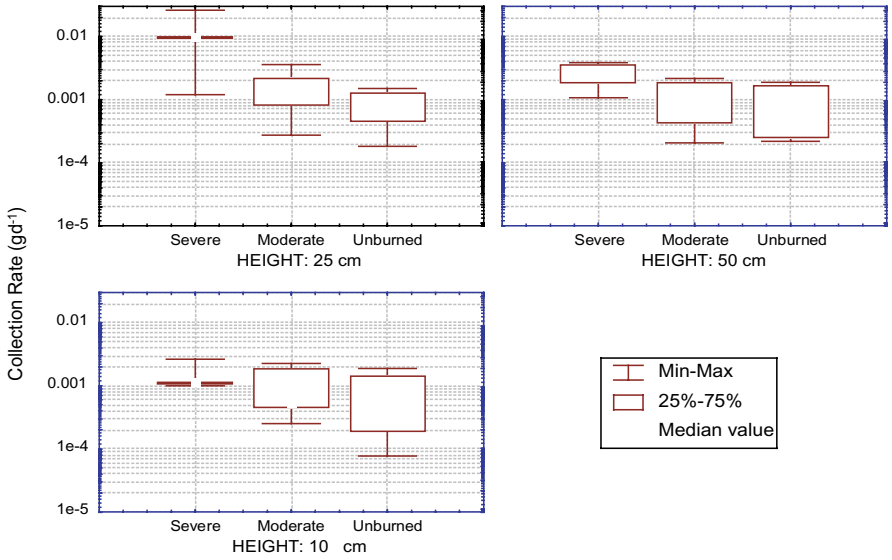

Figure 4. *Mean collection rates categorized by area type and collection height.*

that would attach to the top of the BSNE samplers and minimize the amount of rain and rainsplash collected by the samplers. These hoods have been used by other researchers (Shao et al. 1993).

Wind erosion relationship to meteorological conditions and vegetation cover. There were significant effects of the fire on the vegetation cover that have implications for wind erosion. For example, spherical densiometer estimates of mean live canopy cover were about 60%, 40%, and 0% for the categories of unburned, moderately burned and severely burned areas, respectively. The removal of live canopy cover in severely burned areas means that there is little remaining moderating effect of the trees on wind velocities at the ground surface. This was confirmed by our measurements, which showed highly significant increases in 1-m wind velocities at the severely burned site relative to the unburned site. The greater wind speeds may contribute to greater wind erosion in the severely burned area. In addition, quantitative measures of ground-level vegetation cover are ongoing, but preliminary data indicate a nearly complete removal of ground-level vegetation in both the severely and moderately burned areas. These data also indicate a partial recovery of litter cover on the soil in moderately burned areas because of the fall of the scorched needles. This partial recovery of the litter cover may also moderate wind-erosion rates. In the unburned area, the forest floor has little vegetation but is covered with a thick mat of pine needles. In contrast, there is much more live vegetative ground cover at the severely burned site because of extensive remediation efforts, but the overall ground cover is less because there are more open bare patches of soil. These changes in vegetation and litter cover could have significant implications for wind-erosion rates.

The TSI DustTrak and the TEOM measurements show substantial variation in PM-10 concentrations, especially during high winds. Figure 5 shows an example data set collected during a windstorm last spring. The 1-minute aerosol concentrations show a dramatic rise about 10:00 A.M. This corresponds to an increase in sustained wind velocity of greater than about 5 m s^{-1}, which is generally lower than threshold velocities found at fully vegetated sites (Stout 2001; Whicker et al. 2002). However, more measurements and analyses of the data are planned for the upcoming year to get more accurate estimates of these threshold velocities. A high-volume cascade impactor has been purchased for another project, but we plan on using it to provide detailed measurements of particle size distributions at the TA-6 burned site.

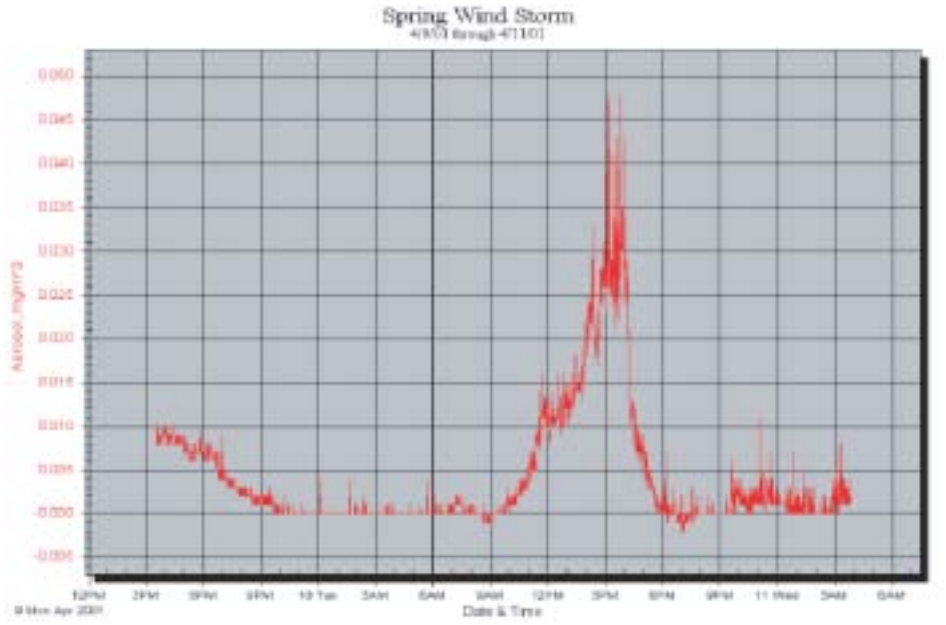

Figure 5. *One-minute PM-10 aerosol concentrations taken at the TA-6 burned area during a wind storm.*

Obtain distribution of resuspension rates at a burned area. Using the vertical gradient (Eqn. 1), one can calculate the vertical flux and the resuspension rate for a particular contaminant. Figure 6 shows the vertical mass flux. Using these values for vertical flux, one can then calculate resuspension rate for any particular soil contaminant. For example, we can examine Pu-239 in LANL on-site soils. Based on a mean vertical gradient at TA-6 of about 0.6 mg m^{-4} (positive values signify upward fluxes and soil loss), a mean friction velocity measured at TA-6 during the sampling period (0.4 m s^{-1}), a sampling height of 2 m, and an average on-site air concentration of Pu-239 in air of 4 aCi m^{-3} (LANL 1996). We obtain an average upward mass flux of soil of about 6 g m^{-2} yr^{-1} or an upward vertical flux of 0.2 Bq m^{-2} yr^{-1} for Pu-239. This translates into a fractional resuspension rate of 5 x10^{-11} s^{-1} or a half-life of 644 years. This resuspension rate is at the faster end of resuspension rate values found by other researchers, but is within the range of values found at other DOE sites (Anspaugh et al. 1975; Shinn et al.1997). In contrast, the site at TA-54 showed little or no net vertical movement (mean about 0) overall measurements. While these calculations

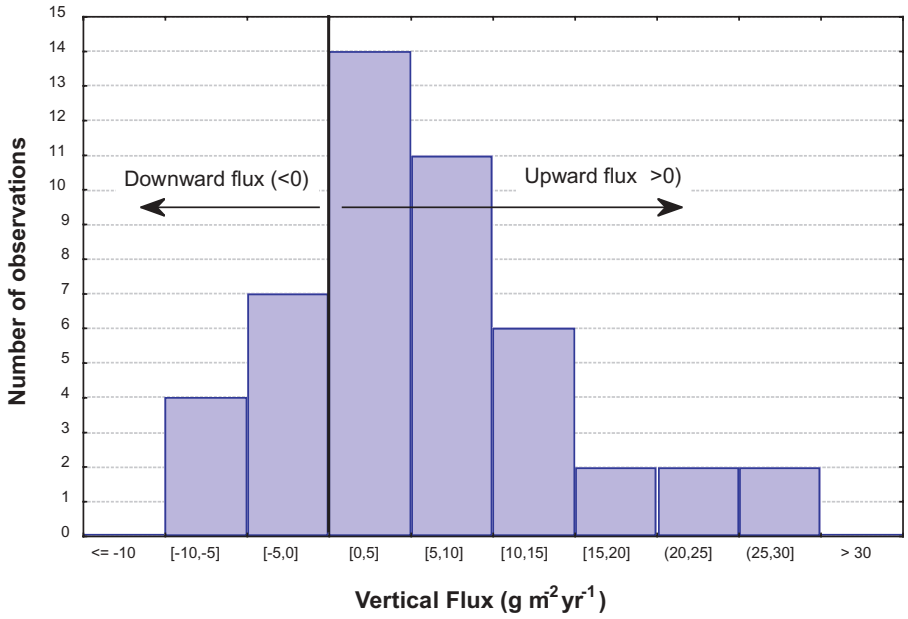

Figure 6. *Distribution of verticle fluxes taken at the burned area at TA-6.*

are preliminary, the illustration shows how the obtained measurements can be directly used to assess risk for many soil contaminants.

Conclusions and Deliverables

Conclusions. Taken together, these preliminary data suggest that wind erosion has increased as a result of the Cerro Grande fire and the effects continue one and a half years later. Based on 1-m-high BSNE sampler results, the median horizontal flux of wind driven soil is about a factor of 3 greater in the severely burned site compared to the unburned site. This difference could be greater than this during windy times. In addition, rainsplash may have been increased significantly.

Measurements of ground cover show significantly more vegetation in the severely burned area as a result of the substantial remediation efforts. These efforts likely reduced wind erosion; however, they were only partially successful because they did not reduce it to the level of the moderately burned sites. Moreover, some observations suggest that these remediation activities may have less effect next year because of the small numbers of perennial plants established. Once the annuals from this year's seeding have died, the soil may be more exposed next year than this year. Measurements also show the effects of the fire on reducing live canopy cover. Preliminary data show that this resulted in greater ground level (1 m) wind velocities in the severely burned area relative to the unburned area. Short-term (minute-to-minute) aerosol concentrations show considerable variation and appear to be strongly related to wind velocities, but additional analyses are needed to confirm this and to determine threshold wind velocities.

The work plan for this year calls for measurements similar to those described above. Making these measurements is critical to capture wind erosion/resuspension rates under a wide variety of conditions, especially during low-frequency, high winds.

Deliverables. This is the first of three years of proposed study. During the first year, we purchased instruments, developed sampling plans, began measurements, and analyzed preliminary data. Over the three years, deliverables include an archived and published data set of resuspension related measurements as correlated to meteorological and vegetation cover conditions at several burned and unburned LANL sites. At some level, these sites will represent the soil and atmospheric conditions of similar forest ecosystems, so the results will have applicability beyond LANL. Also, this work can improve the model predictions of resuspension and subsequent risk. Interest has been expressed in this study and our related research. In fact, our studies at the Waste Isolation Pilot Plant (WIPP) and Rocky Flats were recently highlighted in the DOE publication "Initiatives in Environmental Technology Investment." Further, the results of this investigation can be applied to other contaminants and, therefore, be of interest to a wider audience. Publications in peer-reviewed journals will summarize the research. Finally, this proposal not only provides for timely and valuable information for LANL, it can also serve as seed money for additional collaborations in resuspension and in related areas, such as geographic indexing system (GIS) mapping and modeling of contaminant transport. Already in FY01, money has been obtained for resuspension studies at LANL's Area G ($60K) and at Yucca Mountain ($25+K).

References

Anspaugh, L.R., J.H. Shinn, P.L. Phelps, N.C. Kennedy, "Resuspension and redistribution of plutonium in soils," *Health Phys.* **29**:571–582, 1975.

Bagnold, R.A., "The physics of blown sand and desert dunes," London: Chapman and Hall Ltd., 1941.

Belnap, J. and D.A. Gillette, "Vulnerability of desert biological soil crusts to wind erosion: the influences of crust development, soil texture, and disturbance," *J. Arid Environ.* **39**:133–142, 1998.

Cahill, T.A., T.E. Gill, J.S. Reid, E.A. Gearhart, and D.A. Gillette, "Saltating particles, playa crusts and dust aerosols at Owens (Dry) Lake, California," *Earth Surf. Processes Landforms* **21**:621–639; 1996.

Department of Energy Publication, "Initiatives in Environmental Technology Investment," **8** Fall: 6–8, 2001, http://www.wpi.org.

Driecer, M, T.E. Hakonson, G.C. White, and F.W. Whicker, "Rainsplash as a mechanism for soil contamination of plant-surfaces," *Health Phys.* **46(1)**:177–187, 1984.

Fryrear, D.W., "A field dust sampler," *J. Soil Water Conserv.* **41**:117–120, 1986.

Fryrear, D.W., "Soil cover and wind erosion," *Trans. ASAE* **28**:781–784, 1985.

Giess, P.; A.J.H. Goddard, G. Shaw, "Factors affecting particle resuspension from grass swards," *J. Aerosol Sci.* **28(7)**:1331–1349, 1997.

Gillette, D.A., J. Adams, A. Endo, and D. Smith, "Threshold velocities for input of soil particles into the air by desert soils," *J. Geophys. Res.* **85(C10)**: 5621–5630, 1980.

Goossens, D. and Z.Y. Offer, "Aeolian dust erosion on different types of hills in a rocky desert: wind tunnel simulations and field measurements," *J. Arid Environ.* **37**:209–229, 1997.

Goossens, D. and Z.Y. Offer, "Wind tunnel evaluation of six aeolian dust samplers," *Atmos. Env.* **34**:1043–1057, 2000.

Johansen, M.P., T.E. Hakonson, F.W. Whicker, R.J. Simanton, and J.J. Stone, "Hydrologic response and radionuclide transport following fire at semiarid sites," *J. Env. Quality*. **30**: 2010–2017, 2001a.

Johansen, M.P., T.E. Hakonson, and D.D. Breshears, "Post-fire runoff and erosion from rainfall simulation: contrasting forests with shrublands and grasslands," *Hydro. Process.* **15**: in press, 2001b.

Johnson, S.R., D.D. Breshears, and T.B. Kirchner, "Multi-pathway, multi-site contaminant transport: assessing vertical migration, wind erosion, and water erosion at semiarid DOE sites," *Health Phys.* **78(6)**:S159, 2000.

Liu, B.Y.H. and Y.H. Pui, "Aerosol sampling inlets and inhalable particles," *Atmos. Environ.* **15**:589–600, 1981.

Los Alamos National Laboratory (LANL) "Environment Surveillance at Los Alamos during 1995," Los Alamos National Laboratory report LA-13210-ENV, 1996.

Nyhan, J.W., L.W. Hacker, T.E. Calhoun, and D.L. Young, "Soil survey of Los Alamos County, New Mexico," Los Alamos National Laboratory report LA-677-MS, 1978.

Okin, G.S., B. Murray, and W.H. Schlesinger, "Degradation of sandy arid shrubland environments: observations, process modelling, and management implications," *J. Arid Environ.* **47**: 123–144, 2001.

Rodgers, J.C., P.T. Wasiolek, J.J. Whicker, C. Eberhart, K. Saxton, and D. Chandler, "Performance evaluation of LANL environmental radiological air monitoring inlets at high-wind velocities associated with resuspension," Los Alamos National Laboratory report LA-UR-00-3091, 2000.

Shao, Y., G.H. McTainsh, J.F. Leys, and M.R. "Raupach, Efficiencies of sediment samplers for wind-erosion measurement," *Austrailian J. Soil Res.* **31**: 983–1011, 1993.

Shinn, J.H., D.N. Homan, and W.L. Robinson, "Resuspension studies in the Marshall Islands," *Health Phy.* **73(1)**:248–257, 1997.

Stout, J. E., "Dust and environment in the Southern High Plains of North America," *J. Arid Environ.* **47**: 425–441, 2001.

Stull, R.B., "An Introduction to Boundary Layer Meteorology," Kluwer Academic Publishers: The Netherlands (1998).

Webb, S.A., S.A. Ibrahim, and F.W. Whicker, "A three-dimensional spatial model of plutonium in soil near Rocky Flats, Colorado," *Health Phys.* **73(2)**: 340–349, 1997.

Whicker, J.J., D. Breshears, D. Schoop, P. Wasiolek, R. Tavani, and J. Rodgers, "Temporal and spatial variation in episodic wind erosion in unburned and burned shrubland," *J. Environ. Quality*, **3** in press, 2002.

Woodruff, N.P. and F.H. Siddoway, "A wind-erosion equation," *Soil Sci. Soc. Am. J. Proceedings* **29**:602–608, 1965.

Zobeck, T.M., D.W. Fryrear, and R.D. Pettit, "Management effects on wind-eroded sediment and plant nutrients," *J. Soil Water Conserv.* March–April: 160–163, 1989.

Health Physics

Neutron Extremity Dosimetry Based on Monte Carlo Computations of Magnetic Resonance Images

Laser Illuminated Track Etch Scattering (LITES) Dosimetry System

Personal Continuous Air Monitor (PCAM)

PRESCILA: Proton Recoil Scintillator Los Alamos Rem Meter

Rapid Discrimination of Personnel Contamination Due to Radon versus Other Alpha-Emitting Radionuclides

Studies to Date

FY95

Optimization of Placement of Workplace Continuous Air Monitoring (CAM) Instrumentation

High-Energy Neutron Dosimetry

FY96

Applications of Thermal Ionization Mass Spectrometry to the Detection of Pu-239 and Pu-240 Intakes

High-Energy Neutron Dosimetry and Spectroscopy

Development and Implementation of the LANL Neutron Extremity Dosimeter

Optimization of Continuous Air Monitoring (CAM) Instrument Placement

FY97

Applications of Thermal Ionization Mass Spectrometry (TIMS) to the Detection of Pu-239 and Pu-240 Intakes

High-Energy Neutron Dosimetry and Spectroscopy

Development and Implementation of the Los Alamos National Laboratory (LANL) Neutron Extremity Dosimeter

Optimization of Continuous Air Monitoring (CAM) Instrument Placement

Resuspension of Pu-238 from Surfaces

FY98

Characterization of Photon Radiation Fields in a LANL Plutonium Facility

Detection and Internal Dosimetry of Insoluble Metal Tritides

Determining and Monitoring the Inhalable Fraction of Plutonium Aerosols in an Accident

Implications of Room Ventilation and Containment Design for Minimization of Worker Exposure to Plutonium Aerosols

PRESCILA: Proton Recoil Scintillator Los Alamos Neutron Dose Meter

FY99

Detection and Internal Dosimetry of Insoluble Metal Tritides

Determining and Monitoring the Inhalable Fraction of Plutonium Aerosols in an Accident

Implications of Room Ventilation and Containment Design for Minimization of Worker Exposure to Plutonium Aerosols

Proton Recoil Scintillator Los Alamos Neutron Dose Meter

Rapid Discrimination of Personnel Contamination Due to Radon Versus Other Alpha-Emitting Radionuclides

An XRF Continuous Air Monitor for Metal Tritide Aerosols in the Workplace

FY00

Detection of Low-Energy-Emitting-Radionuclides Using Mobile Platforms

Physical Parameters for the Internal Dosimetry of Insoluble Metal Tritide Particles

Algorithm for Determination of Need for Dosimetry Monitoring

Neutron Extremity Dosimetry Based on Monte Carlo Computations of Magnetic Resonance Images

PRESCILA: Proton Recoil Scintillator Los Alamos Rem Meter

An XRF Continuous Air Monitor for Metal Tritide Aerosols in the Workplace

Rapid Discrimination of Personnel Contamination Due to Radon versus Other Alpha-Emitting Radionuclides

Summary of Progress

TDEA-funded projects in the health physics category have generated 68 presentations and publications from eighteen studies funded since FY95. The fact that a greater number of health physics studies have been funded by TDEA reflects the unique and diverse radiation protection requirements at LANL. The TDEA-funded radiation protection projects have resulted in products at the leading edge of the discipline's technology. The latest example is the PRESCILA neutron probe, commercially available in 2002.

Neutron Extremity Dosimetry Based on Monte Carlo Computations of Magnetic Resonance Images

Principal Investigator: Michael W. Mallett (ESH-4)

Coinvestigator: Jeffrey M. Hoffman (ESH-4)

Funding: FY00 $26K, FY01 $8K

Introduction

This project seeks to advance the protection of Los Alamos National Laboratory (LANL) employees from radiation health hazards, in particular, neutron dose to the extremities. This is in direct support of three University of California contract performance measures: 1) management of routine occupational radiation exposures; 2) hazard analysis and control; and 3) injury/illness prevention. The research will provide the technical basis for reporting measured neutron absorbed dose to the extremities as an equivalent dose, consistent with governing regulations (e.g., 10 CFR 835). In addition, the results will validate newer radiation protection concepts (e.g., ICRP 60's radiation weighting factor, w_R) as applicable to extremity dosimetry. Likewise, the research will address shortcomings in current dosimetry standards (specifically, the lack of Department of Energy Laboratory Accreditation Program (DOELAP) performance testing for neutron extremity dosimetry as a component of HPS N13.32 because of a lack of consistency between current regulations and current protection concepts.)

At present, the new LANL neutron extremity dosimeter is capable of measuring the absorbed neutron dose (e.g., Gy or rad) to the extremities. However, DOE reporting requirements necessitate this dose be reported as an equivalent dose (e.g., Sv or rem). No technical basis exists for "qualifying" the neutron dose to the extremities as measured by personal dosimeters (e.g., thermoluminescent dosimetry/dosimeters, or TLDs). However, it is acceptable to report a neutron extremity dose based upon photon personal dosimeter measurements, and subsequently adjusting the result by a known neutron-to-photon dose ratio. Hence, the capability of the new LANL neutron extremity dosimeter is relegated to a qualitative measure rather than functioning as the dose-of-record. Assessing neutron-to-photon dose ratios across the Laboratory still requires fairly labor and time-intensive field measurements.

By developing the technical basis for reporting an equivalent neutron dose to the extremities consistent with present regulations, these field measurements are made unnecessary. Elimination of the field measurements is estimated as a cost savings of $9K annually, equivalent to 60 hours of effort at $150/hour. The savings would be double should the field measurements be performed on a semiannual schedule. In addition, interruptions of programmatic work at TA-55 because of the performance of these field measurements would also be eliminated, a benefit that is decidedly difficult to quantify. However, it should be noted that the fundamental benefit of this research is a technical contribution that fills a much needed void in the field of extremity dosimetry.

Method

This research seeks to accommodate currently instituted radiation protection concepts. That is, the calculation of a quality factor applicable to the extremities will be made. As currently defined (ICRP 26), the value of Q is a function of the collision stopping power (or unrestricted linear energy transfer), L_∞, in water. This relationship was determined for the whole body using a 30-cm-diameter sphere. As there is no agreement upon a suitable phantom for the extremities as it pertains to neutron radiation, the method proposed here is to use actual physical measurements of the human extremities, as represented by magnetic resonance images (MRIs). In particular, image segmenting techniques generate MRIs that clearly differentiate between muscle, fat, and bone, the three principle tissues of the extremities. This information will be used to define the transport geometry for Monte Carlo computations. Neutron transport through the MRI-defined medium would therefore accurately calculate L_∞ applicable to the extremities. From these results, applying the L_∞-Q relationship of ICRP 26 will yield a consistent, humanly realistic quality factor (function) for reporting a neutron equivalent dose to the extremities. Furthermore, the results can be used to assess the validity of the ICRP 60 methodology as it pertains to the extremities.

Progress and Results

During FY2001, the project completed the collection of MRIs for eleven volunteer subjects. The image field of view consisted of one leg and one arm per volunteer. The images were subsequently postprocessed to grossly segment the various tissues, that is, fat, muscle, bone, and other. The original (non-postprocessed) images were provided as well. Using this image series, computer anatomical mappings of the

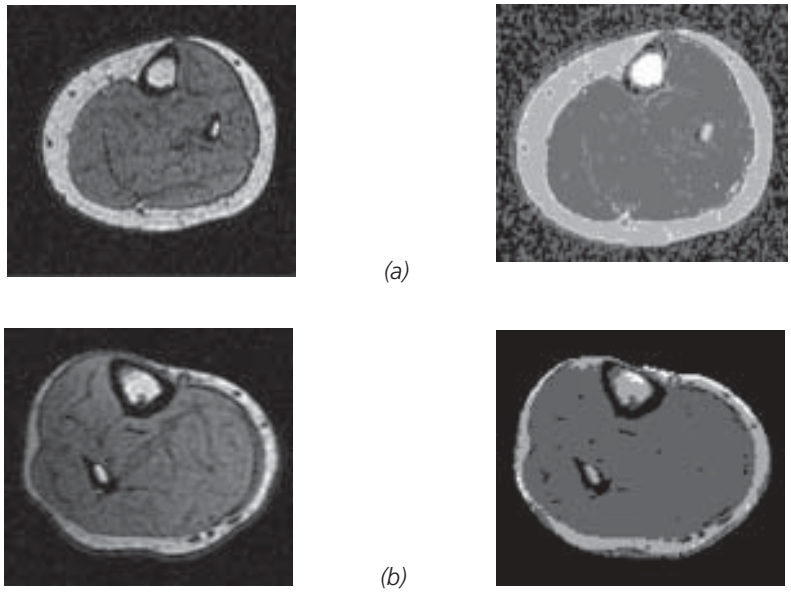

Figure 1. *MR images of the leg, transverse orientation: a) raw image (left), corresponding segmented image (right) using previous technique. b) raw image (left), corresponding segmented image (right) using improved technique.*

body will be constructed as the geometry definitions for neutron transport calculations, i.e., MCNP input file geometry cards.

Additional work was performed to resolve segmenting anomalies. To reduce noise, accurately define tissue boundaries, and limit the segmenting field-of-view once a tissue has been defined, postprocessing techniques were employed to eliminate ambiguous results. Marrow was added as another defined tissue. The improved segmenting technique renders satisfactory anatomy mappings in an automated fashion, rather than painstakingly addressing images voxel by voxel.

Conclusion and Deliverables

A database of magnetic resonance images of the human extremities suitable for structuring the geometry conditions of Monte Carlo computations has been compiled. The result of the Monte Carlo computations using the MRI database will be assembled into a coherent methodology that will serve as the technical basis for reporting the neutron extremity dose consistent with current regulations and standards. The methodology will be presented for peer review among the health physics extremity dosimetry/personnel monitoring community and, following appropriate revision, will be instituted as a component of the LANL Personnel Dosimetry Program, ESH-4.

References

10 CFR 835, *Occupational Radiation Protection*, Code of Federal Regulations, Volume 61, No. 247, December 23, (1996).

American National Standards Institue (ANSI), *Performance Testing of Extremity Dosimeters*, HPS N13.32 (New York: ANSI, 1995).

ICRP Publication 26, *Recommendations of the International Commission on Radiological Protection*, Pergamon Press, Oxford, England (1977).

ICRP Publication 60, 1990 *Recommendations of the International Commission on Radiological Protection*, Pergamon Press, Elmsford, NY (1991).

University of New Mexico Health Science Center, Clinical and Magnetic Resonance Research Center, 1201 Yale NE, Albuquerque, NM 87131.

Laser Illuminated Track Etch Scattering (LITES) Dosimetry System

Principal Investigator: Murray E. Moore (ESH-4)

Coinvestigators: Robert T. Devine, Jeffrey M. Hoffman, Richard J. McKeever (ESH-4), Robert E. Hermes (MST-7), Heather J. Gepford, Nolan E. Hertel, Georgia Institue of Technology

Funding: FY01 $55K

Introduction

The Laser Illuminated Track Etch Scattering (LITES) project proposes to develop and build a "next generation" instrument for measuring the neutron dose equivalent registered by CR-39 track etch foil dosimeters.

The LITES instrument has the potential of replacing one (or possibly two) different instruments, which are presently used for measuring the neutron dose equivalent registered by track etch foils at Los Alamos National Laboratory (LANL).

To satisfy US Department of Energy Laboratory Accreditation Program (DOELAP) requirements, the LANL Personnel Dosimetry Operations (PDO) team uses two different analytical instruments to count track etch foils, depending on the dose exposure recorded by the foil.

The instruments used for track etch counting are (1) the Autoscan 60 (Bicron Instruments), and (2) an optical microscope, which is used to manually count track etch foils. The Bicron Autoscan 60 system routinely works for track etch foils exposed to less than 300 mrem in dose equivalent. An optical microscope manually counts the foils; however, this technique is time-consuming, especially when measuring dose on dozens of individual foils.

If a single automated instrument could be developed to count the foils, there would be monetary savings in the amount of necessary lab equipment. In addition, the accuracy and reliability of the single automated system would simplify the DOELAP certification requirements.

The ESH-4 PDO team leader recently assessed the current state of PDO track etch operations, and welcomed the development of a new reader for track etch dosimeters. The PDO team routinely processes about 2000 foils quarterly, plus several hundred foils classified as "special," also on a quarterly basis. An automated instrument would be both repeatable and reliable, and would be more cost effective because manual counting and visual inspection of track etches would be eliminated.

Method

The basis of the operation of the LITES system is explained in Figure 1 and in the following paragraphs.

To measure the neutron dose equivalent received by a CR-39 plastic foil, neutron tracks are enlarged in the plastic by a chemical etch procedure. The etch protocol begins with a one-hour pre-etch in a 60% methanol and 40% 6.25 N NaOH solution at 70 ºC to remove alpha- and heavy-charged particle tracks. This is followed by a 15-hour etch in 6.25 N NaOH maintained at 70 ºC during the etch cycle. A 10-minute stop etch using room temperature 0.1 N HCl and a final rinse with distilled water and a wetting agent complete the protocol. The etch protocol resulted in an average track diameter of 20 μm for bare ^{252}Cf tracks.

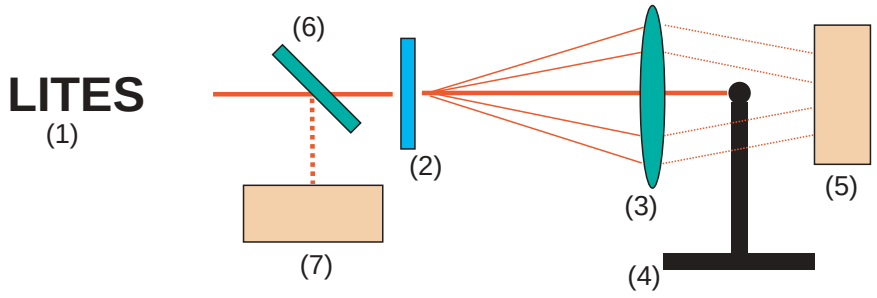

LITES dosimeter and component description

(1) Illuminating laser
(2) Track etch pits in the CR-39 foil scatters laser light
(3) Lens refocuses the scattered light
(4) Beam stop blocks main laser beam
(5) Photodiode measures magnitude of scattered laser light
(6) Flat glass slide diverts small portion of main laser beam
(7) Second photodiode measures main laser output

Figure 1. *Laser Illuminates Track Etch Scattering (LITES) dosimetry system schematic.*

To be measured in the LITES system, a track etch foil dosimeter is placed in the LITES sample holder (see Figure 2). This sample holder is mounted on a YZ motion-control table (providing linear motion, side-to-side and up-down). Light from a helium-neon laser with output power of 6.6 milliWatts is directed through the track etch foil, and the etched pits cause the laser light to be scattered (much as drops of water suspended in the atmosphere scatter incident light)

The optical lens in the LITES system refocuses the scattered light so that it impinges onto the photodiode, which measures the amount of the incident light. A small beam stop placed in between the optical lens and the photodiode prevents the main laser beam from reaching the photodiode, thereby increasing the sensitivity by which the relatively small amount of scattered light may be measured by the photodiode.

A second photodiode is placed at right angles to the direction of the main laser beam, and a glass slide diverts a small portion (about 8%) of the main laser beam to this second photodiode for measurement. This beam-splitter arrangement allows real-time measurement of the laser power output. The LITES system then uses the ratio of the scattered light to diverted light as a measurement metric ("the LITES ratio") for determining the amount of the neutron dose equivalent deposited in the CR-39 foil.

Progress and Results

Calibrating LITES with foils of known dose. The next stage in the process for measuring neutron dose equivalent is illustrated in Figure 3, where the results of foils of known dose are presented.

In this stage of the analysis, 10 LANL "lemon" badge holders were exposed to varying amounts of known neutron dose equivalent, with each badge holder containing 5 different CR-39 foils. Therefore, Figure 3 represents 10 foils, classified by the location within the lemon badge holder. Then, the LITES system was calibrated with this information so that the background corrected

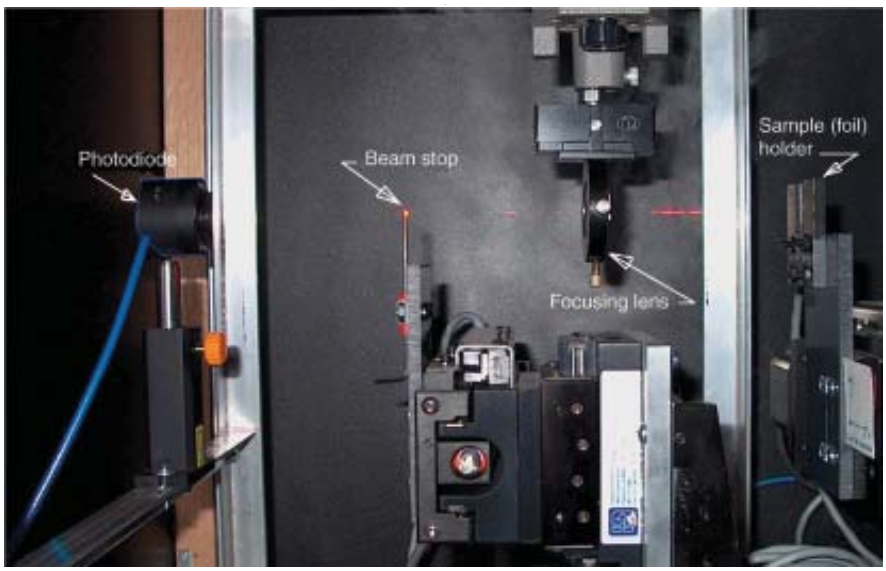

Figure 2. *A photograph of the LITES system shows the vital components in measuring the light scattered from the track etch pits in the CR-39 foil.*

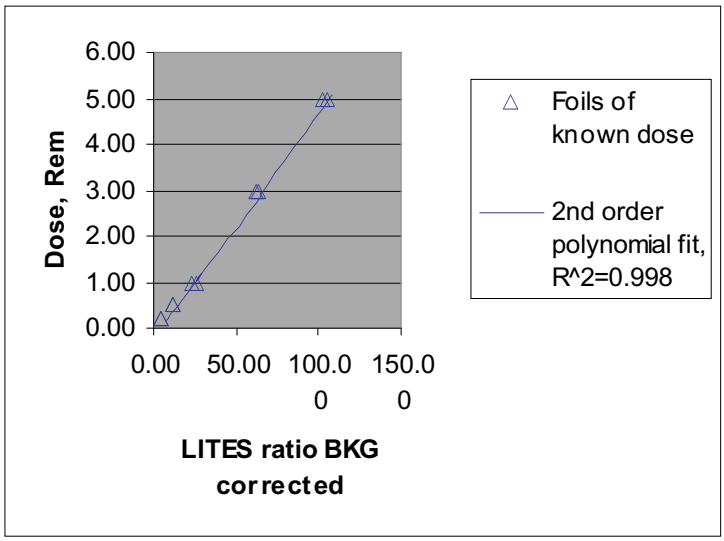

Figure 3. *Scattered laser light is measured for foils of known calibrated dose equivalent, allowing the calculation of a predictive correlation factor.*

LITES ratio could be used to predict the neutron-equivalent dose on foils irradiated with an unknown amount of dose.

Measuring foils of unknown dose with LITES. The PDO team received a test set of track etch dosimeters consisting of 10 LANL "lemon badges" that had been irradiated with varying amounts of unknown dose. These badge holders held a total of 50 foils (5 foils per badge) and these foils were analyzed by four different methods, including:

- the Bicron Autoscan 60,
- the LITES system, and
- manual counting by an optical microscope.

Upon inspection of the graphed results in Figure 4, one may see an upper bound for the valid results from the Autoscan 60. The optical microscope results represent a full three days of manual counting of the track etch pits for each data set. In terms of time, the LITES system was able to process the known calibration foils plus the unknown trial foils in about four hours. This was accomplished using the LITES system in its current format, which is only semi-automated, where the operator must

manually place and remove the individual foils so that they may be counted. These results are encouraging, and the PDO staff are interested in the possibilities available with the new LITES system.

Development of supplemental capabilities: DA-LITES at Georgia Institute of Technology. The DA-LITES (Differential Angle-LITES) system is a modification of LANL-LITES (see Figures 5 and 6) that measures the scattered light intensity from the CR-39 as a function of scatter angle. This work at Georgia Tech involved not only making measurements of the scatter distribution, but also theoretically evaluating the system's ability to extract neutron quality information. The DA-LITES system is comprised of a turntable that rotates the silicon-diode detector about the CR-39 detector at a fixed distance. As is true of the LANL-LITES device, the automated movement of the CR-39 in the horizontal and vertical directions is computer controlled. This allows for measuring and averaging a number of readings from distinct locations on the detector.

A theoretical model of scattering from neutron-induced tracks has been developed. This model has proven useful in evaluating the effects of varying different parameters of the DA-LITES system. Specifically, a significant change is seen in the scatter distribution from normal proton tracks by varying the etch time (15 hours in Figure 7 vs. 6 hours in Figure 8) and by changing the coherent light wavelength (633 nm vs. 514 nm).

Additional work remains to be done on the DA-LITES system. The need for much of this work became evident as a direct consequence of the work performed for this contract. Proposed future work includes experimentally evaluating the result of changing the wavelength of coherent light used. Theoretical models indicate that a change in the scatter distribution will be observed. We have acquired an argon-ion laser for this evaluation. Because of the higher power of this laser, we expect an improvement in the measurement error associated with this method at low dose equivalent.

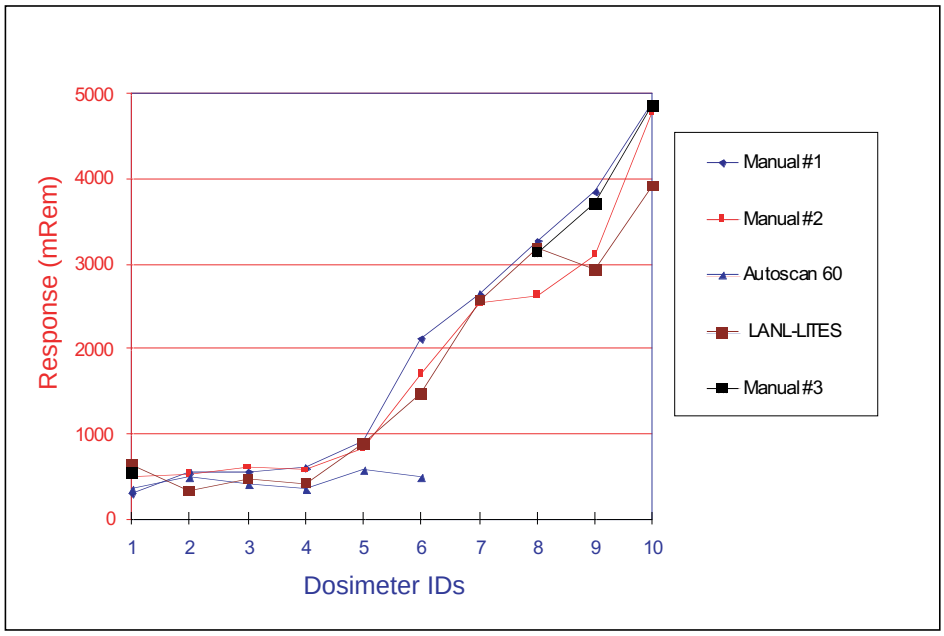

Figure 4. *Results of the analysis of track etch foils of unknown dose. The results from the LITES instrument compare favorably to results from automated Autoscan 60 instrument and to results obtained from manual counting by optical microscope.*

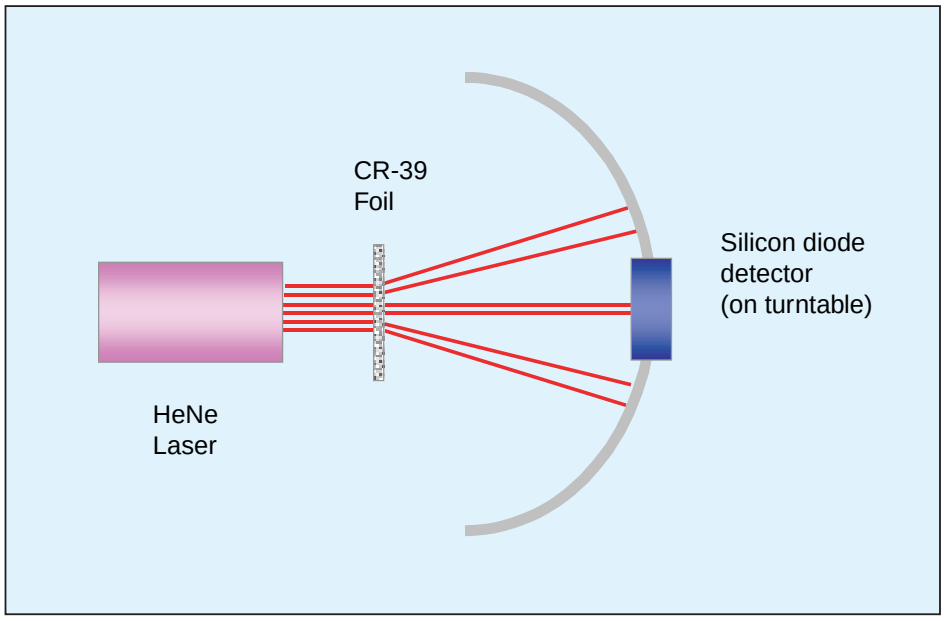

Figure 5. *The DA-LITES system measures the scattered laser light over a range of scattering angles.*

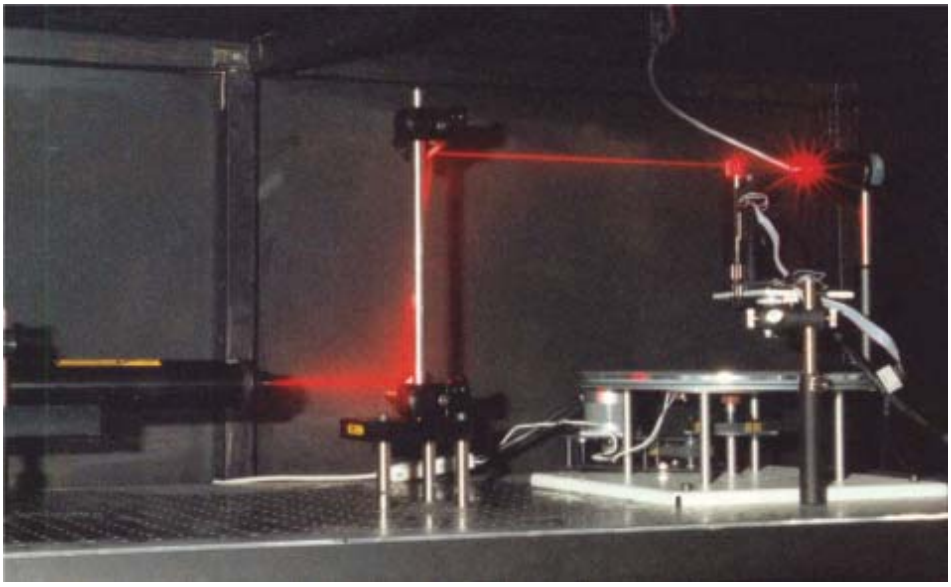

Figure 6. *The DA-LITES instrument had the measurement photodiode mounted on a turntable which can be positioned at the desired angle.*

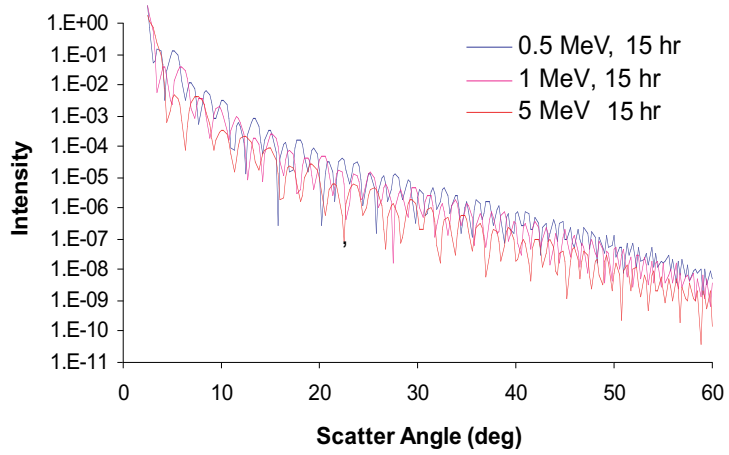

Figure 7. *Results of 15-hour etch time on track etch foils exposed to various neutron energies.*

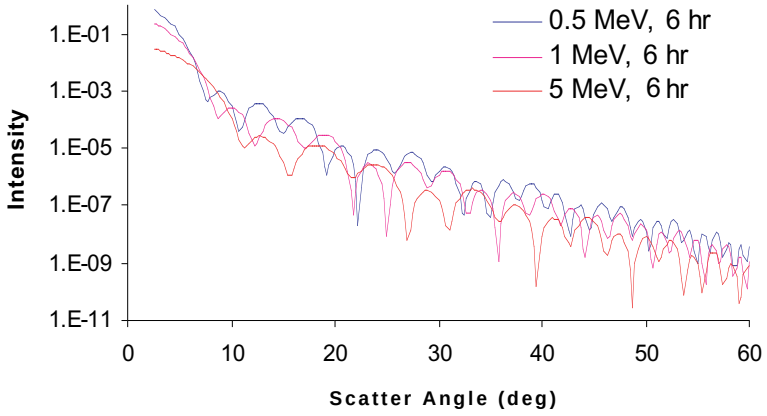

Figure 8. *Results of 6-hour etch time on track etch foils exposed to various neutron energies.*

Theoretical models indicate that a 15-hour etch significantly limits the possibility of extracting neutron quality information, a result which was seen experimentally. Repeating the experimental measurements using a set of CR-39 detectors that were etched for only six hours should produce more promising results. In addition, measurements should be made for additional neutron spectra and monoenergetic neutrons. Determination of the limitations at high-dose because of track overlap for both LANL-LITES and DA-LITES is needed.

From a theoretical standpoint, a number of simplifying assumptions were made that should be addressed. These include the development of a more realistic track model that includes carbon and oxygen recoils, consideration of overetched tracks, and the variation in the track-etch rate as a function of track depth. The effects of polarization, both experimentally and theoretically, also remain to be examined.

Conclusion and deliverables

The LITES system holds promise in providing valuable reinforcement (and hopefully replacement) of the methods and instruments that have been relied upon in the past. In order to completely replace these methods, however, work remains to include the LITES system into the ESH-4 PDO Technical Basis Document.

Personal Continuous Air Monitor (PCAM)

Principal Investigator: Ron G. Morgan (ESH-12)

Coinvestigator: Sam Salazar (ESH-4)

Collaborators: William Murray, Hardware Design (NIS-6), Ken Butterfield, Software Design (NIS-6), Debra Garcia, Financial Mgmt. Support (BUS 3)

Funding: FY01 $44.8K

Introduction

Current monitoring and alarm capabilities for airborne actinides are hampered by delays that can lead to slowed down evacuation of areas with high-actinide concentrations. We proposed to develop a wearable alpha continuous air monitor (CAM) that would sample air in the user's breathing zone and warn the user about high levels of airborne alpha activity very quickly. We believe we have accomplished that goal.

Statement of Problem.

a. Real-time breathing-zone monitoring and alarm capability for airborne actinides does not currently exist. Although fixed CAMs alarm at preset airborne concentration levels, they are hampered by dilution factors, caused by air-circulation patterns and the physical distance from point-of-release. Dilution leads to large delay times between actinide release and CAM alarm. Delays lead, in turn, to further delay evacuating areas with high-actinide airborne concentrations, resulting in potentially larger doses to personnel.

b. The internal dosimetry required for actinide-inhalation uptakes is difficult, imprecise, and expensive.

c. Where actinide environments, or potential actinide environments, cannot be well characterized (such as decontamination and decommissioning [D&D] and environmental restoration [ER] projects) or where environments are seldom entered (pump rooms, attics, etc.), the worker protection often takes the form of overly conservative protective clothing or administrative controls that are time-consuming and difficult to implement, such as the use of remotely-operated devices.

Benefit.

a. Real-time monitoring and alarm capability for actinides would lead to a safer environment for workers, and considerable savings related to the avoidance of occurrences (and the program delays which are often driven by occurrences).

b. The personal CAM (PCAM) provides a representative breathing-zone air sample, which may potentially be used to assign dose. Where the PCAM is used, internal dosimetry investigations may be avoided altogether.

c. Workers in not-well-characterized environments, for example, D&D and ER activities, could use real-time monitoring and alarm capabilities to prevent exposure and avoid overprotection in administrative and protective clothing requirements.

Method and Results

For fiscal year 2001, our main goals were to develop a prototype set of hardware for the PCAM and to develop the alarm algorithm to detect alpha particles from plutonium. To develop the alarm, we measured alpha spectra from filters exposed to air that had been moved through thorium and uranium ore samples. This process provided templates that were used in Monte Carlo simulation of the various alarm algorithms and alarm settings. We calculated the detection likelihood and the false alarm rates for several algorithms. Results from the best algorithm are presented here. We decided to use an algorithm based on two regions of interest (ROIs), one to determine a background and the other for the signal.

Hardware description. The hardware has three main components: a pump and

Photo 1. *Labeled photo of PCAM, November 2001.*

air system to sweep particles to a micropore air filter; a silicon-barrier detector to detect alpha particle emission; and a single board microprocessor based multichannel analyzer (MCA) to do energy-resolved alpha spectroscopy. Data for each detected alpha particle is stored in list mode in battery backed-up RAM for long-term storage. The microprocessor has a keypad and liquid crystal display for the user interface.

Research Results. Our goal was to develop a system that would alarm at about the one-DAC (Pu239) level in the normal radon background present in PF4. First, we needed to obtain an energy calibration and spectral resolution for our detector system. We used several electroplated alpha sources to develop the energy calibration, U^{238}, Th^{230}, Pu^{239}, Pu^{238}, and Pu-Am-U. The sources are shown in Figure 1.

We used two sources for our radon data. These were specially prepared containers of thorium and uranium ore samples that allowed air to be pumped through the sample on its way to the

filter. While these ore samples were mostly one type of ore, both samples contained a mixture or uranium and thorium as would be expected from naturally occurring material. The radon data demonstrates the detector energy resolution when measuring alpha spectra from a filter. See figure 2.

Our alarm algorithm uses two equal-width ROIs, one centered on the 6.05 MeV peak from radon and one centered on the 5.15 MeV peak from Pu^{239}. An ROI centered on the 5.4 peak would be used to detect Pu^{238}. The filter introduces a loss of resolution because the alpha particles lose energy in penetrating the filter material before reaching the detector. This produces the exponential tail toward lower energies evident in Figure 2. Because exponential functions add as linear functions, we only need to account for the one radon region when determining the background under the plutonium region. We assumed a fixed ratio in these two ROIs when only radon is present. We calculate the uncertainty in this ratio given the current number of counts in the radon ROI and set a threshold of four sigma for our alarm level. If the number of counts is small, we use Poisson statistics to determine the alarm level, but the certainty required is about the same as the 4 sigma level for Gaussian statistics. We also include a term for the uncertainty in measuring the mean value in the radon ROI and we can add an extra term to allow setting the false alarm rate if that becomes necessary.

The data will be stored as a list of energy and arrival times. This will allow post processing of the data as well as the real-time analysis planned for the PCAM system. As each count is recorded, the spectrum will be developed by playing the list backward with counts being added to a histogram, and the alarm function being tested. This will continue until the alarm threshold is exceeded in the plutonium ROI or the list is exhausted. Thus, a new plutonium leak will not have to overcome a large background of hours of accumulated radon counts.

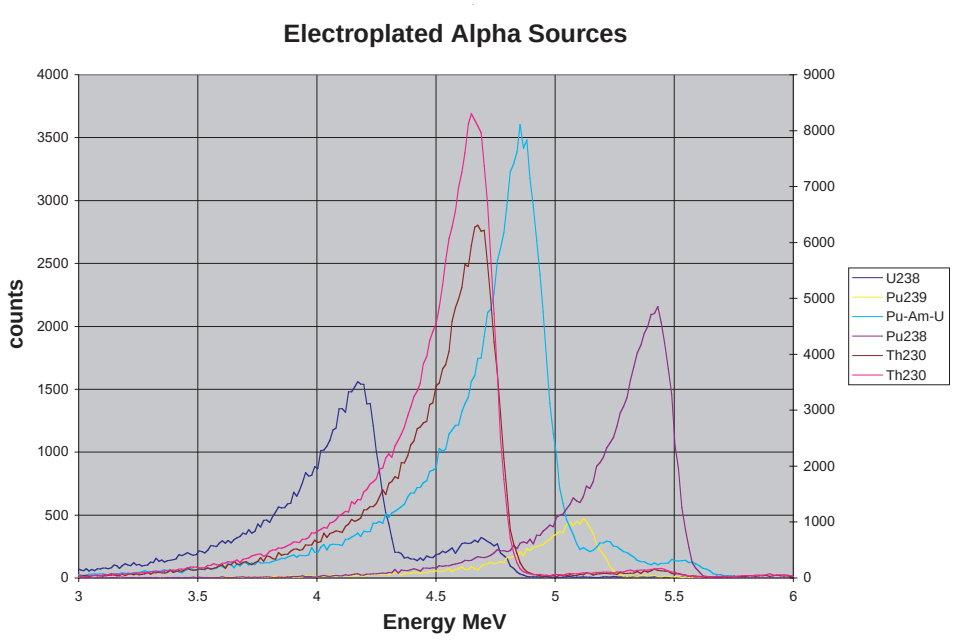

Figure 1. *Electroplated, single and multiple isotope, alpha particle sources measured using the prototype PCAM system.*

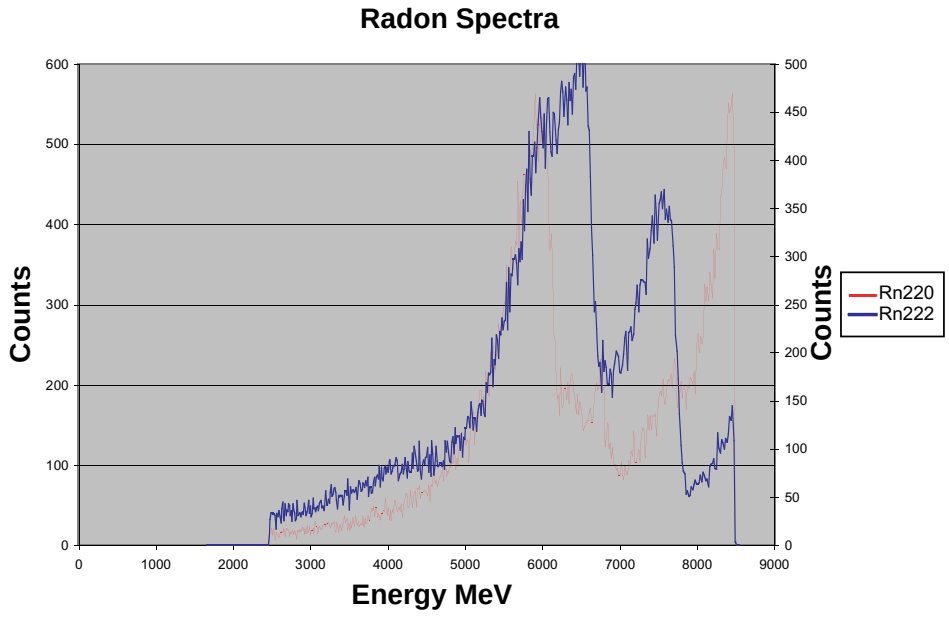

Figure 2. *Radon Spectra from natural uranium and thorium ores. Data represents several hours of collection on a filter with 2 liters per minute air flow rate. Data has been plotted using separate Y axis to normalize the peak counts. Note that both spectra contain mixtures of Rn^{222} and Rn^{220}.*

We tested our alarm algorithm for sensitivity and false alarm rates using a Monte Carlo technique. We randomly sampled a template consisting of the radon spectrum with an injected plutonium spectrum. The peak channel of the plutonium was scaled to be a percentage of the peak channel in the radon spectrum. For a plutonium signal of 100%, the counts in the energy channel at 5.15 MeV from plutonium was equal to the counts in the 6.05 channel because of radon. This situation has roughly one third of the total counts in the spectrum because there are more radon peaks than the 6.05 MeV peak. As each random count was generated, we treated it just as we would the counts arriving from the detector. It was added to the histogram, the background in the ROI and the alarm threshold were calculated, and the alarm function was evaluated. The number of counts required to produce an alarm was recorded. This was repeated for many runs to produce a likelihood function for an alarm. Table 1 has a summary of these results. The table indicates that when the injected plutonium signal is about 100%, then 50% of the alarms were generated within the first 19 counts in the detector. Within 45 counts, 99% of the alarms were generated.

Table 1. *Likelihood for detecting plutonium in a radon background.*

likelihood	10%	20%	25%	33%	50%	100%	injected signal
5%	45	22	15	13	7	7	
10%	88	33	27	21	13	7	
25%	182	57	42	33	21	13	
50%	317	99	68	46	32	19	
75%	497	148	102	68	42	26	
90%	664	203	139	91	55	33	
95%	764	239	164	108	62	38	
99%	986	313	221	142	78	45	

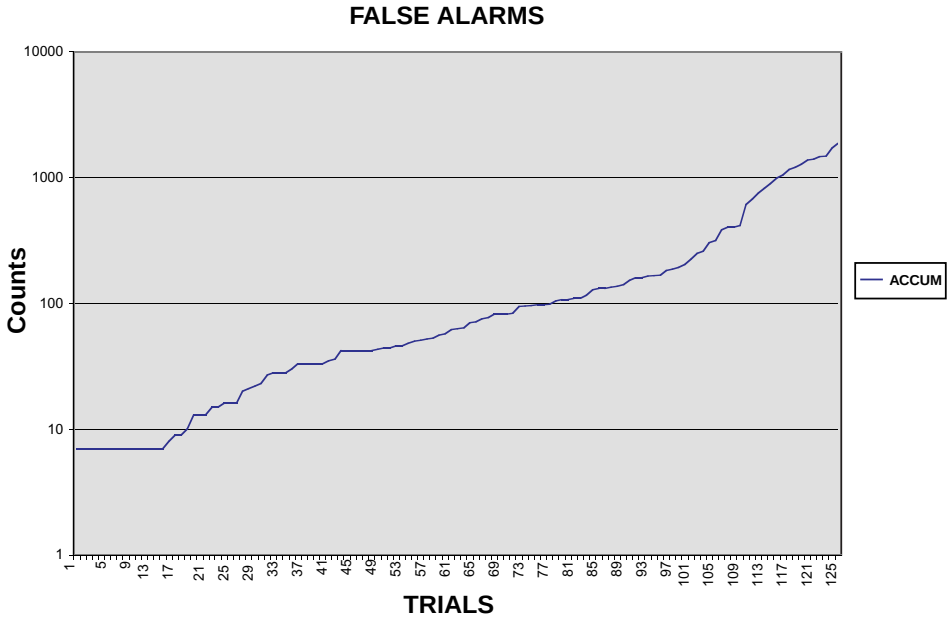

Figure 3. *False alarm level generated for 8500 data trials.*

To determine a false alarm rate, The template consisted of the radon spectrum alone. For each run, sampling was performed until the alarm level was exceeded or 10000 counts were generated. Figure 3 shows the false alarms for 8500 runs. Note that some of the false alarms happened with the minimum number of counts required to exceed the alarm threshold. This probability is similar to that of tossing a coin 7 times and obtaining seven 'heads' in a row. The step in the curve at 7 represents the minimum number of counts given Poisson statistics. A kink in the curve at 42 can be seen where the shift from Poisson to Gaussian statistics occurs. If the total counts expected in the PCAM for a 4 hour shift inside PF4 is 300 counts, then the false alarm rate would be 75/8500 or less than 1% per shift. (One has to look at the full table of 8500 runs to get this number).

Conclusions

We can infer from the results above that, given a radon background comparable to that in PF-4, the instrument will be able to detect a one-DAC plutonium 239 atmosphere and alarm in about 60 minutes, and that it will alarm in a 100-DAC atmosphere in about one minute.

A point of reference : a one-DAC atmosphere delivers about 0.042 mrem/minute to the unprotected worker, and a 100-DAC atmosphere delivers about 4.2 mrem/minute. Therefore, a worker in a one-DAC atmosphere will incur about 2.5 mrem committed effective dose equivalent (CEDE) before the PCAM alarms, and a worker in a 100-DAC atmosphere will incure about 4.2 mrem CEDE prior to the alarm.

The current false alarm rate appears to be less that 1% in units of 4-hr shifts, i.e., we can expect less than one PCAM false alarm for every 100 4-hr shifts worked. We do see some potential for improvement in this false alarm rate.

We plan on placing the PCAM into PF4 and the CMR building in order to obtain actual data in fiscal year 2002.

PRESCILA: Proton Recoil Scintillator Los Alamos Neutron Rem Meter

Principal Investigator: Richard H. Olsher (ESH-4)

Coinvestigators: David T. Seagraves, Shawna L. Eisele, Christopher W. Bjork, and William A. Martinez (ESH-4)

Funding: FY99 $15K, FY00 $12.5K, FY01 $20K

Introduction

Conventional neutron meters currently in use at Los Alamos and elsewhere are based on 1960s technology that relies on a large neutron-moderator assembly surrounding a thermal detector to achieve an accurate dose response. Typically, a BF_3 or ^3He gas-filled counter tube is positioned in the center of a heavy (e.g., 20 pounds) polyethylene moderator. The heavy moderator is necessary to obtain a useful response over a limited neutron energy range, from thermal to 10 MeV

In general, current rem meters are not only heavy and bulky, but possess poor high-energy response above 10 MeV, which makes them inaccurate for applications at high-energy accelerator facilities (e.g., Los Alamos Neutron Science Center (LANSCE)). Other disadvantages are high cost (as much as $6K) and poor ergonomics for field surveys. The photo above demonstrates the ease with which PRESCILA can be used to perform field surveys.

Our goal was to develop a practical proton recoil scintillator (PRESCILA) of low weight (5 pounds) with good sensitivity and gamma rejection, and enhanced high-energy response. PRESCILA offers the potential of replacing thousands of neutron rem meters in field applications around the world with a lightweight and more accurate design.

Benefits

(a) Radiation Protection (Group ESH-1) has requested a lightweight alternative to the standard rem meter to facilitate field surveys. The weight of the commercial version of PRESCILA is about 2 kg (4.5 pounds) versus the 10 kg (22 pounds) of a standard rem meter.

(b) The cost of maintenance of the current inventory is driven by the need to periodically replace the BF_3 detector tube ($300 ea.). Over the life of the inventory (130 rem meters), these costs are estimated to be $60,000. Maintenance costs for PRESCILA should be about 50% lower for a saving of $30,000.

(c) Poor energy response at high-neutron energies limits the ability of a standard rem meter to accurately measure dose around accelerator facilities, such as LANSCE. Standard rem meters with a pure polyethylene moderator seriously underestimate (by up to a factor of ten) neutron dose around accelerator facilities. A recent design trend has been to add heavy metal inserts to the polyethylene moderator to improve the high-energy response via spallation neutron generation. Birattari et al. (1990) were the first to investigate the use of a lead insert to enhance neutron response above the (n,2n) threshold of about 8 MeV. The Los Alamos design WENDI-II (Olsher et al. 2000) uses tungsten powder as both an absorber and neutron generator to extend the response function to 5 GeV. In both cases, there is a serious weight penalty as the moderator assembly exceeds 30 pounds in weight.

(d) As the PRESCILA rem meter is accepted throughout the Department of Energy (DOE) complex, cost savings and improved performance will be realized in every radiation protection program where neutron dose-hazards are present.

(e) The possibility of patenting this detector means royalty income to the Laboratory via licensing agreements with instrument vendors. Currently, Eberline Instruments and Ludlum Measurements, Inc., are in the process of licensing and commercializing the PRESCILA technology.

Objectives

During FY01 the project team investigated a final PRESCILA probe design with the following objectives:

- Finalize the fast and thermal scintillator development in collaboration with Eljen Technology and Ludlum Measurements, Inc.
- Optimize the detector-response function to obtain the most accurate energy response for operational spectra.
- Characterize the probe's performance using both benchmark neutron fields and operational spectra.
- Determine the optimum calibration protocol for the probe and the associated counter.

Methods and Results

Probe Design and Assembly. Figure 1 shows an exploded view of the final PRESCILA probe schematic. Fast and thermal scintillator elements are used to provide a wide energy response from thermal to well beyond 20 MeV. Light produced in the scintillators is collected by the Lucite light guide and transmitted to the photo multiplier tube (PMT), where it is converted into current. An ADIT sideview bialkali 1-inch PMT is positioned in a cylindrical cutout in the light guide. The light guide itself — as well as additional polyethylene — is used as moderating material for the thermal scintillator, which is located below the PMT.

The fast neutron signal is derived primarily from proton recoils in the hydrogenous matrix of the fast scintillator elements. The Eljen Technology EJ-400P scintillator is based on the work of Hornyak (Hornyak 1952) and Emmerich (Emmerich 1954) in the 50s. The original Hornyak detector was made by molding together a blended mixture of ZnS and Lucite powders. The original design suffered from poor efficiency because ZnS(Ag) absorbs its own light and limits the active phosphor volume that can transmit light to the PMT. Emmerich improved the light-collection efficiency by embedding sections of 1/8-in-thick Lucite sheet into the detector. The Lucite acted as a light guide for pulses originating inside the scintillator. This principle is taken to the extreme in the Eljen Technology EJ-410P design (Figure 2), which is the result of a collaborative effort with Eljen Technology and Ludlum Measurements, Inc. The strategy was to increase the surface area from which scintillation light may be emitted and to minimize self-absorption in the phosphor. A total of five phosphor rings is used; the thickness of each ring is approximately 2.5 mm.

The grooves are filled with a mixture of epoxy glue and ZnS(Ag) powder. This geometry minimizes light self-absorption and maximizes the phosphor surface area that can communicate light to the PMT. Some of the proton recoils reach and deposit energy in nearby grains of ZnS(Ag) phosphor. The phosphor grain size is on the order of 8 microns, which gives protons an advantage over secondary electrons for depositing significantly more energy per grain because of their higher stopping power (dE/dx). The resultant voltage pulse height generated by proton tracks is of sufficient magnitude to allow gamma pulse height discrimination. In contrast, plastic scintillators require pulse shape discrimination for effective gamma discrimination. Since standard health physics counters, such as the Eberline E-600, only provide pulse height discrimination, PRESCILA is compatible with existing off-the-shelf commercial counters.

Epithermal and intermediate energy neutron response is generated by the thermal scintillator (Eljen EJ-420P), an improved form of the Stedman scintillator (Stedman 1956). A mixture of ^{6}LiF

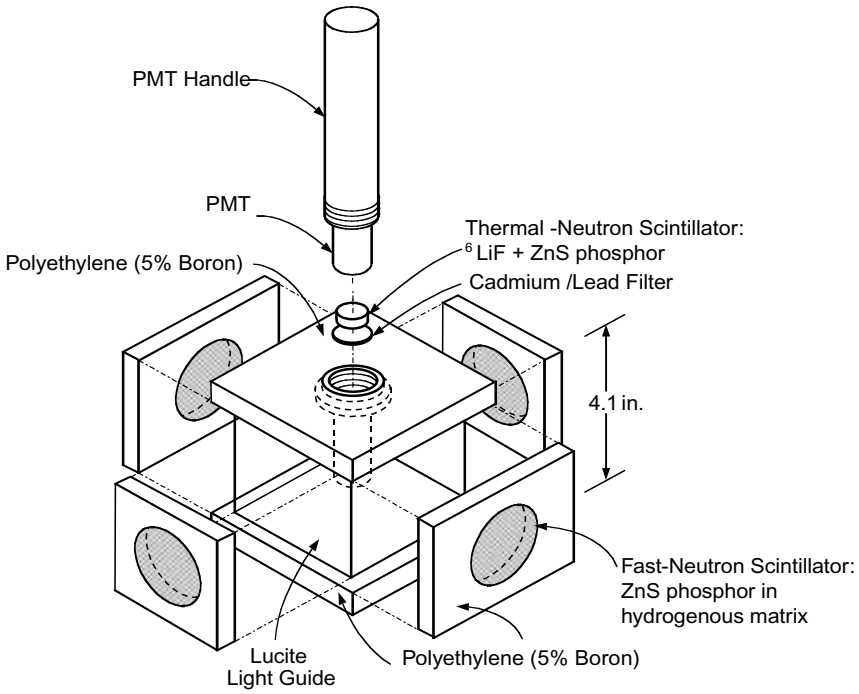

Figure 1. *An exploded view of the PRESCILA neutron rem meter (patent pending).*

Figure 2. *Elijen EJ410-P fast scintillator.*

and ZnS(Ag) powders is hot-pressed onto the back of a Lucite disc, with the active phosphor layer being convoluted to maximize light output. The percentage of ^{6}Li loading is adjusted to properly match the response of the fast scintillators. The $^{6}Li(n,\alpha)^{3}H$ reaction produces the ionizing tracks responsible for excitation of the phosphor. Both the triton and alpha particle have sufficient range to ionize nearby grains of phosphor.

A lead/cadmium filter is located directly below the thermal scintillator in order to further contour its response. The filter consists of a 1.12-in. diameter lead disc (0.015-in. nominal thickness) followed by a 0.75-in. diameter cadmium disc (0.015-in. thick).

Probe Energy Response. The energy response of the final PRESCILA prototype was investigated at the Physikalisch-Technische Bundesanstalt (PTB), the German Bureau of Standards, during July 2001. The irradiations included a series of monoenergetic neutron beams at the PTB Accelerator Facility, as well as bare and D_2O moderated ^{252}Cf irradiations.

The Accelerator techniques included all of the available ISO techniques: 24 keV, 144 keV, 250 keV, 565 keV, 1.2 MeV, 2.5 MeV, 5.0 MeV, 8.0 MeV, 14.8 MeV, and 19 MeV. These beams are produced by accelerating protons or deuterons onto ^{7}Li, tritium, and deuterium targets. The beams have been well characterized by the Neutron Dosimetry staff of the PTB using spectral measurements including time of flight techniques. The irradiations were performed in a low-scatter geometry in a large experimental hall (24 m x 30 m x 14 m). The contribution of room return and background was subtracted for each technique by performing an additional measurement using an appropriate shadow cone between the detector and neutron source. In the case of the 19 MeV technique, a large unwanted neutron contribution is generated because of (d,n) reactions in the target structural materials (Ti and Ag). An additional measurement was performed with a blank (untritiated) target. The blank target count rate was then subtracted from the primary measurement to correct for this source of background neutrons.

The results of these measurements are given in Figures 3, 4, and 5. The response function shown for PRESCILA is supplemented below 0.144 MeVwith Monte Carlo calculations using the Los Alamos code MCNP. A detailed model was used to track neutrons though the probe assembly. The absolute response of the thermal detector was calculated in terms of total number of capture reactions in ^{6}Li. The result was adjusted to match the experimentally determined response at 0.144 MeV. The MCNP calculations agree with experimentally determined response at 24 keV within 1.5%. Also shown are the calculated response functions for the Eberline NRD, Eberline WENDI, and the Andersson-Braun (AB) rem meters. The response per unit dose functions were normalized to a bare ^{252}Cf field to simulate the effect of such a calibration. Figure 3 shows the absolute response per unit fluence in units of counts-cm^2.

The sensitivity of PRESCILA is on par with that of the Eberline WENDI rem meter, and is a factor of 10 higher than that of the Eberline NRD. Sensitivity measurements in standard isotopic fields are summarized in Table 1.

The traditional energy response (per unit dose) is shown in Figures 4 and 5 for PRESCILA [both NCRP-38 and H*(10)], the Eberline NRD, and the Andersson-Braun (AB) or Snoopy rem meters. Figure 5 provides an expanded view of the energy range from 0.1 MeV to 20 MeV. The ideal response per unit dose is, of course, a uniform response of 1.0 at all neutron energies. All rem meters deviate from the ideal significantly. Below 0.1 MeV, PRESCILA's energy response exhibits an over response similar to that of current commercial models. In the range from 0.1 MeV to 1.0 MeV, the probe under responds with the response minima of 0.35 being at energy of 0.565 MeV. PRESCILA was designed so that the over-response balances out the under-response to provide a reasonably uniform response for typical field spectra.

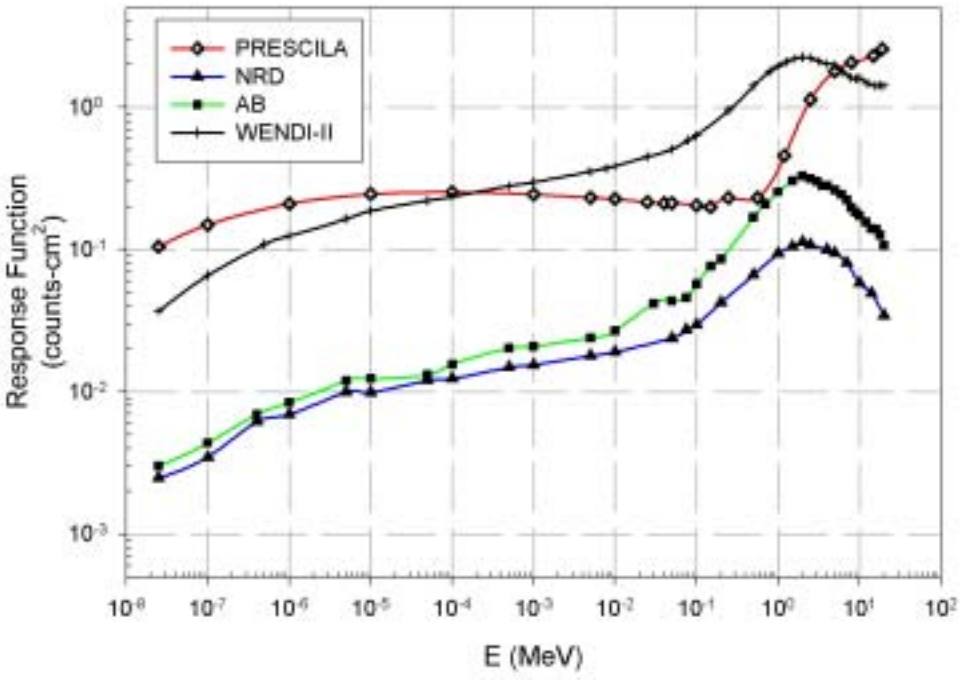

Figure 3. *Response per unit fluence.*

Table 1. *Rem meter sensitivity (NCRP-38 Dose)*

Model	Bare ^{252}Cf (cpm/mrem/h)	D_2O Moderated ^{252}Cf (cpm/mrem/h)	^{241}AmBe (cpm/mrem/h)
PRESCILA	420	690	610
NRD	39	51.4	30.7

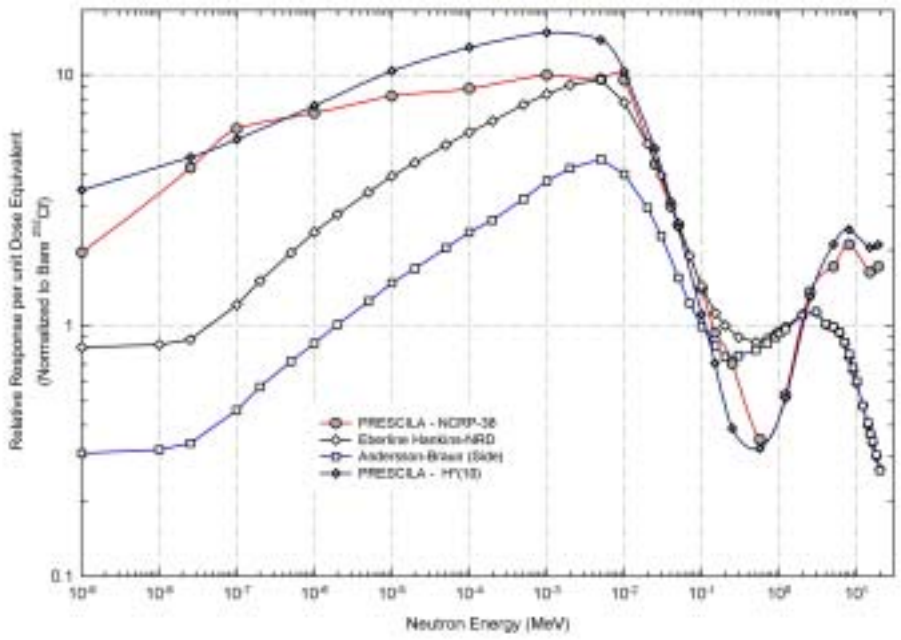

Figure 4. *Energy response functions per unit dose.*

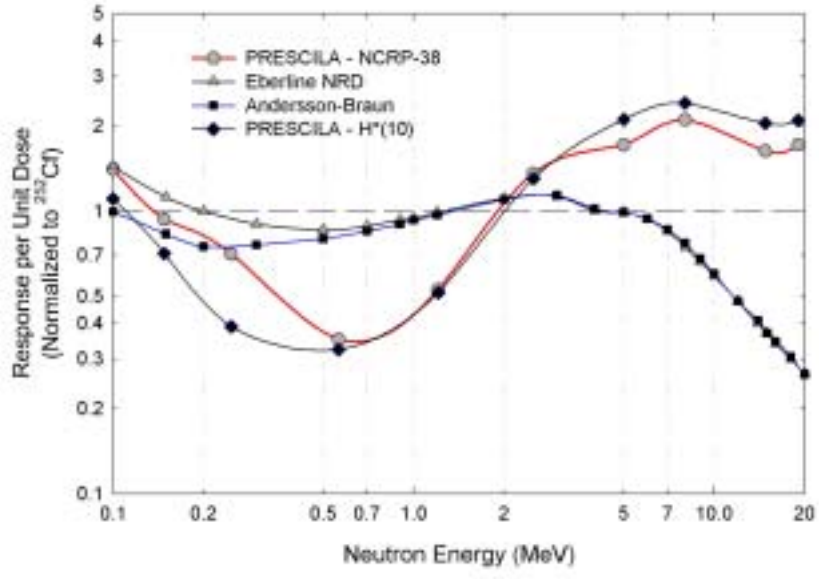

Figure 5. *Energy response functions.*

The predicted response of PRESCILA in a variety of benchmark and operational neutron fields was calculated by folding the fluence response function (Fig. 3) with published neutron spectra. Almost all of the spectra, including a representative selection of pressurized water reactor fields (PWR) were derived from the IAEA's Technical Report 318 (IAEA, 1990). The calculations are summarized in Table 2 and provide a virtual glimpse of PRESCILA's expected field performance. The nomenclature for the neutron fields is identical to that given in the IAEA report. The absolute response (cpm per unit dose) is given as well as the relative response referenced to a bare ^{252}Cf calibration.

For most operational spectra, a bare ^{252}Cf calibration is optimum and gives the most conservative response. For accelerator produced high-energy fields, a ^{241}AmBe calibration is most suitable. Unlike both the NRD and AB meters, which decrease monotonically in response above 7 MeV, PRESCILA's response is quite uniform from 2 MeV to 19 MeV, the high-energy limit of the PTB facility. Indications are that its high-energy response is extended beyond 100 MeV, based on irradiations and field-test measurements obtained at the LANSCE.

Table 2. *PRESCILA Response in various benchmark and operational fields.*

Neutron Spectrum	Response (cpm/mrem/h)		Relative Response: Bare ^{252}Cf Calibration	
	NCRP-38	H*(10)	NCRP-38	H*(10)
Bare ^{252}Cf	413	361	1.00	1.00
^{252}Cf in 18-inch diameter polyethylene sphere	485	433	1.17	1.20
^{252}Cf Skyshine	357	291	0.86	0.81
D_2O moderated ^{252}Cf	689	602	1.67	1.67
^{241}AmBe	617	586	1.49	1.62
Bare $^{238}PuO_2$	443	383	1.07	1.06
Cm_2O_3 power source	416	362	1.00	1.00
Bare PuF_4 source	252	210	0.61	0.58
BWR E/3-X29	366	279	0.88	0.77
PWR I/1-IV	595	451	1.44	1.25
PWR F/5	728	555	1.76	1.54
PWR G/3	602	469	1.46	1.30
PWR H/12	585	455	1.42	1.26
PWR 1L-1	540	414	1.31	1.15
Medical Accelerator: 25 MeV Phot Tungsten, through 90 cm concrete	529	470	1.28	1.30
25 MeV photons on Tungsten, skyshine	384	310	0.93	0.86
Medical Accelerator: U-120 Cyclotron, unshielded	696	684	1.68	1.89
Fusion Reactors: Tokamak, First wall	467	398	1.13	1.10
Natural Uranium pile (5 ton)	400	300	0.97	0.83

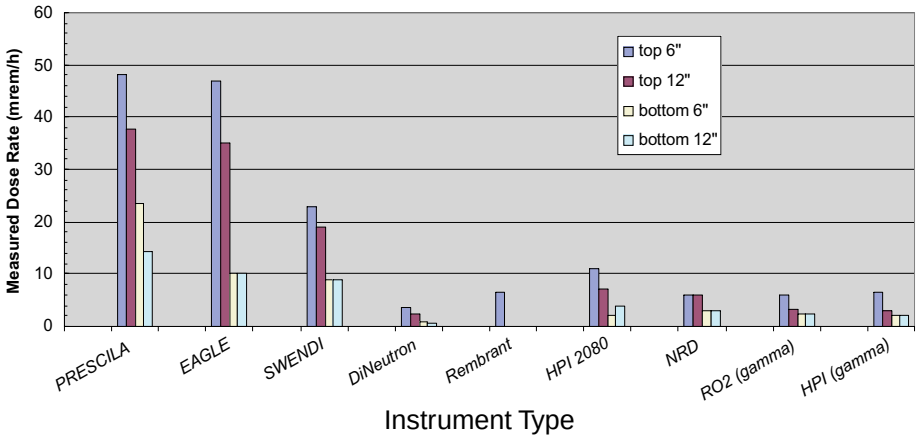

Figure 6. *4WNR15L flight path survey.*

Field Measurements. Limited field testing of two preproduction prototypes was completed at Los Alamos during 2001. Both probes were mated to Eberline E-600 counters.

One probe, calibrated to ^{241}AmBe neutrons, participated in a survey of Flight Path 15L, Target 4, WNR facility south yard, at LANSCE. Target 4 is a tungsten target that is routinely irradiated by a 800 MeV proton beam for spallation neutron production. PRESCILA and several other neutron rem meters obtained dose rate data at several distances from the flight path beam tube. The neutron beam is highly collimated, so the measurements represent scatter primarily because of interactions in the beam tube's walls and air fill. The results are summarized in Figure 6. The EAGLE is a modified version of the HPI 2080 pulsed neutron rem meter, and features a tungsten powder loaded moderator assembly for extended high-energy response to 5 GeV. The PRESCILA data agree closely with the EAGLE measurements.

The second PRESCILA rem meter, calibrated to ^{252}Cf neutrons, was used at a plutonium processing facility at Los Alamos in conjunction with other instruments to map out the neutron dose rates in several rooms. The results are summarized in Table 3.

Under the instrument list, ROSPEC refers to BTI Inc.'s Rotational Spectrometer. SWENDI refers to Eberline's Smart WENDI rem meter, and REMbrandt refers to Apfel Enterprises' neutron survey meter Model AP2001. The ROSPEC was first used to measure the neutron spectrum at the locations indicated, and then it calculated the corresponding dose by folding in an appropriate fluence to dose-conversion function. Based on previous studies, ROSPEC dose measurements are believed to be accurate to within 10%. Where ROSPEC results were available, PRESCILA measurements in general agreed within 21%.

Table 3. *Field survey data for plutonium processing facility.*

Location	Instrument	Dose Rate (mrem/h)
Vault, Room A	PRESCILA	9.8
	ROSPEC	8.1
	SWENDI	10.3
	REMbrandt	6.9
Vault, Room C	PRESCILA	66.2
	ROSPEC	63.1
	SWENDI	83.3
Vault, Room E	PRESCILA	64.6
	ROSPEC	62.1
	SWENDI	77.7
	REMbrandt	21.9
Vault, Room G	PRESCILA	38.4
	ROSPEC	33.3
	SWENDI	39.1
	REMbrandt	31.8
Vault, Room J	PRESCILA	66.0
	SWENDI	73.4
	REMbrandt	37.7
Vault, Room K	PRESCILA	54.0
	SWENDI	60.4
	REMbrandt	26.1
Hallway/Room A	PRESCILA	12.1
	SWENDI	13.2
	REMbrandt	4.8
Hallway/Room G	PRESCILA	18.6
	SWENDI	18.5
	REMbrandt	9.3
Hallway/Room K	PRESCILA	13.2
	SWENDI	12.7
	REMbrandt	7.9
Hallway/Room M	PRESCILA	15.2
	SWENDI	16.1
	REMbrandt	12.3

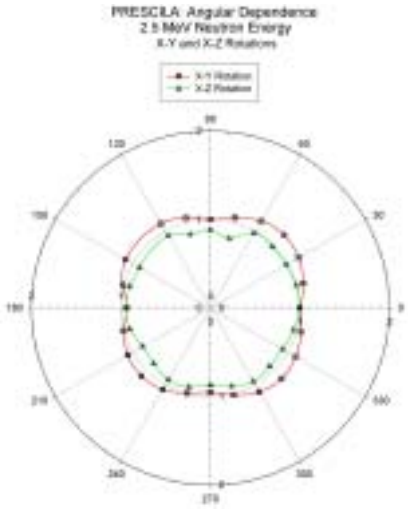

Figure 8.

Angular Dependence. The angular dependence of the PRESCILA probe was investigated at PTB at low (0.144 MeV), intermediate (2.5 MeV), and high-neutron energies (14.8 MeV). Data were collected for both X–Y and X–Z planes of rotation (the Z-axis is defined along the handle of the probe). The results are presented in Figures 7, 8, and 9.

Typically, response uniformity was within +/15% for all three energies tested and both rotations. The maximum deviation, about 22% over response, was measured during the X–Z rotation at 144 keV for the bottom facet of the probe.

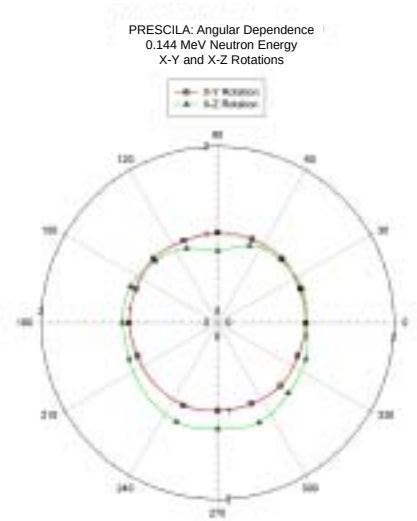

Figure 7.

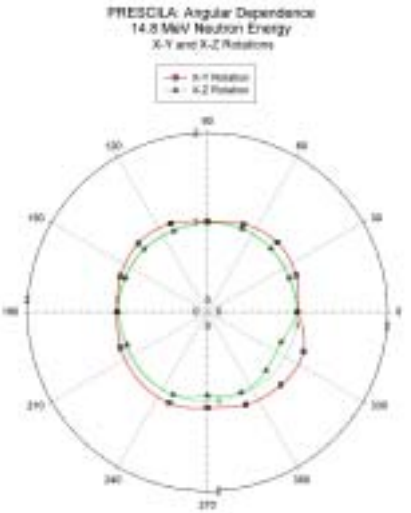

Figure 9.

Response Linearity. The dose rate linearity of PRESCILA was investigated at PTB using the Accelerator Facility's Cyclotron and the $^{2}H(d,n)^{3}He$ reaction, which produces an intense 8 MeV neutron beam. In addition, the response linearity below 100 mrem/h was studied at the PTB Bunker facility using a bare ^{252}Cf source. All of the measurements were conducted with the Eberline E-600 counter. The results are summarized in Figure 10.

The response becomes nonlinear at dose rates in excess of 600 mrem/h because of coincidence counting of small pulse height events. These are proton recoil events that individually would not exceed the upper discriminator setting and trigger a count. However, at high-count rates on the order of 500,000 cpm, coincidence results in increased counting efficiency. As the count rate exceeds about 10^{6} cpm, dead time becomes severe enough to reduce the response per unit dose. The under response is 45% at a dose rate of 2.5 rem/h.

Gamma Rejection. The gamma spillover into the neutron channel was investigated at both Los Alamos and PTB using a ^{137}Cs field, and at Los Alamos using ^{137}Cs and ^{60}Co, and fluorescent x-ray fields. When the neutron channel discriminator is properly set for a neutron response of 410 cpm/mrem/h (bare ^{252}Cf), the gamma spillover was determined to be approximately linear up to an exposure rate of 100 mR/h. The gamma response was also found to be relatively independent of energy over the range from 100 keV to 1.2 MeV. Above 100 mrem/h gamma, the response was found to become nonlinear up to several hundred mR/h and finally saturate in fields over 500 mrem/h gamma.

The gamma spillover magnitude was determined to be typically in the range of 2–3% of the photon exposure rate in pure gamma fields. In a 58 mrem/h gamma field, the corresponding response in the neutron channel was measured to be 1 mrem/h, amounting to only a minor over estimate of the total dose rate. In mixed gamma-neutron fields, the gamma contribution increases because of coincidence counting. Combining a 58 mrem/h gamma field with a 77 mrem/h ^{252}Cf neutron field, resulted in a 14.6% over response in the neutron channel. However, use of the Eberline E-600 counter's spillover correction capability allows for dynamic correction of the gamma signal by subtraction of a small percentage (2%) of the lower channel from the upper (neutron) channel. For the spillover correction to work properly, however, the lower and upper channels need to be defined correctly (see section on calibration protocol).

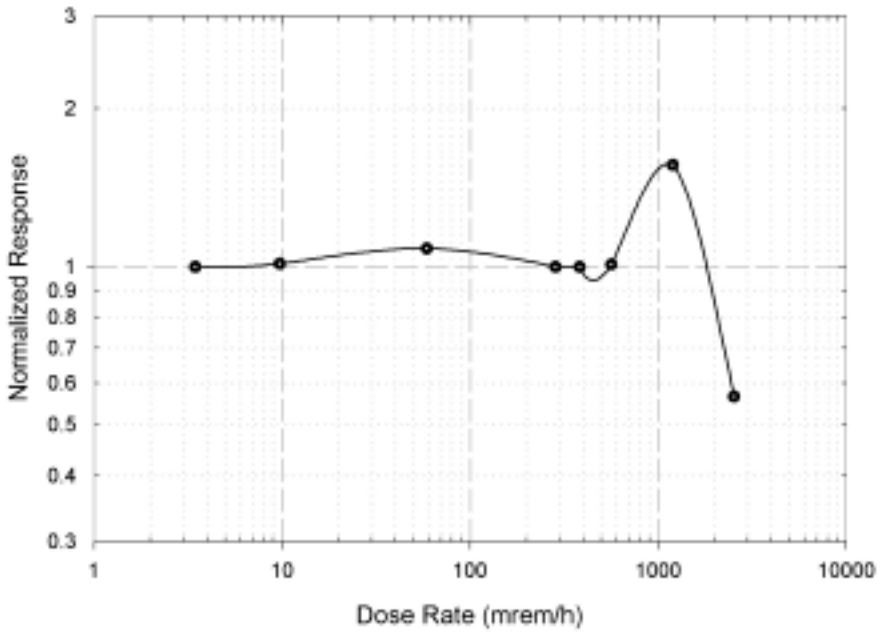

Figure 10. *PRESCILA: response linearity.*

Calibration Protocol. The Eberline E-600 counter's functionality ideally suits the needs of the PRESCILA probe, so one of the research objectives was to determine an optimum calibration procedure for this particular combination. The following general procedure is recommended:

- Set the probe high voltage to 635 V.
- Select the upper window of channel 1 as the neutron channel.
- Set the dead time to 8 μs
- Position the probe in either a ^{252}Cf or $^{241}AmBe$ field—depending on the calibration spectrum desired.
- Adjust the upper discriminator to obtain a response of 410 (+/-5%) cpm/mrem/h for ^{252}Cf or 590 (+/- 5%) cpm/mrem/h for $^{241}AmBe$. The exact discriminator setting is a function of the PMT gain.
- Set the calibration constant in counts/rem equal to: (cpm/mrem/h)(60,000).
- Calculate the lower discriminator setting as 40% of the upper discriminator. Adjust the lower discriminator accordingly.
- Set the lower-to-upper channel crossover to 0.02.

Measurements have shown that the reproducibility of the threshold settings among E-600 counters varies by as much as 30%. Since the proton recoil distribution is uniform from the spectrum maximum to the lower threshold, any relative shift in the upper discriminator setting impacts neutron channel accuracy. For this reason, it is recommended that each probe be dedicated to a particular E-600 counter and be calibrated as a unit.

Conclusion and Deliverables

A final PRESCILA probe design is now ready for licensing. Its salient performance features are as follows:

(a) Extended energy response to beyond 20 MeV

(b) Excellent sensitivity (410 cpm/mrem/h for bare ^{252}Cf)

(c) Uniform directional response over a wide range of energies

(d) Low weight (4.5 pounds)

(e) Good gamma rejection in fields up to 100 mR/h

On March 9, 2001, the Laboratory filed a patent application (DOE Docket No. S-96,584) for the PRESCILA neutron rem meter. Licensing negotiations are in progress with both Eberline Instruments and Ludlum Measurements, Inc. A commercial version of PRESCILA is expected to be available to the health physics community in early 2002.

References

Birattari, C., A. Ferrari, C. Nuccetelli, M. Pelliccioni, and M. Silari, "An extended range neutron rem counter," *Nucl. Instrum. Methods* A**297**:250–257 (1990).

Compendium of Neutron Spectra and Detector Responses for Radiation Protection Purposes, Technical Report Series No. 318, International Atomic Energy, Vienna (1990).

Emmerich, W. S., "A Fast Neutron Scintillator," *Rev. Sci. Instr.* **25**:69–70 (1954).

Hornyak, W. F., "A Fast Neutron Detector," *Rev. Sci. Instr.* **23**:264–267 (1952).

Olsher, R.H., H.H. Hsu, A. Beverding, J.H. Kleck, W.H. Casson, D.G. Vasilik, and R.T. Devine, "WENDI: An Improved Neutron Rem Meter," *Health Phys.* **70**:170–181 (2000).

Stedman, R., "Scintillator for Thermal Neutron using ^{6}LiF and ZnS(Ag)," *Rev. Sci. Instr.* **31**:1156 (1956).

Rapid Discrimination of Personnel Contamination Due to Radon versus Other Alpha-Emitting Radionuclides

Principle Investigator: James T. Voss, Operational Health Physics (ESH-1)

Coinvestigator: William Martinez, Health Physics Measurements (ESH-4)

Funding: FY99, $22.2K; FY00, $18K; FY01, $18K

Introduction

Personnel, clothing, and other items may become contaminated with unknown radioactive isotopes. Naturally occurring radon and thoron progeny impact the determination of the sources of contamination due to their collection on electrostatic surfaces, such as plastic items and synthetic clothing, and their subsequent transfer to personnel or clothing.

The present available methods of determining whether the contamination is because of radon or other radionuclides include:

(1) determining the alpha-to-beta ratio (this may be accomplished with hand-held alpha-beta friskers in the field or by counting samples with gross alpha-beta laboratory counters);

(2) recounting the sample after a short decay period to confirm short-lived or long-lived isotopes;

(3) alpha spectroscopy;

(4) beta spectroscopy; and

(5) gamma spectroscopy.

These methods all take time and may prove to be inconclusive. The time required to determine if contamination comes from radon results in (1) lost productivity while the worker and the surveyor(s) make the determination and (2) increased anxiety in the worker while the determination is made. These methods also potentially impact worker safety and health if medical treatment for a potential uptake is necessary. If the unknown contaminant is one of several possibilities, the investigation of the source of contamination takes longer.

Positively identifying the radioactive contaminant if it is not radon or thoron progeny has several benefits. A summary of the field methods of identifying specific radionuclides is presented later in this report.

Methods of minimizing the presence of radon and thoron progeny have recently come under investigation. A brief discussion of these methods is included in this report.

Timed Coincidence Counting and Alpha-Particle Energy Discrimination

Two additional methods of radon and thoron discrimination are under development. The timed coincidence method is currently in Los Alamos National Laboratory's (LANL, the Laboratory) patenting process, and development of the supporting hardware and software continues. Alpha-particle energy discrimination applied to our standard detectors is also being developed. A discussion of these two methods is included later in this report.

Radiological Incident Reports

There are approximately 300 Radiological Incident Reports (RIRs) written for personal and/or clothing contamination incidents at LANL each year. The number of personnel and/or clothing RIRs written for contamination since our first evaluation in 1996 has not declined. Any personal or clothing contamination due to other than radon or thoron must be reported as an RIR. A simple RIR may cost $10,000 in person-hours per incident (300 incidents times $10,000 = $3,000,000/yr). Radon or thoron progeny are responsible for approximately 150 contamination events each year. The determination that these contamination events are due to radon or thoron may cost as much as $2,000 each event in person-hours (150 events times $2,000 per event = $300,000/yr).

In two large nuclear facilities at LANL, TA-55 and CMR, the number of alarms on PCMs (personnel contamination monitors) averages several each day. The number of individual personnel surveys through the PCMs at these two facilities is several hundred each day. The alarm rates for the two facilities are in the range of less than one percent (<1%) to nearly two percent (2%). Most of these alarms are because of radon and/or thoron progeny contamination. The variations in these false alarms are because of changes in atmospheric conditions and the physical structure of the two facilities. The air ventilation system at TA-55 is high-efficiency particulate air (HEPA) filtered, while the ventilation system at CMR uses typical industrial roughing filters. At both facilities, some areas have less ventilation than others, allowing higher levels of radon and thoron to build up.

Rapidly ruling out radon or thoron progeny as the contaminant allows the investigation of the cause of the contamination to proceed more efficiently. Being able to identify the contamination as radon or thoron also allows normal operations to resume in a timely manner and minimizes worker concerns about radiological safety. Being able to identify the specific isotope allows the investigation into the causes of the incident to be directed to only those operations and locations where that specific isotope is present. In addition, this rapid identifica-

tion of the isotope assists ESH-2's response to personnel contamination events. Reducing the time to determine whether the contamination is from radon or thoron results in a person-hour cost saving equal to the percent reduction in the time required.

The person-hours lost in responding to contamination alarms because of radon or thoron amounts to more than $2,000,000 per year at LANL and is estimated to be more than $20,000,000 in all of DOE.

A small percentage (perhaps 10 %) of those incidents of personal or clothing contamination reported in the RIRs may be caused by radon or thoron, but we do not have the capability or resources to make the determination at the lower regulatory limits for personal contamination. The potential cost savings is (300 incidents/yr x 0.10 x $10,000/incident) $300,000/yr.

Methods of Discriminating Radon and Thoron Progeny from other Alpha Emitters

The radon and thoron interference in alpha contamination discrimination is because of the 7.68 MeV ^{214}Po and 6.0 MeV ^{214}Po alpha-energy peaks from ^{222}Rn decay and the 8.78 MeV ^{212}Po and 6.05 MeV ^{212}Bi alpha-energy peaks from ^{220}Rn decay (see Figure 1). Radon and thoron exist everywhere in our environment and become a source of confusion when personnel or their clothing are contaminated with this natural radioactivity.

It is desired to be able to: (1) detect other alpha-emitting isotopes such as ^{239}Pu, ^{238}Pu, ^{241}Am, ^{238}U, ^{235}U, and ^{234}U in the presence of interferences from radon and thoron progeny; (2) to achieve a detection limit of less than 300 dpm/100 cm^2 for the isotopes of interest using a short count time; and (3) to determine if the contamination is one of tranuranics, uranium, or thorium sources.

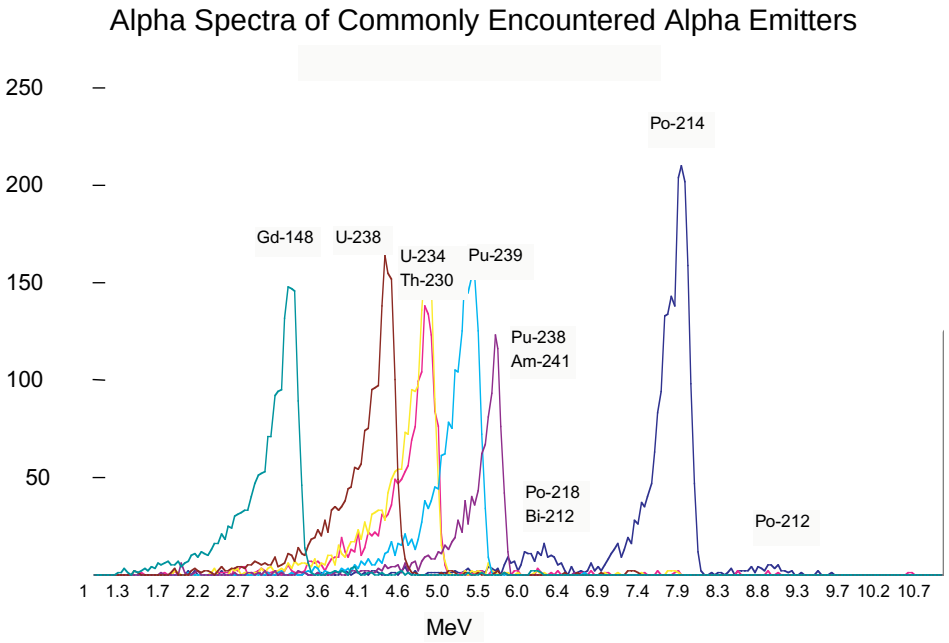

Figure 1. *Alpha Spectra.*

The typical personnel contamination response begins with a contamination alarm on a whole-body frisker such as the Eberline PCM-2 (see Figure 2). The PCM-2 uses multiple P-10 (10% methane and 90% argon) gas-flow detectors for alpha and beta particle detection. A whole-body frisk is then performed by the responding RCT (radiological control technician) using a hand-held contamination detector. A whole-body frisk using a 100-cm^2 detector takes 2 to 3 minutes. The spot of contamination or the article of clothing may be removed and allowed to radioactively decay for a short period of time before another measurement is made. Radon progeny have an effective half-life of approximately 30 minutes while thoron progeny have an effective half-life of approximately 10.5 hours. When the hand-held contamination detector shows no detectable activity and the PCM-2 does not alarm, then the

Figure 2. *Eberline PCM-2.*

activity is determined to have been radon or thoron progeny.

Alpha-to-Beta Ratio using the PCM-2

The determination of the alpha-to-beta ratio using the PCM-2's indication and the hand-held contamination monitor (such as the Eberline E-600/SHP-380) gives further confidence that the contaminant is radon or thoron progeny if the ratio is approximately 1:2. However, this method is not absolute because a mixture of alpha and beta emitters other than radon or thoron progeny could have been encountered. The uranium isotopes also have a similar alpha-to-beta ratio.

A complication arises in comparing the level of contamination reported by the PCM-2 and the level determined with hand-held survey instruments. The 34 detectors on the PCM-2 range in active surface area from about 150 cm^2 to over 600 cm^2. The hand-held survey instruments' active surface areas range from 15.5 cm^2 to 100 cm^2. In many cases the surface area of the spot of contamination is greater than the active surface area of the hand-held instrument. If the spot of contamination is larger than the active surface area of the hand-held instrument, then that instrument will indicate a level of contamination less than that reported by the PCM-2 by a ratio of the instrument's active surface area divided by the area of the spot of contamination. If a 15.5-cm^2 detector is used to monitor an area of contamination of 300 cm^2, then the hand-held instrument will indicate 1/20 (15.5-cm^2 divided by 300 cm^2) of the level reported by the PCM-2.

Alpha-to-Beta Ratio using Hand-held Instruments

The primary hand-held instruments used by the technicians responding to an indication of personnel or clothing contamination are the Ludlum 139, with an air proportional alpha-only detector, and the Eberline E-600, with the SHP-380 detector or the SHP-330 detector. See Figures 3–6. The Ludlum 139 is an early 1980s generation instrument with a detector active surface area of 76 cm^2. The Eberline E-600 is a mid 1990s generation instrument. The SHP-380 and SHP-330 are used with the E-600 for alpha and beta particle detection. The SHP-380 uses ZnS (zinc sulfide-silver actvated) bonded to a plastic scintillator and has an active surface area of 100 cm^2. The SHP-330 is a sealed gas-proportional detector using a mixture of argon and CO_2 and has an active surface area of 15.5 cm^2. Since the Ludlum 139 is an alpha-only instrument, it cannot be used to determine the alpha-to-beta ratio. In addition to the differences in detector active surface areas described earlier, there is another confounding problem in the alpha and beta particle detection efficiencies of the different types of detectors. The different detectors are typically calibrated with similar radionuclides and will indicate correctly when used to monitor radionuclides with energies similar to those used for the calibration. However, the different detectors have different alpha and beta energy versus efficiency slopes. Therefore, the different types of detectors will not indicate the same alpha-to-beta ratios when measuring the same spot of contamination.

Figure 3. *Ludlum 139*

Figure 4. *Eberline E-600*

Figure 5. *SHP-330*

Figure 6. *SHP-380*

Figures 3-6. *The primary hand-held instruments used by technicians.*

Recounting the Sample after a Short Decay Period to Confirm Short-lived or Long-lived Isotopes

Any of the instruments described earlier may be used to recount the sample or spot of contamination. If the contamination is from radon, then this method will work; however, it does require several minutes for the radon progeny to decay to less than detectable limits. Radon progeny have an effective half-life of approximately 30 minutes (see Figure 7). The determination that radon progeny is present does not ensure there are no detectable radionuclides of interest such as plutonium. Unfortunately, we also have to deal with thoron progeny on occasion. Thoron progeny have an effective half-life of approximately 10.5 hours (see Figure 8); so, the option of allowing a period of time for decay does not work if a person is contaminated with thoron progeny. If a sample of the contamination can be taken, then it can be counted locally using an alpha/beta sample counter such as the Ludlum 2929 with the 43-10-1 ZnS/plastic scintillator detector. See Figure 9 below.

Figure 9. *Ludlum 2929.*

Alpha, Beta, and Gamma Spectroscopy

Alpha, beta, or gamma spectroscopy can sometimes be used to identify the specific isotopes.

Alpha-Particle Emitting Isotopes

Figure 10, Radionuclides of Interest, indicates the relative energies of some typical alpha particle emitters. Attenuation of the alpha particle reduces the measure alpha energy and spreads the spectrum, making energy resolution of the various peaks more difficult.

^{222}Rn (radon) decay from ^{238}U

Isotope & Half-life	α Energy (MeV) & abundance	β Energy (MeV) & abundance	γ Energy (MeV) & abundance
^{222}Rn / 3.823 d	5.49 @ 100%	No	0.510 @0.07%
^{218}Po / 3.05 m	6.00 @ 100%	0.33 @ 0.019%	negligible
^{214}Pb / 26.8 m	No	0.65 @ 50% 0.71 @ 40% 0.98 @ 6%	0.295 @ 19% 0.352 @ 36%
^{214}Bi / 19.7 m	negligible	1.00 @ 23% 1.51 @ 40% 3.26 @ 19%	0.609 @ 47% 1.120 @ 17% 1.764 @ 17%
^{214}Po / 164 us	7.69 @ 100%	No	0.799 @ 0.014%
^{210}Tl / 1.3 m	No	1.3 @ 25% 1.9 @ 56% 2.3 @ 19%	0.296 @ 80% 0.795 @ 100% 1.31 @ 21%
^{210}Pb / 21 y	negligible	0.016 @ 85% 0.061 @ 15%	0.047 @ 4%
^{210}Bi / 5.01 d	negligible	1.161 @ 100%	negligible
^{210}Po / 138.4 d	5.305 @ 100%	No	negligible
^{206}Tl / 4.19 m	No	1.571 @ 100%	negligible

Figure 7. *Radon Decay Chain.*

^{220}Rn (thoron) decay from ^{232}Th (thorium)

Isotope & half-life	α Energy (MeV) & abundance	β Energy (MeV) & abundance	γ Energy (MeV) & abundance
^{220}Rn 55s (Thoron)	6.29 @ 100%	No	0.550 @ 0.07%
^{216}Po / 0.15 s	6.78 @ 100%	No	negligible
^{212}Pb / 10.64 h	No	0.346 @ 81% 0.586 @ 14%	0.239 @ 47% 0.300 @ 3.2%
^{212}Bi / 60.6 m	6.05 @ 25% 6.09 @ 10%	1.55 @ 5% 2.26 @ 55%	0.040 @ 2% 0.727 @ 7% 1.620 @ 1.8%
^{212}Po / 304 ns	8.78 @ 100 %	No	negligible
^{208}Tl / 3.10 m	No	1.28 @ 25% 1.52 @ 21% 1.80 @ 50%	0.511 @ 23% 0.583 @ 86% 0.860 @ 12% 2.614 @ 100%

^{212}Bi decays 64% of the time to ^{212}Po through beta decay and 36% of the time to ^{208}Tl through alpha decay.

Figure 8. *Thoron Decay Chain.*

Radionuclides of Interest

Isotope & Half-life	α Energy (MeV) & abundance	β Energy (MeV) & abundance	γ Energy (MeV) & abundance
^{239}Pu 24,100 years	5.105 @ 11.5% 5.143 @ 15.1% 5.155 @ 73.3%	No	0.052 @0.02% 0.129 @0.0062% 0.375 @ 0.0015% 0.414 @ 0.0015% Uranium x-ray 0.014 @ 4.4%
^{238}Pu 87.7 years	5.358 @ 0.1% 5.456 @ 28.3% 5.499 @ 71.6%	No	0.044 @ 0.039% 0.100 @ 0.0075% 0.153 @ 0.0013% Uranium x-ray 0.014 @ 11.6%
^{241}Am 432.7 years	5.388 @ 1.4% 5.443 @ 12.8% 5.486 @ 85.2%	No	0.026 @ 2.4% 0.033 @ 0.1% 0.060 @ 35.9% Neptunium x-ray 0.014 @ 43%

Figure 10. *Radionuclides of Interest.*

Alpha Spectroscopy

Alpha spectroscopy is performed in the field using the SAIC AP-2 hand-held instrument (see Figure11). This instrument has an alpha energy resolution full width at half-maximum peak height (FWHM) of about 200 keV. If the alpha emitters on the spot of contamination are not attenuated, then the AP-2 can resolve the alpha energies well enough to distinguish radon progeny alpha emitters from the other alpha emitters. However, such things as clothing and hair do attenuate the alpha energies and cause the spectrum on the AP-2 to be smeared into the lower energy range. See figures at right.

The AP-2's detector is a 50-mm diameter ion-implanted silicon detector with a honeycomb-like metal cover that collimates the alpha particles to improve the instrument's alpha particle energy resolution (see Figure 11). The liquid crystal display (LCD) on the face of the instrument displays either a bar graph with count rate indication or a real-time alpha spectrum.

Two AP-2s are in use at Los Alamos, one at TA-55 and one at CMR. In general, we have had success in rapidly responding to contamination alarms and determinging the true cause of contamination with these instruments. We are developing our own instruments to address the AP-2's problems of high initial cost, ergonomics, and lack of spectrum processing ability. The prototype of this new instrument uses the Rainbow MCA (multi-channel analyzer, described elsewhere in this report) connected to a solid-state silicon detector.

Figure 11. *SAIC AP-2 Detector, front and back views.*

Beta Spectroscopy

Beta spectroscopy is not routinely performed in the field, but it has some potential for identifying the radioactive contaminant. At present, there are no portable-low-cost beta spectroscopy systems commercially available. We are developing a portable beta spectroscopy system using a 75-mm-diameter plastic scintillator coupled to a 75-mm-diameter photo-multiplier tube (PMT). The first prototype uses the Rainbow MCA. See Figures 12 and 13 on the right.

Beta-Particle Emitting Isotopes

These beta spectra were taken with a plastic scintillator similar to the one pictured (see Figure 12). The short-lived progeny of uranium-238 have a beta energy maximum (e-max) of 193 keV (thousand electron volts) and 2.2 MeV (million electron volts). Tc-99 has a beta energy e-max of 292 keV. These spectra indicate that a plastic scintillator can discriminate between those beta energies. See Figures 14 and 15 at right.

Figure 12. *Plastic scintillator and PMT.*

Figure 13. *Rainbow MCA.*

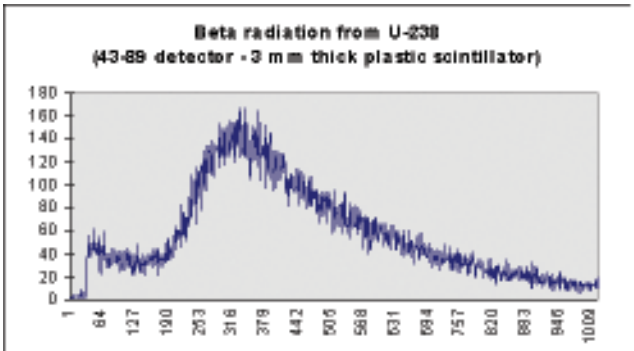

Figure 14. *Beta radiation from U-238 progeny.*

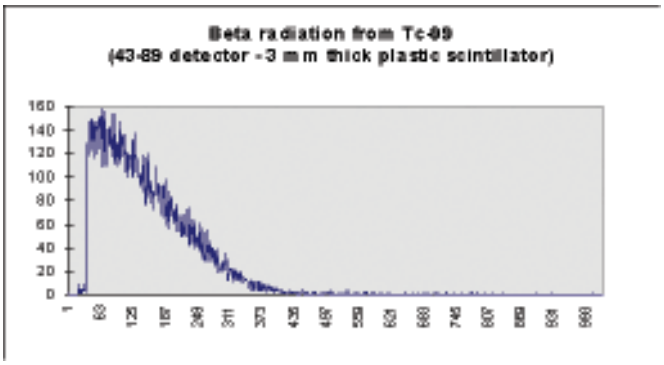

Figure 15. *Beta radiation from Tc-99.*

Gamma Spectroscopy

We are performing gamma spectroscopy in the field using the HPI Rainbow MCA and the 3-inch-diameter by 3-inch-thick sodium iodide detector. The Rainbow MCA is a battery-powered 1024 channel analyzer with an LCD display. The instrument can store 12 spectra and has the capability to subtract background spectra. This instrument has a gamma energy resolution (FWHM) of about 10 keV. The gamma emitters' energies may be attenuated by various materials, but the gamma energies are not shifted as is the case with the alpha-spectroscopy systems. See Figure 16 at right.

Figure 16. *3X 3 Nal detector.*

Gamma Emitting Isotopes

Figure 17 shows the two distinct gamma energies from niobium-94 of 702 keV and 871 keV on the right side of the spectrum. Barium-133 has several distinct gamma energies at 31, 80, 276, and 356 keV. The specific gamma radiation energies of radon and thoron progeny may be used to identify those isotopes. However, the weight of the detector, the ergonomics of its shape, and the lower intrinsic efficiency of all gamma detectors have limited its usefulness in responding to contamination events.

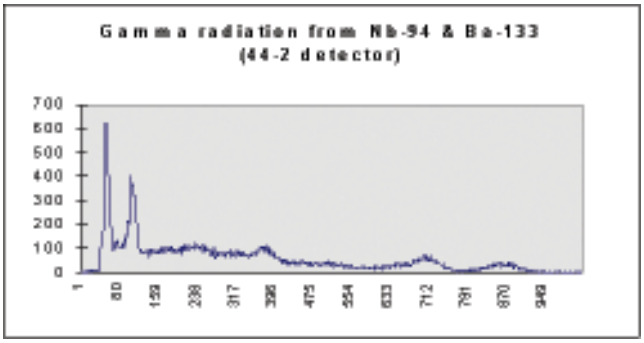

Figure 17. *Gamma radiation from Nb-94 and Ba-133.*

Timed Coincidence Counting Applied to Radon and Thoron Discrimination

Timed coincidence counting can be applied to the subtraction of counts from radionuclides when the immediate progeny of a radionuclide has a very short half-life.

The table of radon decay indicates that ^{214}Po is an alpha-particle emitter with a half-life of 164 μs (micro-seconds). If the instrument detects radioactive decay of the parent, in this case ^{214}Bi, followed by the radioactive decay of its progeny ^{214}Po within a very short time, then we can have a very high degree of confidence that the two radioactive decays were part of the radon decay chain and were not due to other radioactivity. In a typical distribution of radon progeny, ^{214}Po accounts for about 90% of the alpha activity. ^{214}Bi accounts for about half of the beta activity. If we subtract these two activities from the gross radon-progeny activity, then practically no alpha activity is left to initiate an alpha alarm. Typically, beta activity from radon progeny is well below the alarm setpoints of our contamination monitors.

The table of thoron decay indicates that ^{212}Po is an alpha-particle emitter with a half-life of 304 ns (nano-seconds). Its immediate parent is ^{212}Bi. The decay scheme of thoron is different than the radon decay scheme. ^{212}Bi decays by beta particle emission 64% of the time to ^{212}Po, and 36% of the time by alpha particle decay to ^{208}Tl. This difference in decay schemes allows us to subtract all of the alpha activity and about 80% of the beta activity from thoron when we detect the coincidence of ^{212}Bi decay followed by the alpha decay of ^{212}Po.

If we set up our timed coincidence circuit to count an alpha particle following a beta particle within a window of 200 μs as a coincident radon progeny, then what is our confidence that we will not falsely count true activity as radon progeny? First, our typical radon and thoron false alarms have count rates in the range of 500 to 3,000 counts per minute. If we postulate an extreme case where we have 25,000 counts per minute of true alpha activity and 25,000 counts per minute of true beta activity, then the false coincident count rate will happen 4% of the time. The instrument would simply report 96% of the true activity. If the activity were in the range of 2,500 counts per minute for both true alpha and true beta activity, then the instrument would report 99.6% of the true activity after falsely subtracting the radon coincidence. On the other hand, when the activity is due to radon progeny, the

instrument would subtract all of the radon progeny and report no activity.

The application of the timed coincidence method of radon and thoron discrimination requires both hardware and software development. Faster amplifiers are needed to support the 304-ns decay-time coincidence in the thoron decay chain. Software is needed to provide the counting and subtraction logic. The timed coincidence method can be applied to any detector capable of detecting and discriminating both alpha and beta particle emissions. The timed coincidence method is in the Laboratory's patenting process at the present time, and the development of the supporting hardware and software continues.

Alpha-Particle Energy Discrimination

Some hand-held instruments, such as the Harwell A92A (Figure 18) and the Eberline E-600/SHP-380 and E-600/SHP-330 (Figure 5), may be used to discriminate the different alpha particle energies. Stationary personnel contamination monitors, such as the Eberline PCM-2 (Figure 2) and HFM-7 (Figure 21, Hand and Foot Monitor), may also be used to discriminate the different alpha particle energies.

Harwell A92A

The A92A uses a silicon solid-state detector with a surface area of 9 square inches (75-mm by 75-mm square) to detect alpha emitters. The A92A does not have a MCA, but uses an upper level discriminator that eliminates the instrument's response to alpha energies above the upper level cutoff. The upper level discriminator is typically set just above the highest alpha expected to be encountered. The 5.8 MeV alpha particle energy from ^{244}Cm may be used effectively to set the instrument's upper level cutoff. By eliminating alpha energy response above 5.8 MeV, more than 90% of the typical interference from radon progeny is eliminated from the instrument's response. Also, if the contamination is from radon progeny only, then using the upper level discriminator on the A92A limits its response to only the 6.00 MeV alpha energy from ^{214}Po, which has a 3 minute half-life. This allows for a much more rapid determination that the activity is radon by allowing for the decay of this single radon progeny isotope. See Figures 18 and 19 below.

Our success with the A92A has not been as good as we had anticipated because of the electronics that were designed in the late 1980s. The lack of a response time switch and an integrate mode has prevented this instrument from meeting our expectations. We plan to use the instrument's large area detector, the instrument's best feature, in two prototypes. One prototype uses the Eberline E-600 to provide two levels of alpha particle energy discrimination, and one uses the Rainbow MCA to provide an alpha energy spectrum. The A92A's detector with a 56-cm^2 active surface area is substantially greater than the 15.5-cm^2 active surface area of the SAIC AP-2.

Figure 18. *Harwell A92A.*

Eberline SHP-380

The SHP-380 was described earlier in this report (page 56). Its ability to discriminate alpha particle energies was unacceptable because of light scattering in the ZnS phosphor and in the detector case. This light scattering spreads the energy response of the detector over too broad a range to discriminate the different alpha particle energies.

Eberline SHP-330

The SHP-330 was described earlier in this report (page 56). Its ability to discriminate alpha particle energies was unacceptable because of the thickness of the detector entrance window. Alpha particles entering the detector window at an angle are attenuated more than alpha particles entering the window perpendicularly. This spreads the energy response of the detector over too broad a range.

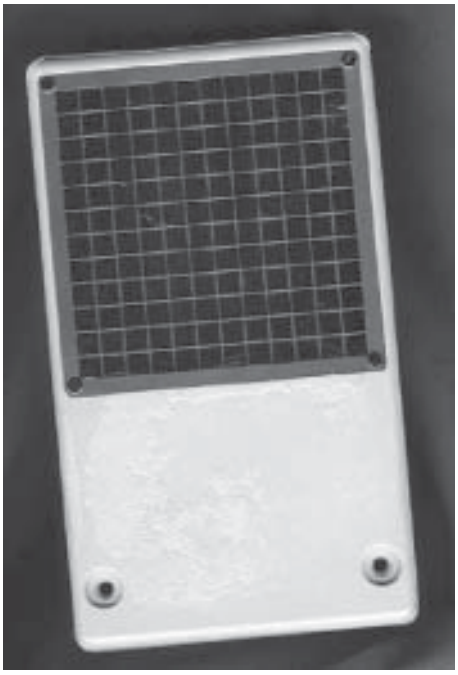

Figure 19. *A92A Detector.*

Eberline PCM-2 and HFM-7

The PCM-2 was described earlier in this report (page 55). The HFM-7 is similar in operation to the PCM-2, but is used to detect contamination on the hands and feet (bottom of the shoes) of personnel. We are investigating the possibility of modifying the calibration procedure of one of these instruments to allow it to discriminate alpha particles of different energies. These instruments have two discriminator levels: the low-level is for beta detection, and the upper-level is for alpha detection. After we have modified the instrument, the lower discriminator level will be for the alpha particles of less than 6.00 MeV, and the upper discriminator level will be for those alpha emitters of 6.00 MeV and higher.

Figure 20. *Eberline HFM-7.*

Once we have proven the ability of the PCM-2s and HFM-7s to discriminate alpha particle energies, the users will have two options. First, they can have their instruments recalibrated to detect alpha only, but to discriminate between radon or thoron progeny and the isotopes of interest. Second, the PCM-2s and HFM-7s can be modified to have three discriminator levels—the lowest for beta particle detection, the middle for alpha particle emitters of interest, and the highest for radon and thoron progeny. The first option is the cheapest, for it will only be a matter of scheduling the recalibration. The second option will cost approximately $10K for a PCM-2 and $5K for an HFM-7, but will give the user the most options on how the instrument can be used.

Ion Generators to Minimize Radon and Thoron Interference

Ion generators are being investigated to minimize radon and thoron progeny interference. In the introduction, we stated that radon and thoron progeny become attached onto plastic and other synthetic materials through electrostatic attraction. If the electrostatic charge on materials can be reduced or eliminated, then much less radon and thoron progeny will become attached to those materials. By applying techniques used in electronics manufacturing and explosives manufacturing, we can reduce those electrostatic charges. Electrostatic charges on plastics and other synthetic materials can build up to several thousand volts. These electrostatic charges typically exist as separate areas of positive and negative charges. Ion generators neutralize these areas of positive and negative charges by supplying many thousands of positive and negative ions to the areas of charge. This causes the separate areas of charge to blend together. With no electrostatic charges to attract fresh radon or thoron progeny, a short decay time will reduce the radon and thoron activities to much lower levels. If the plastic or synthetic material is treated with the ion generator before they attract radon or thoron progeny, then we can achieve the same final result without waiting for decay time. For most plastic and synthetic materials, this neutralization of electrostatic charge will last up to two hours before the materials again build up electrostatic charges.

Conclusions

In most cases of personnel contamination, it is possible to rapidly discriminate between radon and thoron progeny and other alpha-emitters using hand-held detectors.

It is not possible for the present automatic personnel contamination monitors to discriminate between radon and thoron progeny and other alpha-emitters.

Using more sophisticated electronics in the personnel contamination monitors may allow for discrimination of the different alpha energies. This could make the personnel contamination monitors much more effective in discriminating between radon and thoron progeny and other alpha emitters.

Ion generators have some potential to minimize the problems associated with radon and thoron progeny becoming attached to personnel and clothing.

Field identification of the specific isotopes will require more sophisticated portable detectors. However, those portable detectors do not need to be expensive and the operators do not need extensive training if adequate procedures are developed.

References

Evans, R. D., “Engineers’ Guide to the Elementary Behavior of Radon Daughters” (Health Physics, Pergamon Press, 1969).

Hoover, M. D., personal communication (2000).

Knoll, G. F., “Radiation Detection and Measurement” (John Wiley and Sons, New York, 2000).

10 CFR 835 “Occupational Radiation Protection”

Rasmussen, R., personal communication (2000).

Industrial Hygiene

Development of Methods for Determining Physiochemical Properties of Respirable Beryllium Aerosol Materials Associated with Chronic Beryllium Disease

Studies to Date

FY95

Pilot Program for the Risk-Based Surveillance of Lung Cancer

A Polymeric Barrier Monitor to Protect Workers

Evaluation of a Real-Time Beryllium Detection Instrument

FY96

A Polymeric Barrier Monitor to Protect Workers

Evaluation of Commercial Air-Purifying Respirator Cartridges for Protection against Vapors of Nitric Acid

FY97

Reusability of Organic Vapor Air-Purifying Respirator Cartridges

FRHAM-TEX II Cool Suit Material Testing for Water (and therefore, Tritium) Protection

A Polymeric Barrier Monitor to Protect Workers

FY98

Pressure-Deformation Correlation in Waste Containers (PDCWC)

Reusability of Organic Vapor Air-Purifying Respirator Cartridges

FY99

Development of Methods for Determining Physiochemical Properties of Respirable Beryllium Aerosol Materials Associated with Chronic Beryllium Disease

Pressure Effects and Deformation of Waste Containers

Service Life Modeling for Using Organic Vapor Air-Purifying Respirator Cartridges and Setting Change-Out Schedules

FY00

Development of Methods for Determining Physiochemical Properties of Respirable Beryllium Aerosol Materials Associated with Chronic Beryllium Disease

Service Life Modeling for Using LANL Organic Vapor Air-Purifying Respirator Cartridges and Setting Change-Out Schedules

Summary of Progress

Industrial hygiene and safety projects have produced 31 professional papers and presentations since the TDEA program started in FY95. One industrial hygiene study was funded in FY01. That study alone has resulted in 6 professional papers and presentations, with 2 of the papers published in peer reviewed journals. The project is a comprehensive study of respirable beryllium, which has become very important to workers from the former Cold War weapons complex. The study has resulted in collaboration among four LANL organizations and many organizations external to the Lab, including Lovelace Respiratory Research Institute, Brush Wellman Inc., and the Institut de Protection et de Surete Nucleaire.

Development of Methods for Determining Physicochemical Properties of Respirable Beryllium Aerosol Materials Associated with Chronic Beryllium Disease

Principal Investigators: Ronald C. Scripsick, Industrial Hygiene and Safety (ESH-5) and Kendall J. Hollis, Materials Technology: Metallurgy (MST-6)

Investigators: Gregory A. Day, Mary Ann Hill, and R. Scott Lillard (MST-6), Robert M. Dickerson (MST-8), Eric J. Peterson (MST-STC), Aleksandr B. Stefaniak (ESH-5), Yolanda E. Valdez (B-5), Mark D. Hoover, Lovelace Respiratory Research Institute, Albuquerque, NM (LRRI), Michael S. Kent, Brush Wellman Inc., Elmore, OH, Marie-Hélène Hengé-Napoli, Institut de Protection et de Sûreté Nucléaire, Cedex, France

Funding: FY99, TDEA - $88K; MST-6 $90K; FY00, TDEA - $89K; ESH-5 - $40K (unburdened); MST-6 - $40K (unburdened); FY01, TDEA - $100K; ESH-5 - $40K (unburdened); MST-6 - $120K (unburdened)

Introduction

Traditionally, beryllium (Be) aerosol mass concentration has been used to develop exposure controls for Be facilities. Recent epidemiological studies and exposure assessments (Kr97, Ei98) indicate investigation into exposure indices other than Be aerosol mass concentration may be needed to control exposures to levels that assure protection. Development of such indices requires information on the physical and chemical properties of Be aerosol exposures that may affect occurrence of disease. The objective of this study is to adapt methods for evaluating these properties in actinides and other hazardous materials to evaluations of respirable Be aerosol materials.

Epidemiological studies find that exposure to insoluble Be aerosol materials is associated with development of chronic beryllium disease (CBD) in workers (Ei83, Kr93, St96, Kr96, Kr97). At the cellular and molecular level, it is thought that a dissolved Be species is the Be input to the immunopathologic process that results in disease (Ne93). This project is focusing on physical and chemical properties of beryllium particles that control conversion from particle to dissolved species. The study hypothesis is that the rate of dissolution and dissolution lifetime of particles deposited in the alveolar region of the lung may influence the disease process and that exposure indices based on physicochemical properties that govern dissolution may lead to protection of workers.

This is an annual report of progress for the third and final year of the project. In fiscal year (FY) 2001, progress was made in two areas: 1) development of cellular methods for determining dissolution rate constants (k) for Be, and 2) development of a framework for data interpretation. Progress made in each of these areas is described below.

Development of cellular methods for determining dissolution rate constants (k) for Be

The intracellular dissolution behavior of insoluble particles is often modeled using macrophage cells maintained in vitro (Kreyling et al., 1990; Eidson et al., 1991). From the dissolution data, the chemical dissolution rate constant, k, with units of g/cm^2-day, can be determined and used to model the dissolution behavior of a given material.

The appropriate in vitro compartment within which to measure the dissolved mass of analyte of interest is not well established. Kreyling et al. (1990) investigated the in vitro dissolution of cobalt oxide particles and found that the dissolved species diffused out of the cell. This observation indicates that the mass of particle dissolved should most appropriately be measured in the extracellular culture medium. In contrast, Eidson et al. (1991) observed that dissolved beryllium produced by dissolution of beryllium particles in vitro accumulated within cells until a cytotoxic concentration was reached, then released to extracellular media upon cell death. These data suggest that the mass of dissolved analyte should be measured for the intracellular compartment only to avoid overestimating the value of k. Based on these conflicting data, an approach was devised to compare both methods in our in vitro studies of the dissolution behavior of respirable beryllium aerosol particles.

Prior to undertaking full-scale studies, we reviewed the methods of Kreyling et al. and Eidson et al. Their techniques were practiced and/or modified based on results of our own pilot studies and a methodology, depicted in Figure 1, capable of comparing the results obtained from the two in vitro approaches. For the purposes of our studies, the method based on Eidson et al. (1991) is referred to as sequential sacrifice because the dissolution rate constant was calculated from the mass of dissolved beryllium within the macrophage cell phagolysosome at predetermined harvest-time points. The sequential sacrifice method entails dosing a number of tissue culture dishes containing macrophage cells and harvesting a subset of dishes at fixed time points until all dishes have been harvested. The method based on Kreyling et al. (1990) is referred to as serial decanting because the dissolution rate constant was determined from the mass of dissolved beryllium in the extracellular culture medium at predetermined time points. In the serial decanting method, a set number of tissue culture dishes are dosed and at fixed time points the culture medium from each dish was removed, then replaced with fresh culture medium, maintaining the same number of dishes throughout the study

period. Sacrificed tissue culture dishes and cell culture media were then subject to a series of fractionation steps, described below, to separate dissolved from particulate beryllium so that k could be calculated from the dissolution data. Several techniques were developed for this methodology, including 1) preparation of liquid-beryllium particle dosing suspensions, 2) dose delivery, 3) maintenance of cell cultures for a period sufficient for quantifiable dissolution to occur, and 4) fractionation of particulate from dissolved beryllium within the cell and in the culture media:

Preparation of liquid-beryllium particle dosing suspensions. Techniques were developed to suspend beryllium particles in liquid. All possible combinations of beryllium particles (beryllium metal or beryllium oxide), container (plastic centrifuge tube or glass scintillation vial), and liquid matrix (water or phosphate buffered saline [PBS]) were tested with the goal of finding an optimum set of variables for suspension preparation. Results indicated that beryllium oxide could be suspended in water or PBS, and that beryllium metal could only be suspended in PBS using a glass scintillation vial to prevent the loss of particles to the container wall.

Dose delivery technique. Gravimetric determination of a mass of powder is often used to dose cell cultures with a known amount of beryllium (Andre et al., 1987; Eidson et al., 1991) in dissolution studies. To circumvent analytical weighing balance sensitivity limitations, the dose mass of beryllium was determined using inductively coupled plasma-mass spectrometry (ICP-MS). This technique involves estimating a dosing suspension concentration gravimetrically and verifying the exact dose mass by submitting multiple samples of the cell culture medium supplemented with dosing suspension for ICP-MS analysis.

Maintenance of cell cultures during dissolution studies. The J774A.1 monocyte-macrophage cell line was planned for use in our dissolution studies because these cells are highly phagocytic (Ralph and Nakoinz, 1975). A potential limitation to using this cell line is that the cell population doubling time is 12–24 hours (Ralph et al. 1976), and once confluent (e.g., having formed a monolayer of cells on the dish surface), the cells must be sub-cultured or they will begin to die. As a result, a balance was needed between having a sufficient cell population per dish to ensure rapid and complete beryllium particle uptake while avoiding confluence prior to sufficient dissolution having occurred to meet ICP-MS analytical limit of detection. We investigated two options for delaying time to confluence, using a cytostatic agent and increasing tissue culture dish surface area.

Lipopolysaccharide (LPS) is a chemostatic agent, i.e., at 10 μg LPS/ml media J774A.1 growth rate is reported to be static but physiologic functioning is not altered (Ralph and Nakoinz, 1977). In a pilot study, we investigated the effects of LPS at two concentrations, 2 or 9 mg LPS/ml media, on J774A.1 cell proliferation and viability. Cell population doubling time was 2.4 to 3.0 times slower for cells cultured in either 2 or 9 μg LPS/ ml medium than in control medium; however, LPS was cytotoxic after 4 days.

Based on the negative results of the LPS pilot study, we investigated a second technique to delay the time to confluence, increasing the tissue culture dish surface area available for growth. For this pilot study, six of each sized sterile tissue culture dishes, 60 x 15 mm, 100 x 20 mm, and 150 x 25 mm were seeded with 2×10^6 J774A.1 cells per dish in minimum essential media (MEM). Every other day, cells in each dish were suspended and assayed for cell concentration and viability by trypan dye exclusion technique. Results indicated that using a 150 mm culture dish rather than a 100 mm dish in vitro dissolution studies could be maintained for 12 days prior to cells reaching confluence.

Fractionating particulate from dissolved beryllium. Kreyling et al. (1990) and Eidson et al. (1991) used filtration to fractionate particulate from dissolved species, both in the extracellular medium and within the cells; however, an exact technique was not specified. We investigated the feasibility of using several different filtration techniques, including an open face filter holder or a lure lock filter unit that attaches to a syringe. Results from pilot studies indicated that filtration using an open face filter holder was subject to wall losses, and that 0.1, 0.22, and 0.45 μm pore size filters used by Kreyling et al. (1990) and Eidson et al. (1991) were apt to clog while filtering particle free cultured medium. Lure lock filter units that attach to the end of disposable syringes were also subject to clogging with 0.1, 0.22, and 0.45 μm pore size filters, resulting in spillage of culture medium or rupture of the filter, yielding unfiltered sample breakthrough into the filtrate.

The negative results from the pilot studies investigating filtration prompted development of an alternative approach combining low- and high-speed centrifugation, depicted in Figure 2, to separate particulate from dissolved beryllium. First, the culture medium from each sequential sacrifice and serial decanting dish was aspirated and placed into separate labeled 50-ml centrifuge tubes, and centrifuged at 1100 rpm and 4° C for 6 minutes. The supernatant from each centrifuge tube was then aspirated and transferred to separate labeled 50 ml high-speed centrifuge bottles and centrifuged at 10000 rpm and 4° C for 45 minutes. The supernatant from this high-speed spin, which contains the mass of dissolved beryllium in the extracellular culture medium, M_{DE}, was aspirated and transferred to separate labeled glass sample jars. The undissolved mass of beryllium in the extracellular medium, M_{UDE}, from particles that were free or inside floating cells at the time of aspiration remained in the pellet. Next, the PBS rinse from each serial decanting and sequential sacrifice was added to the appropriate 50 ml centrifuge tube containing the cell pellet from the low-speed spin, and centrifuged at 1100 rpm and 4° C for 6 minutes. The resulting supernatant contained any residual dissolved beryllium captured by the PBS

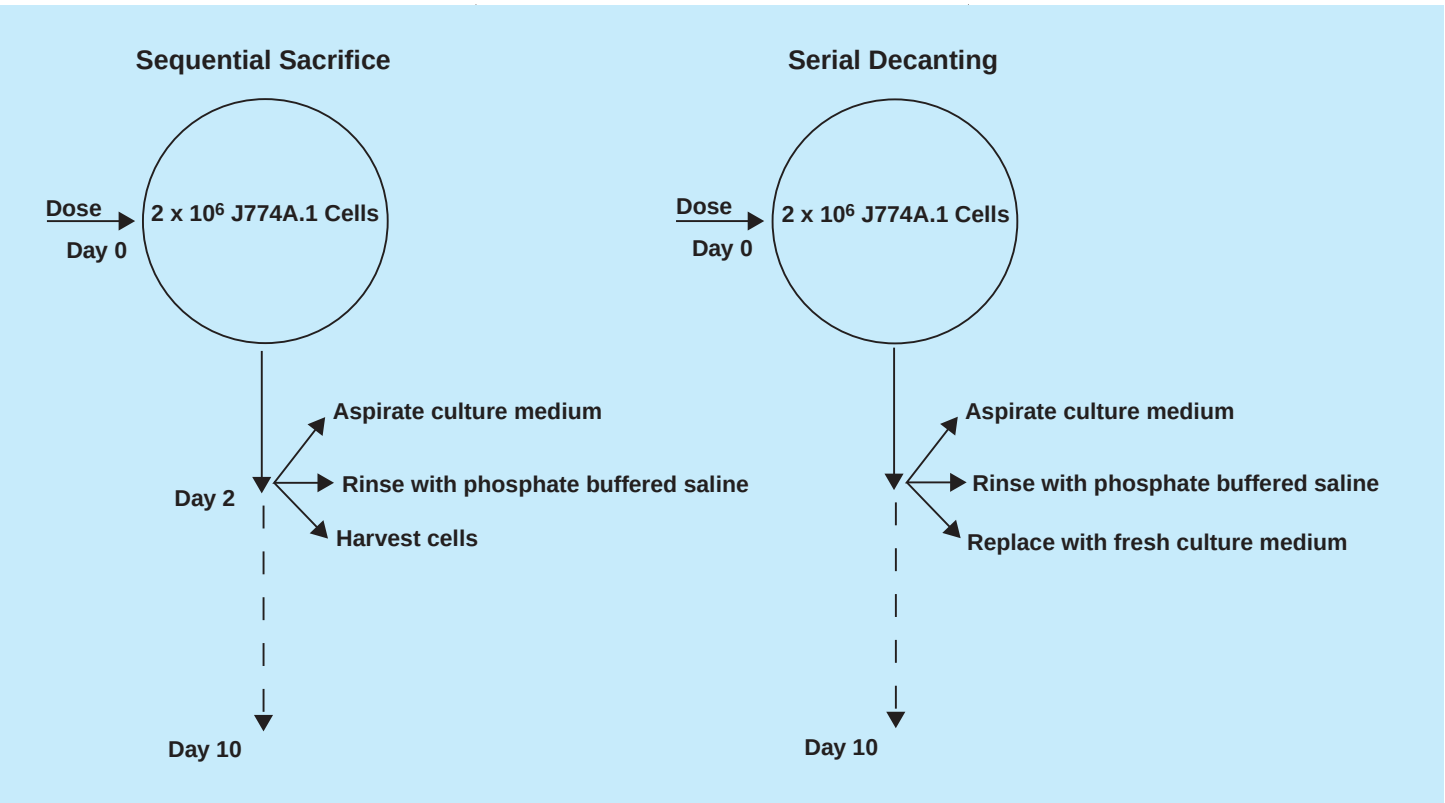

Figure 1. *Method for fractioning particulate from dissolved beryllium in the intracellular and extracellular compartments.*

rinse, M_{DE}, and the cell pellet potentially contained dissolved intracellular, M_{DI}, and undissolved intracellular, M_{UDI}, beryllium. The supernatant containing M_{DE} was aspirated and combined with the M_{DE} sample previously obtained from the high-speed spin to yield a single sample containing all M_{DE} for a given dish. For the serial decanting dishes, the dissolution rate constant is determined from the M_{DE}, which represents dissolved beryllium that has diffused out of the cell, so the cell pellet containing M_{DI} and M_{UDI} was resuspended in 5 ml PBS and submitted for ICP-MS analysis to complete the mass balance. For sequential sacrifice dishes, the dissolution rate constant is calculated from the M_{DI}; therefore, the cell pellet was subject to further fractionation. The cells in the sequential sacrifice dishes were suspended using 4 x 10 ml aliquots of PBS and transferred to the appropriate high-speed centrifuge bottle containing the cell pellet with M_{DI} and M_{UDI} and centrifuged at 10000 rpm and 4° C for 45 minutes. The resulting supernatant, containing M_{DI} was aspirated and transferred to a glass sample jar and the particle-cell debris pellet containing M_{UDI} resuspended in 5 ml PBS and all samples were submitted for beryllium analysis by ICP-MS.

Determination of the dissolution rate constant of beryllium oxide. Using the method described above, we performed two experiments to determine the dissolution rate constant of beryllium oxide particles (aerodynamic diameter 1.5–2.5 μm, specific surface area = 11.1 m^2/g). A suspension containing approximately 780 μg beryllium oxide was prepared in a glass scintillation vial. An aliquot of the suspension was added to supplemented MEM to achieve a target dose of 80 μg beryllium oxide (29 μg Be) per dish. Next, 15 sequential sacrifice, 3 serial decanting, and 3 cellular control dishes were prepared by seeding 150 x 25 mm dishes with 2 x 10^6 J774A.1 cells per dish, incubated for 2 hours to allow cells to adhere, then the culture medium aspirated and replaced with medium containing beryllium oxide. The exception to this protocol was that cellular control dishes were not dosed, but 3 acellular control dishes consisting of dosing medium only were prepared and all 24 dishes were returned to the incubator. Six samples of equal volume of dosing medium as that used to culture dishes were prepared and submitted for ICP-MS analysis to determine the exact initial beryllium dose mass. The media from 9 random dishes aspirated prior to dosing were also submitted as blanks to confirm the absence of beryllium in cells at the start of the study. Every other day for 10 days three sequential sacrifice dishes were harvested and the medium from 3 serial decanting dishes was aspirated and replaced as described in Figure 1 and the cell cultures and medium manipulated as depicted in Figure 2 until all dishes were harvested on day 10.

The efficiency of certain steps outlined in Figures 1 and 2 were unknown, so three pilot studies were embedded in the experiment. The efficiency of the PBS rinse step in removing residual M_{DE} from the cells, the efficiency with which beryllium was

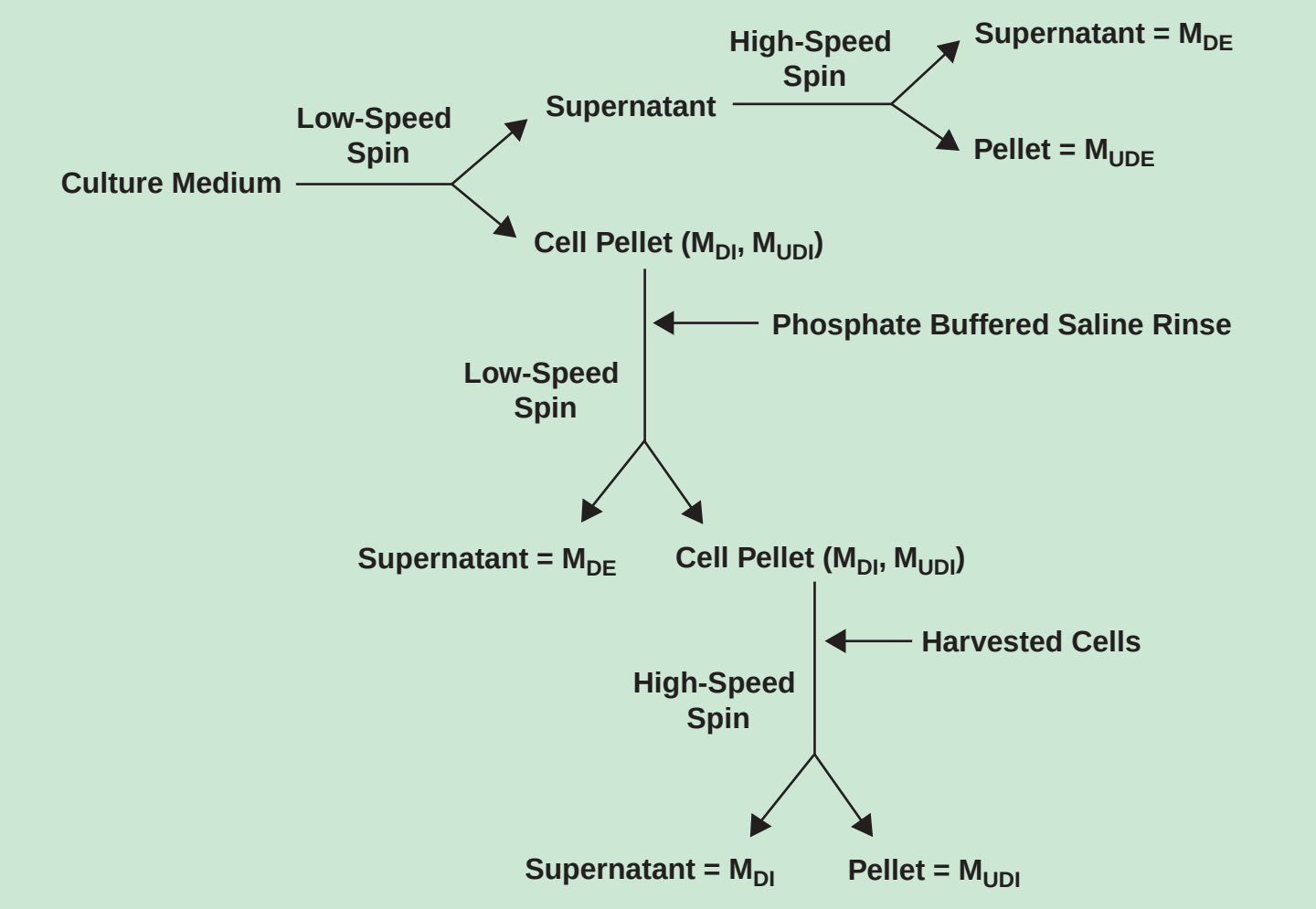

Figure 2. *In vitro method for determination of dissolution rate constants of beryllium aerosols.*

removed from dishes when cells were harvested, and the beryllium recovery efficiency of the high-speed centrifuge step were determined. The results of these pilot studies will be used to calculate efficiency correction factors for data analysis.

Preliminary Results. A portion of the samples generated during the first dissolution experiment has been analyzed and a preliminary summary of the results is provided here for the serial decanting method. The analysis of the remaining serial decanting and all sequential sacrifice samples is ongoing. The initial dose mass as determined from 6 samples of dosing medium analyzed by ICP-MS is 20.7 μg Be and no beryllium was detected in blank samples. For the serial decanting dishes (N = 3), M_{DE} on day 2 after dosing was 0.122 μg Be while no beryllium was detected in the M_{UDE} samples, e.g., <LOD. Analysis of the cell pellet from the low-speed spin detected 0.270 μg Be in the pellet containing M_{DI} and M_{UDI}, indicating 99% of beryllium was retained intracellular within 48 hours of dosing. It is known that beryllium oxide dissolution is biphasic, comprised of an early rapid dissolution phase during the first 48 hours followed by a slower long-term dissolution phase (Finch et al. 1988). Analysis of the data yields a rapid phase value of $k = 2.2 \times 10^{-4}$ g/m^2-day. This rate constant is consistent with values reported for the rapid dissolution phase of beryllium oxide in 0.1 N HCl, $k = 3.3 \times 10^{-4}$ g/m^2-day, and a simulant of extracellular lung fluid (pH 7.4), $k = 6.3 \times 10^{-6}$ g/m^2-day (Finch et al. 1988).

Development of framework for data interpretation

Exposure-disease relation. At a fundamental level, Be exposure controls CBD. The disease is observed in cohorts with exposure to Be and has not been reported in the absence of exposure (Cu87, Ne92, Mi98, Wa00). There is evidence of an exposure threshold for CBD. Beryllium is commonly found in soil and air at trace levels, yet cases of disease are not observed in the general public. From studies of past beryllium environmental releases (Wa00), an airborne exposure concentration threshold for CBD of 0.01 μg Be/m^3 has been derived. To date, no clear exposure-disease relation has been found for CBD (Ei98, Kr97). However, there is evidence suggesting that chemical form may affect this relation. Kreiss (Kr96) found a positive association between beryllium exposure and sensitization at a facility that only worked with beryllium oxide whereas no such association was found at a facility where there were exposures to multiple beryllium species (Kr97). Recently, at two facilities having comparable beryllium exposure levels, Deubner et al. (De01) attributed an eight-fold difference in disease incidence to differences in the chemical form of exposures at the facilities.

Dose-Response Relation. Studies (Ha70, Ep82, Ro88, Sa89) contributing to development of the beryllium lymphocyte proliferation test show an in vitro dose-response relation between added beryllium and T cell activation in individuals with CBD. Epstein et al. (Ep82), Rossman et al. (Ro88) and Saltini (Sa89) observed a positive dose response in both brochoalveolar lavage (BAL) and peripheral blood cell cultures for treatments of soluble beryllium (e.g., $BeSO_4$).

Hanifin (Ha70) made similar observations with cells from peripheral blood for treatments with beryllium oxide particles. This is the only dose-response study to use beryllium particulate found in our literature review. Hanifin's results for three CBD patients (cases A, B, and C) are shown in Figure 3. The results include a positive response region where response [R] increases with added mass M – R = f(M).

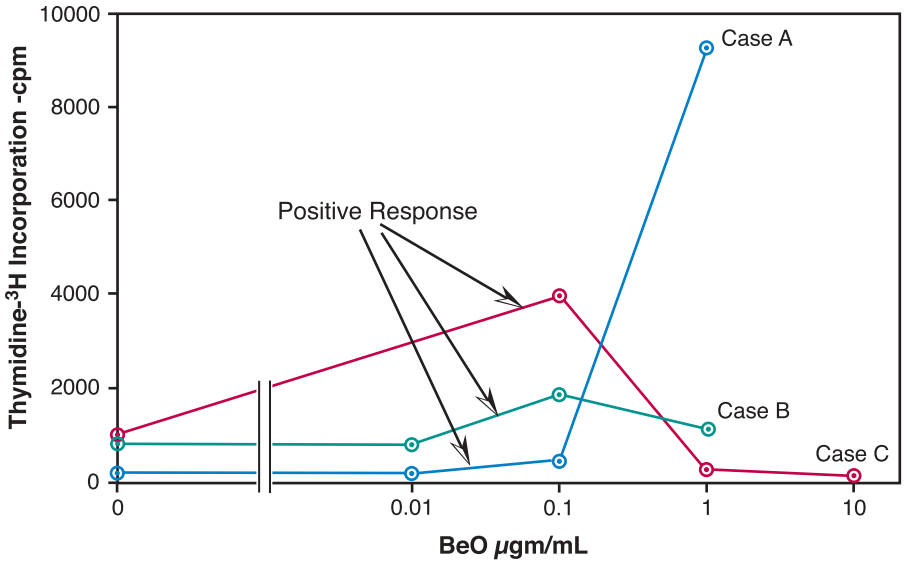

Hanifin, J.M., W.L. Epstein, and M.J. Cline: In Vitro Studies of Granulomatous Hypersensitivity to Beryllium. J. Invest. Derm. 55: 284-288 (1970).

Figure 3. *Dose-response data from Hanifin et al. showing a positive response region.*

Added mass can be interpreted as added BeO surface area (S) using the relation with specific surface area (Sp):

$$M = S/Sp \quad (1).$$

Thus, the functional dependence of response observed by Hanafin et al. can also be expressed in terms of added BeO surface area. For BeO particles, the production rate of dissolved beryllium depends on total particulate surface area. Such a functional dependence on S is expected if response is limited by the availability of beryllium dissolved from added beryllium particles. This interpretation of Hanifin's results suggests that the kinetics of lymphocyte activation, here represented by lymphocyte proliferation, may depend on the kinetics of particle dissolution.

Conclusion and Deliverables

In FY 2001, major activity areas included development of cellular methods for determining dissolution rate constants (k) for Be (Development of methods section), and the development of a framework for data interpretation section. Progress made in each area is described in detail above and is summarized below.

Uncertainty in whether intracellularly dissolved beryllium remained within cells or is transported out of the cell across the cell membrane drove our decision to look for dissolved beryllium both within cells and in extracellular fluid. Our method consists of two components: 1) serial sacrifice of cell cultures and determining dissolved beryllium associated with lysed cells and 2) sequential decanting where dissolved beryllium is analyzed for in cell culture extracellular fluid. Two studies were completed using this two component method. Analysis of samples from these studies is ongoing.

We collaborated with Theoretical Biology group (T-10) to investigate the exposure-disease and dose-response relations for chronic beryllium disease. The literature supports a disease exposure threshold concentration of 0.01 μg Be/m^3. Ambient exposure levels below this value do not appear to result in cases of CBD. Determining an exposure-disease relation has been elusive. Our review of certain recent studies suggests that the presence of such exposure-disease relations may be obscured by a dependence on the chemical form of exposure.

Dose-response relations have been observed in cultures of lymphocytes from the peripheral blood and BAL fluid of CBD patients when treated with soluble beryllium (e.g., Be_2SO_4). One study has been found where positive dose-response was also observed for doses of insoluble BeO particulate. Through conversion of added beryllium particulate mass to added beryllium particle surface area, results of this study can be interpreted to suggest that the kinetics of the lymphocyte response may be limited by dissolution of BeO particulate.

References

An87 **André, S., H. Métivier, G. Lantenois, M. Boyer, D. Nolibé, and R. Masse:** Beryllium Metal Solubility in the Lung, Comparison of Metal and Hot-pressed Forms by in vivo and in vitro Dissolution Bioassays. *Human Toxicol.* **6**:233–240 (1987).

Cu87 **Cullen, M.R., J.R. Kominsky, M.D. Rossman, M.G. Cherniack, J.A. Rankin, J.R. Balmes, J.A. Kern, R. P. Daniele, L. Palmer, G.P. Naegel, K. McManus, and R. Cruz:** Chronic Beryllium Disease in a Precious Metal Refinery. *Am Rev Respir Dis* **135**:201–208 (1987)

De01 **Deubner, D., J. Kelsh, M. Shum, L. Maier, M. Kent, and E. Lau:** Beryllium sensitization, chronic beryllium disease, and exposures at a beryllium mining and extraction facility. *Appl. Occup. Env. Hyg.* **16**(5):579–592 (2001).

Ei83 **Eisenbud, M., and J. Lisson:** Epidemiological Aspects of Beryllium-Induced Nonmalignant Lung Disease: A 30-Year Update. *J. Occ. Med.* **25**(3):196–202 (1983).

Ei91 **Eidson, A.F., A. Taya, G.L. Finch, M.D. Hoover, C. Cook:** Dosimetry of Beryllium in Cultured Canine Pulmonary Alveolar Macrophages. *J. Toxicol. Environ. Health* **34**:433–448 (1991).

Ei98 **Eisenbud, M.:** The Standard for Control of Chronic Beryllium Disease. *Appl. Occup. Environ. Hyg.* **13**(1):25–31 (1998).

Ep82 **Epstein PE, Dauber JH, Rossman MD, and RP Daniele:** Bronchoalveolar Lavage in a Patient with Chronic Berylliosis: Evidence for Hypersensitivity Pneumonitis. *Ann. Intern. Med.* **97**:213–216 (1982).

Fi88 **Finch, G.L., J.A. Mewhinney, A.F. Eidson, M.D. Hoover, and S.J. Rothenberg:** In Vitro Dissolution Characteristics of Beryllium Oxide and Beryllium Metal Aerosols. *J. Aerosol Sci.* **19**(3):333–342 (1988).

Ha70 **Hanifin, J.M., W.L. Epstein, and M.J. Cline:** In Vitro Studies of Granulomatous Hypersensitivity to Beryllium. *J. Invest. Derm.* **55**:284–288 (1970).

Kr90 **Kreyling, W.G., J.J. Godleski, S.T. Kariya, R.M. Rose, and J.D. Brain:** In Vitro Dissolution of Uniform Cobalt Oxide Particles by Human and Canine Alveolar Macrophages. *Amer. Jou. of Resp. Cell and Molecular Bio.* **2**:413–422 (1990).

Kr93 **Kreiss, K., M.M. Mroz, B. Zhen, J.W. Martyny, and L.S. Newman:** Epidemiology of Beryllium Sensitization and Disease in Nuclear Workers. *Am. Rev. Respir. Dis.* **148**:985–991 (1993).

Kr96 **Kreiss, K., M.M. Mroz, L.S. Newman, J. Martyny, and B. Zhen:** Machining Risk of Beryllium Disease and Sensitization with Median Exposures Below 2 μg/m3. *Amer. J. Ind. Med.* **30**:16–25 (1996).

Kr97 **Kreiss, K., M.M. Mroz, B. Zhen, H. Wiedeman, and B. Barna:** Risks of Beryllium Disease Related to Work Processes at a Metal, Alloy, and Oxide Production Plant. *Occ. Env. Med.* **54**(8):605–612 (1997).

Mi98 **Middleton, D.C.,** Chronic beryllium disease: uncommon disease, less common diagnosis. *Environ Health Perspect* 1**06**:765–767 (1998).

Ne92 **Newman, L.S. and K. Kreiss.,** Non-occupational beryllium disease masquerading as sarcoidosis: identification by blood lymphocyte proliferative response to beryllium. *Am Rev Respir Dis* **145**:1212–1214 (1992).

Ne93 **Newman, L.S.:** To Be2+ or Not to Be2+: Immunogenetics and Occupational Exposure. *Science* **262**:197–198 (1993).

Ra75 **Ralph P and I Nakoinz:** Phagocytosis and cytolysis by a macrophage tumor and its cloned cell line. *Nature.* **257**:393–393 (1975).

Ra76 **Ralph P, Moore-Malcolm AS, and K Nilsson:** Lysosome Synthesis by Established Human and Murine Histiocytic Lymphoma Cell lines. *J. Exp. Med.* **143**:1528–1533 (1976).

Ra77 **Ralph P and I Nakoinz:** Direct toxic effects of immunopotentiators on monocytic, myelomonocytic, and histiocytic or macrophage tumor cells in culture. *Cancer Res.* 37:546–550 (1977).

Ro88 **Rossman MD, Kern JA, Elias JA, Cullen MR, Epstein PE, Preuss OP, Markham TN, and RP Daniele:** Proliferative Response of Bronchoalveolar Lymphocytes to Beryllium: A Test for Chronic Beryllium Disease. *Ann. Intern. Med.* **108**:687–693 (1988).

Sa89 **Saltini C, K. Winestock, M. Kirby, P. Pinkston and R.G. Crystal:** Maintenance of Alveolitis in Patients with Chronic Beryllium Disease by Beryllium Specific Helper T-Cells. *N. Engl. J. Med.* **320**(17):1103–1109 (1989).

St96 **Stange, W., D.E. Hilmas, F.J. Furman:** Possible Health Risks from Low Level Exposure to Beryllium. *Toxicology* **111**:213–224 (1996).

Wa00 **Wambach, P.F., R.M. Tuggle:** Development of an eight-hour occupational exposure limit for beryllium. *Appl. Occup. Environ. Hyg.* **15**(7):581–587 (2000).

Publications and Presentations Resulting from TDEA Projects

The publications and presentations listed below have received full or partial funding from the TDEA Program. In some instances, a project has been ongoing, and TDEA contributed support toward its progress**.**

Balice et al.

Selected Presentations and LA Reports for the Duration of the Project

Balice, R.G., "Ecological risk assessment and extreme events analysis: applications to wildfire management." Presented at the symposium Extreme Event Analysis in Ecology, held at the 86th Annual Meeting of the Ecological Society of America, Madison, WI 2001.

Balice, R.G. and S.W. Koch, "Regression modeling to enhance spatial representations of fuel loads and fire hazards." LA-UR-01-1090, presented at the ESH Division Review Committee Meeting, Los Alamos National Laboratory, March 13–15, 2001.

Balice, R.G., S.W. Koch, and S.R. Yool, "Modeling the spatial patterns of forest fuels in the Los Alamos region." Presented at the 85th Annual Meeting of the Ecological Society of America, Snowbird, UT 2000.

Balice, R.G., B.P.Oswald, and S.R. Yool, "Fuels inventories and spatial modeling of fire hazards in the Los Alamos Region." Pages 138-147 in *Proceedings of the Crossing the Millennium: Integrating Spatial Technologies and Ecological Principles for a New Age in Fire Management Conference and Workshop, Volume 1,* (L. Neuenschwander et al., Technical Editors), University of Idaho and the International Association of Wildland Fire, Moscow, ID 2000.

Balice, R.G., J.D. Miller, B.P. Oswald, C. Edminster, and S.R. Yool, "Forest surveys and wildfire assessment in the Los Alamos Region; 1998-1999." Los Alamos National Laboratory, report LA-13714-MS 2000.

Koch, S.W. and R.G. Balice, "Input data development for the FARSITE fire area simulator for the Los Alamos National Laboratory Region." Presented at the ESRI User Conference, San Diego, CA June 26, 1999.

Koch, S.W. and R.G. Balice, "Interactions of wildfire components: modeling the Cerro Grande Fire." Oral presentation at the 86th Annual Meeting of the Ecological Society of America, Madison, WI, August 5–10, 2001.

Koch, S.W, R.G. Balice, J.W. Nyhan, and S.R. Loftin, "Validation and sensitivity analyses of a wildfire behavior model." Presented at the ESH Division Review Committee Meeting, Los Alamos National Laboratory, April 11–13, 2000.

Koch, S.W., R.G. Balice, S.R. Loftin, J.W. Nyhan, P. Valerio, and J. Baars, "Modeling wildfire behavior and effects in the Los Alamos Region following the Cerro Grande Wildfire." Oral presentation at the Fall Meeting of the New Mexico Geographic Information Council, Albuquerque, NM, November 3, 2000.

Nyhan, J., S.W. Koch, R.G. Balice, S. Loftin, and P. Valerio, "Estimation of soil erosion in burned forest areas resulting from the Cerro Grande Fire." Poster presented at the ESH Division Review Committee Meeting, Los Alamos National Laboratory, LA-UR-01-1356, March 13–15, 2001.

Valerio, P, "Tree thinning saves lives and property. Poster presentation at the Fire Conference 2000: The First National Congress on Fire Ecology, Prevention and Management." Held in San Diego, California, by the California Association of Fire Ecology, November 27–December 1, 2000.

Yool, S.R., J.D. Miller, R.G. Balice, B.P. Oswald, and C. Edminster, "Mapping fuel risk at the Los Alamos urban-wildland interface." Pages 228–234 in *Proceedings of the Crossing the Millennium: Integrating Spatial Technologies and Ecological Principles for a New Age in Fire Management Conference and Workshop, Volume I,* (L. Neuenschwander et al., Technical Editors), University of Idaho and the International Association of Wildland Fire, Moscow, ID 2000.

Peer Reviewed Publications and Presentations

Miller, J.D., J.W. Nyhan, and S.R. Yool, "Modeling potential erosion due to the Cerro Grande Fire with a GIS-based implementation of the Revised Universal Soil Loss Equation." *Landscape Ecology* submitted, in review, 2001.

Nyhan, J.W., S.W. Koch, R.G. Balice, and S. Loftin, "Estimation of soil erosion in burnt forest areas of the Cerro Grande Fire in Los Alamos, New Mexico." *Catena,* submitted, in review, 2001.

Oswald, B.P., R.G. Balice, and K.B. Scott, "Fuel loads and overstory conditions at Los Alamos National Laboratory, New Mexico." Pages 41–45 in *Fire and Forest Ecology: Innovative Silviculture and Vegetation Management* (W. Keith Moser and Cynthia F. Moser, Editors). Tall Timbers Fire Ecology Conference Proceedings, No. 21. Tall Timber Research Station, Tallahassee, FL 2000.

Biggs et al.

Presentations:

Quintana, E. and H. Alexander, "The evaluation of techniques to collect hair and scat samples from free-ranging carnivores." Los Alamos National Laboratory report LA-UR-01-3845 2001.

Peer Reviewed Publications:

Alexander H., J. Longmire, J. Biggs, L. Hansen, C. Bare, and S. Frybarger, In preparation, "Tetranucleotide microsatellite loci for mountain lion *(Puma concolor)."*

Gonzales et al.

Publications and Presentations

In September 2001, a poster on this project was presented at the annual Wildlife Society meeting in Reno, Nevada. In November 2001, a poster was presented at the annual Society for Environmental Toxicology and Chemistry conference in Baltimore, Maryland.

Planned publications and presentations for this project include a presentation at the Society for Environmental Toxicology and Chemistry, publication in the *J. Environ. Tox. and Chem.*, satisfaction of the thesis requirement for the M.S. degree (Ms. Sarah Mitchell), and a poster presentation at the annual Environment, Safety and Health Division Review.

Mallett et al.

Publications

TDEA Progress Report, "Neutron Extremity Dosimetry Based on Monte Carlo Computations of Magnetic Resonance Images," Los Alamos National Laboratory report LA-13901-PR 2000.

Presentations

Poster presentation to the ESH Division Review Committee: March 12, 2001, LA-UR-01-1245.

Moore et al.

Publications

Moore, M.E., H.J. Gepford, R.E.. Hermes, N.E. Hertel, and R.T. Devine, "Laser Illuminated Track Etch Scattering (LITES) Dosimetry System" to be printed in Radiation Protection Dosimetry, accepted for publication in Solid State Dosimetry—Proceedings of the Thirteenth International Conference (Athens, Greece July 9–13, 2001).

Presentations

Moore, M.E., R.T. Devine, H.J. Gepford, R.E. Hermes, N.E. Hertel, J.M. Hoffman, and R.J. McKeever, Poster presentation to the ESH Division Review Committee: March 12, 2001. Title: "Laser Illuminates Track Etch Scattering (LITES) Dosimetry System," Received a "Best-in-Class" designation from the DRC committee.

Conference presentation (Heather Gepford): Laser Illuminated Track Etch Scattering (LITES) Dosimetry System. M.E. Moore, R.E. Hermes, R.T. Devine (LANL), H.J. Gepford, and N.E. Hertel (Georgia Tech). Thirteenth International Conference on Solid State Dosimetry July 9–13, 2001, Athens, Greece.

Awards

LITES team received a "Los Alamos Achievement Award" from the Environment, Safety, and Health Division. Los Alamos National Laboratory, September 20, 2001.

Rodgers et al.

Presentations and LA Reports

Rodgers, J.C., M.J. Koskelo, and S. Homann, "Features of the environmental continuous air monitor (ECAM)," Los Alamos National Laboratory report LA-UR-01-1390 presented at, DOE Air Monitoring Users Group Meeting, Oak Ridge, TN, March 19, 2001.

Rodgers, J.C., and S. Huang, "Modification of the Los Alamos / Canberra Environmental Continuous Air Monitor (ECAM) inlet for enhanced performance by removal of fine particles," Los Alamos National Laboratory report LA-UR-01-0763 presented at TDEA Committee Review and Division Review Committee June 2001.

Rodgers, J.C., "Monitoring for alpha-emitting radionuclides in the environment using the Los Alamos / Canberra alpha-ECAM," presented at, CRMG Meeting, Santa Clara Pueblo, NM August 22, 2001.

Huang, S., R. Alcantara, S.D. Schery, P.T. Wasiolek, and J.C. Rodgers, "Investigations of techniques to improve continuous air monitors under conditions of high dust loading in environmental settings," presented at, *EMSP National Workshop*, Atlanta, GA, April 24–28, 2000.

Peer Reviewed Publications

Huang, S., S.D. Schery, R.E. Alcantara, N.V. Dale, and J.C. Rodgers, "Micrometer-sized short-lived radioactive aerosol particles for convenient use in laboratory measurements," *Health Physics* (in press, submitted April 2001).

Huang, S., S.D. Schery, R.E. Alcantara, J.C. Rodgers, and P.T. Wasiolek, "Influence of dust loading on the alpha-particle energy resolution of continuous air monitors for thin deposits of radioactive aerosols," *Health Physics* (in press, submitted September 2001).

Scripsick et al.

Presentations

LANL Divisional Review Committee Poster Session, March 2001

Surface area of beryllium metal, oxide and copper alloy aerosol particles: Stefaniak, A.B., M.D. Hoover, G.A. Day, and R.C. Scripsick.

Chronic beryllium disease dosimetry: particle dissolution to lymphocyte activation: Scripsick, R.C., and B.B. Goldstein.

AIHCE01 Poster Session June 2001

Surface area of beryllium metal, oxide and copper alloy aerosol particles: Stefaniak, A.B., M.D. Hoover, G.A. Day, and R.C. Scripsick.

Microscopy and Microanalysis (August 2001)

TEM of BeO aerosol: materials aspects of method development in studying chronic beryllium disease: Dickerson, R.M., R.C. Scripsick, G.A. Day, A.B. Stefaniak, and E.J. Peterson.

Peer Reviewed Publications

Scripsick, R.C.: On the role of particle dissolution in chronic beryllium disease. (In preparation)

Stefaniak A.B., M.D. Hoover, R.M. Dickerson, E.J. Peterson, G.A. Day, P.N. Breysse, and R.C. Scripsick: Surface Area of Respirable Beryllium Metal, Oxide, and Copper Alloy Aerosols and Implications for Assessment of Exposure Risk of Chronic Beryllium Disease. (In preparation)

Stefaniak A.B., R.S. Lillard, R.M. Dickerson, P.N. Breysse, and R.C. Scripsick: Evidence to Support the Potential Importance of Chloride Ion and pH in Phagocytic Dissolution of Beryllium Metal Particles. (In preparation).

Whicker et al.

Peer Reviewed Publications

Whicker, J.J., D.D. Breshears, P.T. Wasiolek, T.B. Kirchner, R.A. Tavani, D.A. Schoep, and J.C. Rodgers, "Temporal and spatial variation of episodic wind erosion in unburned and burned semiarid shrublands," *J. of Environmental Quality*, **31**, 2002.

Los Alamos, New Mexico 87545